Molecular Sieve Synthesis using Imidazolium Structure Directing Agents
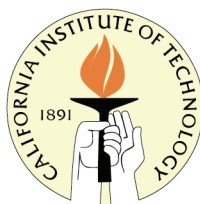
Thesis by

Raymond Humphrey Archer

In Partial Fulfillment of the Requirements for the

degree of

Doctor of Philosophy

California Institute of Technology

Pasadena, California

2009

(Defended May 29, 2009)

Acknowledgements

I would like to thank my advisor, Professor Mark Davis, for his contribution throughout my graduate career. Through the many disappointments and failed projects he always had suggestions and ideas on how to move forward. I would also like to thank the other members of my committee, Professor Dave Tirrell, Dr. Jay Labinger, and Dr. Stacey Zones. I am particularly indebted to Stacey for his time and contribution to all aspects of this thesis. I am particularly glad I made the effort to visit with him when I was in the Bay Area over the last 11 months. Our various meetings in Richmond, Berkeley, and the Beach Chalet were valuable to my research and offered a different perspective on what life might entail after graduate school. I am also indebted to the help Allen Burton provided, particularly with the molecular modeling and for his keen eye to look at X-ray patterns. All work presented in this thesis received financial support from the Chevron Energy Research Company and the constant support is appreciated.

I would also like to thank the members of the Davis Group, both past and present, for their help and guidance. Most of the training I received was from Hyunjoo Lee and Jon Galownia and they both made Room 31 a pleasant office. John Carpenter also deserves credit for running the CI tests on my materials. Another person I would like to thank is Sonjong Hwang for his help with solid-state NMR experiments. Tom Dunn and Larry Henling were always willing to help troubleshoot equipment and their assistance helped to speed repairs. Through the many projects I was involved with I received valuable assistance from Mona Shahgholi, Nathan Dalleska, Bill Tivol, and Carol Garland.

Finally, I could not have completed my studies without the love and support of my family. My parents and siblings have been a source of constant support from my formative school years through the University of Canterbury and on to Caltech. My time at Caltech would have been far less enjoyable without my wife, Melissa, to share the experience and I cannot wait to be reunited with her in the near future. Also, the welcome her family gave me was appreciated, being so far from home.

Abstract

The synthesis of high-silica molecular sieve SSZ-70 is investigated through a guest/host study of imidazolium structure directing agents (SDAs). The original borosilicate synthesis is extended to pure-silica and aluminosilicate compositions using six imidazolium SDAs. Physical characterization using powder X-ray diffraction (XRD), ^{29}Si solid-state NMR, electron microscopy, thermogravimetric analysis, and nitrogen adsorption shows SSZ-70 to be layered with similarity to MCM-22 (MWW). Aluminum-containing SSZ-70 is evaluated for catalytic activity using the constraint index (CI) test and shows a similar cracking rate to SSZ-25 (MWW structure). Distinct differences in CI as a function of time on stream are observed between MWW and SSZ-70 materials. Additional molecular sieve phases observed in this guest/host study included Theta-1 (TON), ZSM-5 (MFI), ZSM-23 (MTT), ZSM-12 (MTW), Beta, Mordenite (MOR), CIT-5 (CFI), SSZ-16 (AFX), and SSZ-35 (STF).

Attempts to synthesize Beta enriched in chiral polymorph A are investigated in a second guest/host study using five chiral imidazolium SDAs. Two SDAs successfully gave Beta, but no enrichment in polymorph A is observed. The remaining SDAs do not direct the formation of any molecular sieve phases. Molecular modeling indicates both SDAs occupy the straight [100]/[010] 12 membered ring (MR) pores of Beta. In this configuration, no chirality could be projected across the [001] fault planes and this offers an explanation for not observing enrichment. Modeling shows careful consideration must be given to efficiently filling the entire void volume when large SDAs are used. Additional molecular sieve phases observed in the guest/host study are EU-1 (EUO) and MOR.

Finally, attempts to synthesize novel materials using supramolecular SDAs are described. Supramolecular SDAs are created through adamantyl/β-cyclodextrin inclusion complex formation. Both 2:1 and 1:1 inclusion complex stoichiometries are attempted. Significant cyclodextrin degradation occurs at temperatures above 90°C and no structure-directing effect can be attributed to the cyclodextrin. Molecular sieve phases observed in the study are SSZ-16 (AFX), MOR, B-SSZ-13 (CHA), VPI-8 (VET), and SSZ-24 (AFI).

Table of Contents

List of Figures

List of Tables

Chapter One: Introduction

1.1: Molecular Sieve Synthesis

Molecular sieves comprise a family of porous inorganic materials. The crystalline nature of these materials offers defined pore diameters and high internal void volume. Pore dimensions are often on the order of small molecules and hence selective adsorption can be achieved. Materials are classified as microporous (pore diameter ≤2 nm) or mesoporous (2 <pore diameter ≤50 nm). Framework structures are assigned by the International Zeolite Association with an online database available[1]. Structure codes are three-letter designations of the material name; e.g., ZSM-5 has the MFI structure code. Various inorganic compositions have been reported with significant efforts devoted to high-silica molecular sieves. Pure-silica materials represent one molecular sieve subset where [SiO_4] tetrahedra are linked to form a three-dimensional SiO_2 framework. In the absence of lattice substitution the framework is neutral. Introducing tetrahedral aluminum into the framework results in negative framework charge and a cation is required for neutrality. This is shown schematically in Figure 1.1. If a proton is the cation a Brønsted acid is formed and the resulting material can be active in acid catalyzed reactions. In addition, the defined pore structure offers shape-selective catalysis. Aluminosilicate molecular sieves form the zeolite family, although all silica-based molecular sieves are often called zeolites. Research emphasis has been placed on zeolites due to applications in petrochemical and refining transformations, adsorption and as ion-exchange materials.
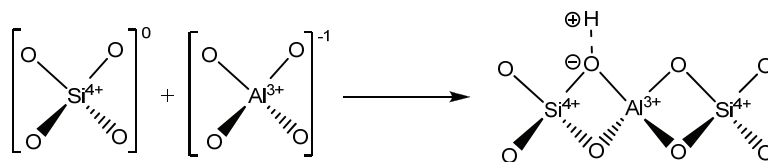
Figure 1.1: Schematic of Brønsted acid site

Figure 1.1 shows aluminum incorporation into a silicate lattice and this is just one example of possible substitution. Other examples of elements incorporated in silica-based molecular sieves include B, Ga, Ge, Be, Zn and Ti. Any lattice substitution must obey the bonding rules outlined by Pauling[2] and Loewenstein[3]. Molecular sieves of non-silica composition have been synthesized with the aluminophosphate (AlPO) family extensively studied. These materials have strictly alternating -Al^{3+}-O-P^{5+}-O- sequences and represent another family of neutral frameworks. Substitution of Si^{4+} for phosphorus creates negative framework charge as above and the resulting silicoaluminophosphate (SAPO) materials can show activity in acid catalyzed reactions. Similarly, substituting M^{2+} (e.g., Co^{2+}, Zn^{2+}) for Al^{3+} also produces negative framework charge. Most phosphate-based materials have significantly lower hydrothermal stability compared to high-silica materials and this has limited applications.

Early investigations into zeolite synthesis aimed to replicate geothermal conditions where natural zeolites are formed[4, 5]. Reaction gels containing alkali hydroxide, silica, alumina and water lead to materials such as Linde Type A (LTA) and zeolites X and Y (both isostructural with the mineral faujasite (FAU)). Further advances occurred with the introduction of quaternary ammonium molecules, starting with tetramethylammonium

hydroxide[6]. Extension to tetraethylammonium lead to the discovery of zeolite Beta, with this being the first example of a high-silica zeolite (Si/Al≥5)[7]. Continued expansion of organic reaction components has lead to the discovery of numerous frameworks, with 179 structure codes assigned by the International Zeolite Association (as of May, 2009).

High-silica reactions involving organic molecules result in the organic species occluded within the product phase. Most organic molecules were capable of making more than one product depending on the reaction conditions (e.g., SiO_2/Al_2O_3 ratio, alkali cation addition, temperature). In addition, any given product could often be made using many different organic molecules. This lead to a proposed restriction of the term "template" to cases where one organic specified only one product[5]. One commonly cited example of a template is the tris-quaternary molecule used to make ZSM-18 (MEI)[8]. For all other cases the organic was deemed a structure directing agent (SDA). This latter designation covers the majority of organic molecules investigated to date and will be used in this thesis.

The organic-silicate distances observed in molecular sieves are of the order where van der Waals attractions can occur. This lead to experiments aimed at understanding organic-silicate interactions as the reaction gel transformed from X-ray amorphous to crystalline. Fundamental insights into the steps involved in high-silica material nucleation and crystal growth have been achieved using a model system. This system is the tetrapropylammonium hydroxide/sodium hydroxide/silica/water system that produces pure-silica MFI. The synthesis is reproducible and relatively fast making it ideal for temporal analysis. Solid-state magic angle spinning (MAS) NMR ^{1}H-^{29}Si experiments revealed polarization transfer from organic to silicate species before long-range order was observed by X-ray diffraction (XRD)[9]. Further experiments indicated overlap of silicate and SDA

hydrophobic hydration spheres with ordered water release[10, 11]. These studies gave the first conclusive evidence of short-range association before crystallization occurred. Modification of the synthesis gel by using tetraethyl orthosilicate (TEOS) results in optically clear gels. These gels were examined under synthesis conditions by *in situ* dynamic light scattering (DLS) and were shown to contain particles ~3–10 nm in diameter[12]. Additional *in situ* experiments using synchrotron radiation confirmed the presence of these particles and a synthesis pathway was proposed[13, 14]. The proposed pathway is shown in Figure 1.2 and involves overlap of hydrophobic hydration spheres leading to ~3 nm diameter particles that can aggregate under appropriate conditions to form ~10 nm diameter particles. Nucleation was proposed to occur from these aggregates with subsequent crystal growth from the 3 nm "primary" units.
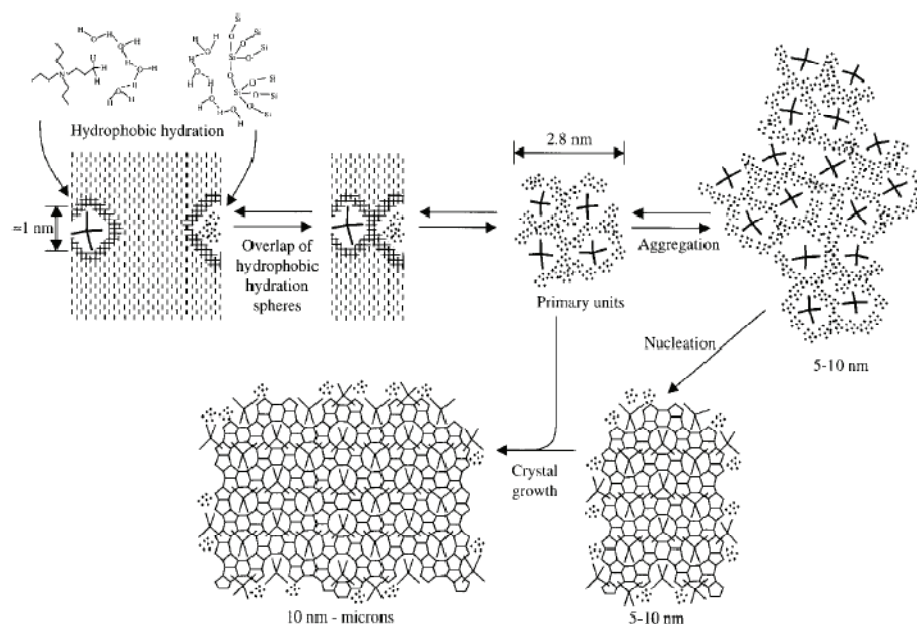
Figure 1.2: Scheme for Si-MFI-TPA crystallization (from Reference 13)

Another important aspect of high-silica molecular sieve synthesis was understanding synthesis thermodynamics. Calorimetry experiments for pure-silica molecular sieves showed enthalpies of transition between 6.8–14.4 kJ mol^{-1} relative to quartz[15]. The enthalpies span approximately twice the thermal energy (RT) at synthesis conditions indicating small energetic differences between porous frameworks and relatively small metastability compared to quartz. Accounting for the full synthesis cycle indicated enthalpy and entropy contributions were of comparable magnitude and were within several RT at synthesis temperature[16]. The study revealed a relatively flat energy landscape indicating product selectivity was largely determined by kinetic factors.

Recent developments in the use of fluoride and germanium have lead to many new framework discoveries. Reaction conditions for high-silica molecular sieves evolved from attempts to mimic geological conditions with hydroxide employed to mineralize silica. Early investigations into reactions containing fluoride showed no difference in product compared to hydroxide reactions[17, 18]. These studies were performed at relatively high water to silica ratios ($H_2O/SiO_2 > 20$) based on existing hydroxide preparations. Significantly reducing the water content ($2 < H_2O/SiO_2 < 10$) resulted in the discovery of several new frameworks[19]. Many products under fluoride conditions show very few framework defects and trends have emerged where low framework density products become favored at low H_2O/SiO_2[20, 21]. In addition, pure-silica frameworks containing double-four membered rings (D4Rs, a cube) have emerged. This structural feature had not been observed in high-silica molecular sieves derived from hydroxide reactions. The addition of germanium also promotes the formation of D4Rs. Combining germanium, fluoride and low water content has lead to several very open structures being discovered,

e.g., ITQ-21 (three-dimensional 12MR)[22] and ITQ-33 (18x10 MR)[23]. The longer Ge-O bond[24] results in preferential Ge substitution in D4R structures[25].

The advances in understanding high-silica molecular sieve synthesis are still not sufficient to predict what product will result from a given SDA. Molecular modeling has proven useful in certain cases to predict suitable SDAs for known products[26]. Without appropriate retrosynthetic methodologies the discovery of novel frameworks has relied on synthesizing various SDAs and observing what product is obtained. Some general guidelines for desirable SDA characteristics have been accumulated through these studies[27]. The inorganic conditions also play a significant role in determining the product with subtle changes in reagent selection offering different reaction outcomes[28]. Recent application of high-throughput (HT) techniques has resulted in several new discoveries through thorough reaction variable exploration[29]. Discovery of new frameworks will continue to rely on a combination of new SDAs coupled with appropriate inorganic conditions.

1.2: Previous Examples of Imidazolium Structure Directing Agents

Imidazolium SDAs have been used in molecular sieve synthesis with the first investigations in the 1980s[30, 31]. The phases obtained were ZSM-5 (MFI), ZSM-12 (MTW), ZSM-23 (MTT), Theta-1 (TON), KZ-2 (TON) and ZSM-48 (*MRE). All products are 10MR structures except MTW that is a puckered 12MR. In addition, all products are one-dimensional except MFI. SDAs with notable selectivity to the same product with decreasing SiO_2/Al_2O_3 ratios were 1,3-dimethylimidazolium (TON), 1,3-

diisopropylimidazolium (MTT) and 1,2,3-trimethylimidazolium (MTW). The SDAs were synthesized by imidazole alkylation, with cyclopentyl, neo-pentyl and benzyl groups the largest investigated. No products were reported using 1,3-dibenzylimidazolium or 1,3-dicyclopentylimidazolium, while MTT was reported for 1,3-bis(neo-pentyl)imidazolium. In addition, the early investigations used the SDAs as halide salts together with sodium silicate as silica source. This corresponded to $Na^+/SiO_2 \geq 0.59$ for all cases. Subsequent evolution in gel compositions now see SDAs used as hydroxide solutions with $Na^+/SiO_2 \sim 0.1\text{-}0.2$ and $SDA^+OH^-/SiO_2 \sim 0.15\text{-}0.25$ typical.

Further studies were performed under hydroxide conditions with a series of diquaternary imidazolium SDAs[32]. The SDAs studied were based on the selective SDAs outlined above with methylene spacers of varying length between imidazoliums. Starting imidazoles were 1-methylimidazole, 1-isopropylimidazole and 1,2-dimethylimidazole. Again, one-dimensional products TON and MTW were favored with three-dimensional MFI more common than above. In contrast, MTT was absent indicating sensitivity to periodicity along the pore. Several original imidazolium SDAs were revisited after the breakthroughs in fluoride mediated reactions at low water to silica ratios[19]. The results showed TON and MTT for 1,3-dimethylimidazolium and 1,3-diisopropylimidazolium respectively at all water to silica ratios[33]. In addition, a new phase named ITQ-12 (IWW) was discovered using 1,3,4-trimethylimidazolium[34]. IWW is a small pore material constructed from linked D4Rs forming slit-shaped cages. Obtaining a material rich in D4Rs is in contrast to the structures listed above that are rich in five membered rings (pentasil structures). Subsequent work showed 1,2,3-trimethylimidazolium also made IWW at all water to silica ratios[21]. Observing the same product at all H_2O/SiO_2 ratios was

rarely observed across an entire SDA library. The implication was the imidazolium dominated nucleation selectivity to a greater extent than the fluoride anion. Single-crystal analysis of pure-silica MTT synthesized using 1,3-diisopropylimidazolium revealed the isopropyl lobes had similar periodicity to the undulating MTT framework. This guest/host pair appeared particularly favorable due to mutual periodicity.

Additional studies under boron-rich fluoride conditions with 1,3-diisopropylimidazolium lead to the discovery of a new material denoted SSZ-70[35]. Chapter Two of this thesis explores the synthesis of SSZ-70 as described below. Independent studies using 1-ethyl-3-methylimidazolium under germanosilicate fluoride conditions lead to the discovery of IM-16 (UOS)[36]. This material has a 10x8x8 MR pore topology and is rich in D4Rs owing to high Ge content (Si/Ge~1.4).

Finally, the unique properties of imidazolium ionic liquids were exploited to synthesize several new AlPO materials SIZ-1 to SIZ-11[37, 38]. This "ionothermal" method is unique in that the solvent also acts as the SDA. Reactions have been demonstrated at atmospheric pressure and solvent recycling has also been shown. Imidazolium ionic liquids 1-ethyl-3-methylimidazolium bromide, 1-isopropyl-3-methylimidazolium bromide, and 1-butyl-3-methylimidazolium bromide are examples used in this approach. No reports of high-silica molecular sieve synthesis have appeared although active research is expected in this area.

The examples listed above show imidazolium SDAs to be well suited in molecular sieve synthesis. Most studies have focused on small imidazoliums available through imidazole alkylation and therefore larger substituent groups have not been thoroughly investigated. Since the initial studies in the 1980s, alternative synthetic methods for 1,3-

disubstituted imidazoliums have emerged[39]. This allows expansion of previous studies with an emphasis on larger imidazolium SDAs.

1.2: Thesis Overview

The focus of this thesis was exploring larger imidazolium SDAs in molecular sieve synthesis. Chapter Two explores the synthesis of new material SSZ-70 using a library of 16 imidazolium SDAs. The majority of the SDAs studied had not been reported in molecular sieve synthesis before. Chapter Three evolved from the SSZ-70 work where Beta was a common product. This separate study explored chiral imidazolium SDAs with the aim of synthesizing Beta enriched in chiral polymorph A. The underlying theme of Chapters Two and Three was exploring guest/host relationships. The aim for these studies was to observe product (host) changes across different SDAs (guest) to find appropriate SDAs for the desired product. Both studies involved synthesis and characterization of imidazolium SDAs plus screening all SDAs in inorganic reactions. Of general interest in both studies was whether larger SDAs would show strong specificity to one product as in the case of 1,3-diisopropylimidazolium to MTT. Chapter Four sought to expand the results obtained with 1,3-bis(1-adamantyl)imidazolium in Chapter Two by creating supramolecular SDAs through adamantyl/β-cyclodextrin inclusion complexes. Finally, Chapter Five offers conclusions and considerations for future directions.

1.3: References

1.   http://www.iza-structure.org/databases/.

2.   L. Pauling, Journal of the American Chemical Society **51** (4), 1010–1026 (1929).

3.   W. Loewenstein, American Mineralogist **39** (1–2), 92–96 (1954).

4.   C. S. Cundy and P. A. Cox, Chemical Reviews **103** (3), 663–702 (2003).

5.   M. E. Davis and R. F. Lobo, Chem. Mater. **4** (4), 756–768 (1992).

6.   R. M. Barrer and P. J. Denny, Journal of the Chemical Society (MAR), 971–& (1961).

7.   R. L. Wadlinger, G. T. Kerr and E. J. Rosinski, US Patent No. 3,308,069 (1967).

8.   S. L. Lawton and W. J. Rohrbaugh, Science **247** (4948), 1319–1322 (1990).

9.   S. L. Burkett and M. E. Davis, The Journal of Physical Chemistry **98** (17), 4647–4653 (1994).

10.   S. L. Burkett and M. E. Davis, Chemistry of Materials **7** (5), 920–928 (1995).

11.   S. L. Burkett and M. E. Davis, Chemistry of Materials **7** (8), 1453–1463 (1995).

12.   B. J. Schoeman, Zeolites **18** (2–3), 97–105 (1997).

13.   P. de Moor, T. P. M. Beelen, B. U. Komanschek, L. W. Beck, P. Wagner, M. E. Davis and R. A. van Santen, Chemistry—a European Journal **5** (7), 2083–2088 (1999).

14.   P. de Moor, T. P. M. Beelen, R. A. van Santen, K. Tsuji and M. E. Davis, Chemistry of Materials **11** (1), 36–43 (1999).

15.   P. M. Piccione, C. Laberty, S. Y. Yang, M. A. Camblor, A. Navrotsky and M. E. Davis, Journal of Physical Chemistry B **104** (43), 10001–10011 (2000).

16. P. M. Piccione, S. Y. Yang, A. Navrotsky and M. E. Davis, Journal of Physical Chemistry B **106** (14), 3629–3638 (2002).

17. E. M. Flanigen and R. L. Patton, US Patent No. 4,073,865 (1978).

18. J. L. Guth, H. Kessler, J. M. Higel, J. M. Lamblin, J. Patarin, A. Seive, J. M. Chezeau and R. Wey, ACS Symposium Series **398**, 176–195 (1989).

19. M. A. Camblor, L. A. Villaescusa and M. J. Diaz-Cabanas, Topics in Catalysis **9** (1–2), 59–76 (1999).

20. M. A. Camblor, M. J. Diaz-Cabanas, J. Perez-Pariente, S. J. Teat, W. Clegg, I. J. Shannon, P. Lightfoot, P. A. Wright and R. E. Morris, Angewandte Chemie International Edition **37** (15), 2122–2126 (1998).

21. S. I. Zones, S. J. Hwang, S. Elomari, I. Ogino, M. E. Davis and A. W. Burton, Comptes Rendus Chimie **8** (3–4), 267–282 (2005).

22. A. Corma, M. J. Diaz-Cabanas, J. Martinez-Triguero, F. Rey and J. Rius, Nature **418** (6897), 514–517 (2002).

23. A. Corma, M. J. Diaz-Cabanas, J. L. Jorda, C. Martinez and M. Moliner, Nature **443** (7113), 842–845 (2006).

24. R. D. Shannon, Acta Crystallographica Section A **32** (SEP1), 751–767 (1976).

25. T. Blasco, A. Corma, M. J. Diaz-Cabanas, F. Rey, J. Rius, G. Sastre and J. A. Vidal-Moya, Journal of the American Chemical Society **126** (41), 13414–13423 (2004).

26. A. W. Burton, Journal of the American Chemical Society **129** (24), 7627–7637 (2007).

27. Y. Kubota, M. M. Helmkamp, S. I. Zones and M. E. Davis, Microporous Materials **6** (4), 213–229 (1996).

28. S. I. Zones, Y. Nakagawa, G. S. Lee, C. Y. Chen and L. T. Yuen, Microporous and Mesoporous Materials **21** (4–6), 199–211 (1998).

29. M. Moliner, J. M. Serra, A. Corma, E. Argente, S. Valero and V. Botti, Microporous and Mesoporous Materials **78** (1), 73–81 (2005).

30. S. I. Zones, US Patent No. 4,483,835 (1984).

31. S. I. Zones, Zeolites **9** (6), 458–467 (1989).

32. S. I. Zones and A. W. Burton, Journal of Materials Chemistry **15** (39), 4215–4223 (2005).

33. S. I. Zones, R. J. Darton, R. Morris and S. J. Hwang, Journal of Physical Chemistry B **109** (1), 652–661 (2005).

34. X. B. Yang, M. A. Camblor, Y. Lee, H. M. Liu and D. H. Olson, Journal of the American Chemical Society **126** (33), 10403–10409 (2004).

35. S. I. Zones and A. W. Burton, US Patent No. 7,108,843 (2006).

36. Y. Lorgouilloux, M. Dodin, J.-L. Paillaud, P. Caullet, L. Michelin, L. Josien, O. Ersen and N. Bats, Journal of Solid State Chemistry **182** (3), 622–629 (2009).

37. E. R. Cooper, C. D. Andrews, P. S. Wheatley, P. B. Webb, P. Wormald and R. E. Morris, Nature **430** (7003), 1012–1016 (2004).

38. E. R. Parnham and R. E. Morris, Accounts of Chemical Research **40** (10), 1005–1013 (2007).

39. A. J. Arduengo, Accounts of Chemical Research **32** (11), 913–921 (1999).

Chapter Two: Imidazolium Structure Directing Agents in Molecular Sieve Synthesis: Exploring Guest/Host Relationships in the Synthesis of SSZ-70

2.1: Introduction

The synthesis of novel molecular sieves has relied on combining an organic structure directing agent (SDA) with appropriate inorganic reaction conditions. The combination of high boron to silica ratios and fluoride lead to a new material denoted SSZ-70[1]. The synthesis employed 1,3-diisopropylimidazolium hydroxide as SDA with previous studies showing strong specificity to ZSM-23 (MTT)[1] materials [2, 3]. The MTT framework comprises an undulating one-dimensional pore topology delimited by 10 tetrahedral atoms (10MR) with 5Å periodicity. Single crystal X-ray diffraction studies show the spacing between isopropyl groups is well aligned with the framework periodicity. Furthermore, this observation was used to predict suitable SDAs for MTT synthesis[4]. Given the strong structure directing ability to MTT we were interested if SSZ-70 showed similar framework periodicity.

---

[1] Molecular sieve frameworks are denoted by three-letter codes assigned by the Structure Commission of the International Zeolite Association. The full structure database can be found at http://www.iza-structure.org/databases/.

In addition to the structure directing ability of 1,3-diisopropylimidazolium, several other imidazolium SDAs give the same product across all dilutions under pure silica fluoride synthesis conditions[5]. The majority of organic SDAs studied do not give the same product across all water-to-silica ratios, with low framework density products favored at low H_2O/SiO_2 ratios (<4) and relatively high framework density products at high H_2O/SiO_2 (>14). The imidazolium SDAs discussed above were synthesized via imidazole or substituted imidazole quaternization with an alkyl halide[6]. This strategy works well for small alkyl groups but larger groups are expected to react slowly (secondary halides) or possibly not at all (tertiary halides)[7]. Since the early investigations of imidazolium SDAs alternative synthetic methodologies have been developed for imidazolium salt synthesis driven by their suitability as N-heterocyclic carbene (NHC) precursors [8, 9] as outlined in Scheme 2.1. The alternative synthetic methods enable a wider range of substituent groups to be synthesized. With established synthetic methods we were also interested if the same product specificity would be encountered with larger imidazolium SDAs.
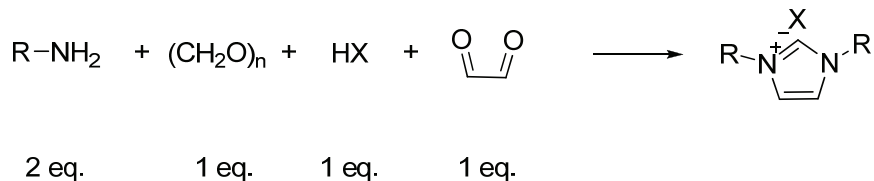
Scheme 2.1: 1,3-disubstituted imidazolium synthesis

Layered silicate materials have been widely investigated as catalysts and adsorbents. This is best exemplified by the MCM-22 (MWW)[10] family of molecular sieves. These materials contain layers in the as-made form that condense to a fully four-

connected framework upon calcination. Different inorganic compositions define other MWW materials (borosilicate ERB-1, aluminosilicate SSZ-25 and pure silica ITQ-1). Several other materials with less order have also been investigated and shown to be active catalysts for a variety of reactions (MCM-56 and ITQ-30 for example)[11, 12]. Another aspect of this family is the ability to modify the layered precursor to create a pillared material (MCM-36)[13] and even a delaminated/exfoliated material (ITQ-2)[14]. The high external surface area of these materials has attracted attention due to the possibility of catalytic reactions occurring on the external surface with substrates too large to fit inside the pores of a regular zeolite. In addition to MWW, other layered precursor materials that convert to four-connected products have been reported. These include SSZ-71 (precursor to SSZ-42 (IFR))[15] and CDS-1 (CDO)[16].

The original SSZ-70 synthesis with 1,3-diisopropylimidazolium and boron required greater than two months heating at 150°C under fluoride conditions with this being reduced to 1–2 weeks without fluoride (at 170°C). Modest catalytic activity in acid catalyzed hydrocarbon reactions was reported in the original discovery. Post synthetic aluminum insertion was required for catalytic activity with the modest catalytic activity possibly due to incomplete Al-exchange[17]. Therefore, an exploration of guest/host relationships using an expanded imidazolium library was warranted with an objective to directly synthesize aluminum-containing SSZ-70. Also, product formation kinetics could be improved using an alternative SDA.

The SDAs selected were anticipated to show changes in product distribution that could offer insight into structural features of SSZ-70. Figure 2.1 presents the sixteen guest molecules studied. The SDA library shows variation in steric demand at the charge center

(**1**, **2**, **5** and **11** less sterically demanding), periodicity (**5** and **11** have larger spacing between substituent groups) and substituent rigidity (branched and cyclic alkyl groups to rigid bicyclic and tricyclic alkyl groups). In addition, aromatic substituent groups were explored using **14** and **16**. The organocations span a wide carbon to charge range of 5 to 27 representing moderately hydrophilic for 1,3-dimethylimidazolium **1** to very hydrophobic for 1,3-bis(1-adamantyl)imidazolium **15** and 1,3-bis(2,6-diisopropylphenyl)imidazolium **16**. The zeolite chemistry of 1,3-diisopropylimidazolium has been well documented but is included here for completeness. In addition, boron rich conditions were explored using 1,3-dimethyl- and 1,3-diethylimidazolium as both SDAs show strong selectivity to ZSM-22 (TON)[3] under aluminosilicate and pure silica conditions. Many recently discovered large- and extra large pore zeolite topologies have employed organocations with $C/N^+ \geq 17$ (e.g. SSZ-24 (AFI), CIT-5 (CFI), ITQ-21, SSZ-53 (SFH) & SSZ-59 (SFN)). Generally these materials are synthesized under a narrow range of inorganic conditions with germanium required for ITQ-21 and low trivalent substitution (boron or aluminum) for the other one-dimensional products.
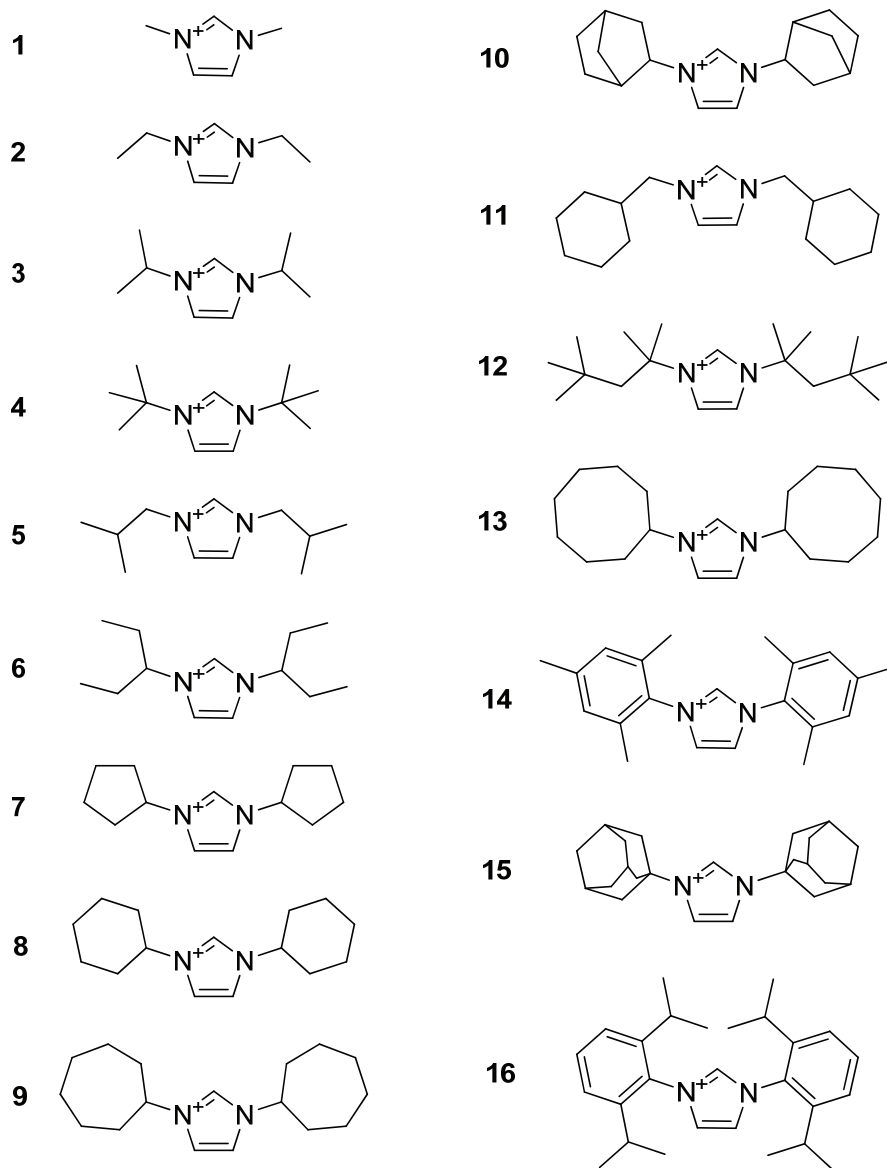
Figure 2.1: Imidazolium Structure Directing Agents Studied

As touched on above, inorganic reaction conditions play an important role in determining product formation. To study SSZ-70 formation five inorganic composition areas were investigated. The first was pure silica fluoride reactions where the water to silica ratio was varied from 3.5 to 14.5 in accordance with previous reports. Under

concentrated conditions beta is often produced (three dimensional large pore framework), with ZSM-12 (MTW, one dimensional large pore framework) a common product at high water to silica ratios. For these reactions low framework density products are favored at low water to silica ratios with higher framework densities emerging at high water to silica ratios. Second was borosilicate fluoride conditions modeled after those where SSZ-70 was originally discovered. Here the water to silica ratio was held constant around 15 and SiO_2/B_2O_3 varied. Low boron substitution at relatively high water to silica ratios could be expected to give similar phase selectivity to pure silica fluoride reactions at similar dilution (one-dimensional products favored). As more boron is incorporated into the reaction gel a transition to lower framework density phases (two or three dimensional) is possible. In addition borosilicate and aluminosilicate hydroxide reactions were explored. The product under borosilicate and aluminosilicate conditions is often different with the same guest molecule [18]. The reactions at silica to alumina (SAR) of 35 used sodium Y (FAU) zeolite as the aluminum source after the success in crystallizing SSZ-26[19]. Finally, the results from these four conditions were used to select SDAs for aluminosilicate fluoride reactions. The aluminosilicate fluoride reactions were performed at water to silica ratio of 15 with SiO_2/Al_2O_3 varied in accordance with the borosilicate fluoride reactions. All reactions were performed at 150°C in the initial reaction scheme. As described below, several reactions were repeated at 170 or 175°C to further explore the structure directing role of select guest molecules.

2.2: Experimental Section

2.2.1: Structure Directing Agent Synthesis

All reagents were purchased from commercial vendors and used as received. SDAs 1–3 were synthesized by quaternizing an imidazole with the appropriate alkyl halide[6]. 1,3-bis(2,4,6-trimethylphenyl)imidazolium chloride **14** (1,3-bis(mesityl)imidazolium chloride) and 1,3-bis(2,6-diisopropylphenyl)imidazolium chloride **16** were purchased from Sigma-Aldrich and used as received. All other SDAs were synthesized by adapting published procedures[20, 21]. Crude tetrafluoroborate salts were purified by recrystallization. Similar recrystallization attempts for halide salts were largely unsuccessful, therefore, an aqueous activated carbon treatment was employed[22]. Liquid NMR spectra were recorded on 300 MHz Varian Mercury spectrometers. Combustion analysis was performed at the Chevron Energy Technology Center (Richmond, CA) using a Carlo-Erba Combustion Elemental Analyzer. All SDAs were exchanged to the hydroxide form using Dowex Monosphere 550A UPW hydroxide resin (Supelco). Final hydroxide concentration was determined by titration with 0.01N HCl solution to a phenolphthalein end point. Several reactions with 1,3-bis(cyclohexyl)imidazolium **8** and 1,3-bis(1-adamantyl)imidazolium **15** were performed with SDA$^+$OH$^-$ solutions obtained after ion-exchange from commercially available tetrafluoroborate salts (Sigma-Aldrich). Ion exchange of **15**·BF$_4$ took approximately one week at room temperature due to the low solubility of the parent salt (>90% ion exchange by titration).

1,3-dimethylimidazolium iodide (**1**): 1-methylimidazole (4.11g, 50 mmol, Sigma-Aldrich, 99%) in 50mL ethyl acetate (J.T. Baker, HPLC Grade) was cooled to 0°C in an ice bath. Once cool, iodomethane (7.77g, 54.7 mmol, Sigma-Aldrich, 99%) was added dropwise via addition funnel. The solution was allowed to warm slowly to room temperature. Stirring was continued for approximately 60 hours then the solution was filtered and the residue was washed with diethyl ether. The product dried under high vacuum overnight yielding 10.74g (47.9 mmol, 96% yield) of white solids (used without further purification). ^{1}H NMR (300 MHz, DMSO-d_6): 9.07, 7.70, 3.85. ^{13}C NMR (75MHz, DMSO-d_6): 136.9, 123.4, 35.8. Analysis calculated for $C_5H_9IN_2$: C, 26.80; H, 4.05; N, 12.50 (C/N=2.14). Found: C, 26.90; H, 4.23; N, 12.31 (C/N=2.19).

1,3-diethylimidazolium iodide (**2**): 1-ethylimidazole (4.81g, 50 mmol, Sigma-Aldrich, 99%) in 50mL ethyl acetate was cooled 0°C in an ice bath. Once cool, iodoethane (8.69g, 55.7 mmol, Sigma-Aldrich, 99%) was added dropwise via an addition funnel. The solution was allowed to warm slowly to room temperature then stirred overnight. The precipitate was filtered off and washed with diethyl ether. The filtrate was collected and an additional 8.96g (57.4 mmol) iodoethane was added and stirring continued at room temperature for six days. The solution was filtered again and the residue was washed with diethyl ether. The combined solids were dried overnight under high vacuum yielding 9.76g white solids (38.7 mmol, 77% yield) that were used without further purification. ^{1}H NMR (300 MHz, DMSO-d_6): 9.25, 7.83, 4.20, 1.42. ^{13}C NMR (75MHz, DMSO-d_6): 135.4, 122.1, 44.2, 15.1. Analysis calculated for $C_7H_{13}IN_2$: C, 33.35; H, 5.20; N, 11.11 (C/N=3.00). Found: C, 33.26; H, 5.29; N, 10.95 (C/N=3.04).

1,3-bis(*tert*-butyl)imidazolium tetrafluoroborate (**4**): *tert*-butylamine (7.32g, 100 mmol, Alfa-Aesar, 98%) in 100mL toluene (EMD, ACS Reagent) was placed in a room temperature water bath then paraformaldehyde (3.16g, 100 mmol, Fisher, 95%) was added with strong stirring. The solution was stirred at room temperature for 30 minutes then ice was added to the water bath. After cooling for one hour another 7.32g (100 mmol) *tert*-butylamine was added dropwise via addition funnel. Tetrafluoroboric acid (18.30g, 100 mmol, Alfa-Aesar 48 wt% in water) was diluted to 30wt% with 9.16g water then added dropwise via addition funnel. The ice bath was removed and the solution warmed for 30 minutes then glyoxal solution (14.488g, 100 mmol, Alfa-Aesar, 40 wt% in water) was added dropwise. The flask was heated at 40°C overnight then allowed to cool to room temperature. The solution was filtered and the residue washed with 50 mL water and 100 mL diethyl ether then dried overnight under high vacuum yielding 13.28g white solids (49.5 mmol, 50% yield) that were used without further purification. ^{1}H NMR (300 MHz, DMSO-d$_6$): 8.98, 8.05, 1.60. ^{13}C NMR (75MHz, DMSO-d$_6$): 132.2, 120.5, 59.6, 29.1. Analysis calculated for $C_{11}H_{21}BF_4N_2$: C, 49.28; H, 7.90; N, 10.45 (C/N=4.72). Found: C, 48.87; H, 8.18; N, 10.34 (C/N=4.73).

1,3-diisobutylimidazolium bromide (**5**): Isobutylamine (7.32g, 100 mmol, Alfa-Aesar, 99%) in 100mL toluene (EMD, ACS Reagent) was placed in a room temperature water bath then paraformaldehyde (3.16g, 100 mmol, Fisher, 95%) was added with strong stirring. The solution was stirred at room temperature for 30 minutes then ice was added to the water bath. Hydrobromic acid solution (16.87g, 100 mmol, Sigma-Aldrich, 48 wt%) was diluted to 20 wt% with 23.66g water then placed on ice for approximately one hour. After cooling the toluene solution for one hour another 7.32g (100 mmol) isobutylamine

was added dropwise via addition funnel. The cold hydrobromic acid solution was added dropwise via addition funnel. The ice bath was removed and the solution warmed for approximately two hours then glyoxal solution (14.52g, 100 mmol, Alfa-Aesar, 40 wt% in water) was added dropwise. The reaction was stirred at room temperature for approximately 36 hours. The solution was concentrated by rotary evaporation to give a viscous yellow/orange oil. Purification was achieved by adding 125 mL water and 20mL saturated $KHCO_3$ and extracting with diethyl ether (2x100 mL). The aqueous phase was treated with 1.55g activated carbon (Sigma-Aldrich) and stirred overnight at room temperature. The carbon was filtered off and washed with a small amount of water. This process was repeated three times until the filtrate was colorless to the eye. The filtrate was concentrated by rotary evaporation and the residue extracted with chloroform (2x100 mL) then filtered. The chloroform extracts were combined, dried over $MgSO_4$, filtered and stripped down by rotary evaporation to give a waxy residue. Further drying under high vacuum yielded 20.57g off-white solids (78.7 mmol, 79% yield). ^{1}H NMR (300 MHz, DMSO-d_6): 9.41, 7.88, 4.06, 2.11, 0.85. ^{13}C NMR (75MHz, DMSO-d_6): 136.4, 122.8, 55.4, 28.7, 19.0. Analysis calculated for $C_{11}H_{21}BrN_2$: C, 50.58; H, 8.10; N, 10.72 (C/N=4.72). Found: C, 50.27; H, 8.23; N, 10.61 (C/N=4.74).

1,3-bis(pentan-3-yl)imidazolium bromide (**6**): Using 3-aminopentane (2x70 mmol, Alfa-Aesar, 98%) the procedure described for **5** was followed yielding 14.82g white solids (51.2 mmol, 73% yield). ^{1}H NMR (300 MHz, DMSO-d_6): 9.75, 8.10, 4.24, 1.84, 0.70. ^{13}C NMR (75MHz, DMSO-d_6): 135.2, 121.3, 64.0, 27.2, 9.9. Analysis calculated for $C_{13}H_{25}BrN_2$: C, 53.98; H, 8.71; N, 9.68 (C/N=5.58). Found: C, 53.69; H, 8.57; N, 9.51 (C/N=5.64).

1,3-bis(cyclopentyl)imidazolium tetrafluoroborate (**7**): Using cyclopentylamine (2x147 mmol, Alfa-Aesar, 99%) the procedure for **4** was followed. Unlike **4**, no solid precipitate was visible so layers were separated after adding 150 mL diethyl ether and 75 mL saturated $NaHCO_3$ solution. The top ether/toluene layer was discarded and the aqueous layer plus oily residue were extracted with chloroform (3x100 mL). Combined $CHCl_3$ extracts and washed with brine (100 mL), dried over $MgSO_4$, filtered and stripped down by rotary evaporation to obtain a dark, waxy residue. Further drying under high vacuum did not change the waxy residue. The residue was finely ground using a mortar and pestle then extracted with diethyl ether using a Soxhlet apparatus. The extracted solids were recrystallized from 4:1 tetrahydrofuran/ethyl acetate to give 16.09g light tan solids. Further purification using activated carbon treatment as described for **5** (added 80 mL water plus 30 mL ethanol to dissolve) yielded 15.33g light yellow solids (52.5 mmol, 36% yield). ^{1}H NMR (300 MHz, DMSO-d_6): 9.36, 7.90, 4.74, 2.23-2.16, 1.91–1.78, 1.75–1.63. ^{13}C NMR (75MHz, DMSO-d_6): 134.6, 121.4, 60.6, 32.6, 23.2. Analysis calculated for $C_{13}H_{21}BF_4N_2$: C, 53.45; H, 7.25; N, 9.59 (C/N=5.57). Found: C, 55.54; H, 7.82; N, 10.00 (C/N=5.55).

1,3-bis(cyclohexyl)imidazolium tetrafluoroborate (**8**): Using cyclohexylamine (2x200 mmol, Alfa-Aesar, 98+%) the procedure for **4** was followed. The solid precipitate was filtered off and washed with 150 mL water then 150 mL diethyl ether and dried overnight under high vacuum. Recrystallization from 2:1 ethyl acetate/dichloromethane yielded 33.72g off-white solids after drying under high vacuum (105.3 mmol, 53% yield). ^{1}H NMR (300 MHz, DMSO-d_6): 9.19, 7.88, 4.24, 2.07–2.03, 1.84–1.62, 1.43–1.30, 1.24–1.15. ^{13}C NMR (75MHz, DMSO-d_6): 133.5, 120.8, 58.8, 32.4, 24.6, 24.4. Analysis

calculated for $C_{15}H_{25}BF_4N_2$: C, 56.27; H, 7.87; N, 8.75 (C/N=6.43). Found: C, 56.56; H, 7.67; N, 8.68 (C/N=6.52).

1,3-bis(cycloheptyl)imidazolium bromide (**9**): Using cycloheptylamine (2x110.4 mmol, Alfa-Aesar, 97%) the procedure for **5** was followed yielding 23.60g white solids after drying under high vacuum (69.1 mmol, 63% yield). ^{1}H NMR (300 MHz, DMSO-d$_6$): 9.44, 7.93, 4.50, 2.08–1.97, 1.95–1.97, 1.77–1.69, 1.65–1.56, 1.54–1.46. ^{13}C NMR (75MHz, DMSO-d$_6$): 133.5, 120.8, 61.1, 34.7, 26.8, 23.3. Analysis calculated for $C_{17}H_{29}BrN_2$: C, 59.82; H, 8.56; N, 8.21 (C/N=7.29). Found: C, 59.45; H, 8.33; N, 8.08 (C/N=7.36).

1,3-bis(bicyclo[2.2.1]heptan-2-yl)imidazolium bromide (**10**) (1,3-bis(norbornyl) imidazolium bromide): Using exo-2-aminonorbornane (2x19.1 mmol, Sigma-Aldrich, 99%) the procedure for **5** was followed yielding 3.69g off-white waxy solids (10.9 mmol, 57% yield). ^{1}H NMR (300 MHz, DMSO-d$_6$): 9.39, 7.91, 4.38, 2.55, 2.39, 1.94–1.91, 1.62–1.50, 1.32–1.21. ^{13}C NMR (75MHz, DMSO-d$_6$): 134.1, 121.5, 62.4, 42.70, 42.68, 37.82, 37.79, 35.71, 35.11, 27.49, 26.31. Analysis calculated for $C_{17}H_{25}BrN_2$: C, 60.53; H, 7.47; N, 8.31 (C/N=7.28). Found: C, 60.23; H, 7.22; N, 8.20 (C/N=7.35).

1,3-bis(cyclohexylmethyl)imidazolium bromide (**11**): Using cyclohexanemethylamine (2x110.4 mmol, Alfa-Aesar, 98%) the procedure for **5** was followed yielding 26.57g off-white waxy solids (77.8 mmol, 70% yield). When performing the activated carbon treatment 250 mL water plus 50 mL methanol was used to dissolve the residue. ^{1}H NMR (300 MHz, DMSO-d$_6$): 9.29, 7.82, 4.06, 1.79, 1.69–1.66, 1.52–1.48, 1.20–1.13, 0.99–0.91. ^{13}C NMR (75MHz, DMSO-d$_6$): 136.4, 122.8, 54.3, 37.5,

29.3, 25.6, 24.9. Analysis calculated for $C_{17}H_{29}BrN_2$: C, 59.82; H, 8.56; N, 8.21 (C/N=7.29). Found: C, 59.43; H, 8.35; N, 8.07 (C/N=7.37).

1,3-bis(2,4,4-trimethylpentan-2-yl)imidazolium tetrafluoroborate (**12**) (1,3-bis(isooctyl)imidazolium tetrafluoroborate): Using 2-amino-2,4,4-trimethylpentane (2x120 mmol, TCI America, 95%) the procedure for **7** was followed omitting Soxhlet extraction. Recrystallization from dichloromethane/tetrahydrofuran yielded 11.76g off-white solids (30.9 mmol, 26% yield). ^{1}H NMR (300 MHz, DMSO-d$_6$): 9.19, 8.13, 1.95, 1.66, 0.79. ^{13}C NMR (75MHz, DMSO-d$_6$): 133.5, 120.9, 62.8, 52.7, 31.3, 30.3, 29.3. Analysis calculated for $C_{19}H_{37}BF_4N_2$: C, 60.00; H, 9.81; N, 7.37 (C/N=8.14). Found: C, 61.38; H, 9.94; N, 7.50 (C/N=8.18).

1,3-bis(cyclooctyl)imidazolium bromide (**13**): Using cyclooctylamine (2x98.3 mmol, Alfa-Aesar, 97+%) the procedure for **5** was followed yielding 20.315g off-white solids (55.0 mmol, 56% yield). Similar to **11**, methanol was added during the activated carbon treatment to dissolve the residue. ^{1}H NMR (300 MHz, DMSO-d$_6$): 9.50, 7.91, 4.56, 2.01–1.87, 1.67–1.55. ^{13}C NMR (75MHz, DMSO-d$_6$): 133.8, 120.9, 60.2, 32.3, 26.1, 24.9, 23.2. Analysis calculated for $C_{19}H_{33}BrN_2$: C, 61.78; H, 9.00; N, 7.58 (C/N=8.15). Found: C, 63.93; H, 9.79; N, 7.99 (C/N=8.00).

1,3-bis(1-adamantyl)imidazolium bromide (**15**): An aqueous solution of 1-adamantylamine hydrochloride (Alfa-Aesar, 99%) was treated with potassium hydroxide and extracted with toluene, dried over Na_2SO_4, filtered and stripped down by rotary evaporation to give 30.3g 1-adamantylamine (200 mmol). The procedure for **5** was followed except the reaction was heated at 45°C overnight yielding 26.23g white solids (62.8 mmol, 63% yield). When performing the activated carbon treatment 2:1

water/absolute ethanol was used to dissolve the residue. ^{1}H NMR (300 MHz, CD$_3$OD): 9.02, 7.94, 2.27, 1.91, 1.85. ^{13}C NMR (75MHz, CD$_3$OD): 132.2, 120.6, 61.4, 43.4, 36.4, 31.0. Analysis calculated for C$_{23}$H$_{33}$BrN$_2$: C, 66.18; H, 7.97; N, 6.71 (C/N=9.86). Found: C, 62.37; H, 8.26; N, 6.44 (C/N=9.68).

2.2.2: Inorganic Reactions

All reactions were performed in 23 mL or 45 mL PTFE-lined stainless steel autoclaves (Parr Instruments). Hydroxide mediated reactions were tumbled at approximately 40 rpm using spits built into convection ovens. Fluoride mediated reactions were not tumbled. Silica sources were tetraethylorthosilicate (TEOS, Sigma-Aldrich, 98%) for fluoride reactions and Cab-O-Sil M5 fumed silica (Cabot) for hydroxide reactions. Boric acid (J.T. Baker, ACS Reagent) was used for borosilicate reactions and Reheis F-2000 (50–53 wt% Al$_2$O$_3$) or Na-Y zeolite (Tosoh HSZ-320NAA) were used in aluminosilicate reactions. Germanosilicate reactions used germanium dioxide (99.98%, Alfa-Aesar) and TEOS.

Gels for fluoride reactions were prepared by adding boric acid or aluminum hydroxide gel (if required) to the SDA$^+$OH$^-$ solution then adding TEOS. The vessel was covered and stirred overnight to ensure complete TEOS hydrolysis then left uncovered in a 40°C oven to evaporate the required water and ethanol. Once the desired mass had been reached 48 wt% hydrofluoric acid (Mallinckrodt) was added with care and the gel stirred to form a stiff paste. The autoclave was sealed and placed in a 150°C (or 175°C) oven and opened every 7–10 days to assess reaction progress. After homogenizing, a small sample

was dispersed in 10 mL water and inspected under an optical microscope. For certain reactions at $H_2O/SiO_2=7.5$ and 14.5 small crystals were often visible. If no clear sign of crystallinity could be seen by optical microscope a small sample was filtered periodically and the XRD pattern inspected. All reactions were monitored to at least 60 days with the product labeled amorphous if no crystalline material was observed.

Gels for hydroxide reactions were prepared by adding water, 1N sodium hydroxide solution (if required), boron or aluminum source then silica and homogenizing by hand. Borosilicate reactions were run at $SiO_2/B_2O_3=8$ with no alkali hydroxide (gel composition 1.0 SiO_2:0.125 B_2O_3:0.25 SDA^+OH^-:23 H_2O); and the remaining reactions added sodium hydroxide with slightly increased water content (gel composition 1.0 SiO_2:x B_2O_3:0.20 SDA^+OH^-:0.10 NaOH:30.0 H_2O where $0.00 \leq x \leq 0.02$). Aluminosilicate reactions with NaY at SAR=35 had gel composition 1.0 SiO_2:0.029 Al_2O_3:0.20 SDA^+OH^-:y NaOH:30.0 H_2O where y=0.25 or 0.05 (except where NaOH content was varied in a separate series). The remaining reactions used unstructured Reheis F-2000 aluminum hydroxide gel as aluminum source with gel composition 1.0 SiO_2:z Al_2O_3:0.20 SDA^+OH^-:0.10 NaOH:30.0 H_2O with z=0.02 or 0.01. Finally, several germanosilicate reactions were performed with gel composition 1.0 SiO_2:0.11 GeO_2:0.5 SDA^+OH^-:3.5 H_2O at 170°C[23] (not tumbled).

Reactions at 150°C were monitored every four to six days by measuring solution pH and looking for signs of phase separation (checked every two days for 170°C reactions). The reactions were checked until a pH maximum was observed then filtered. If no pH maximum was observed the reaction was continued until a sustained pH decline was observed (indicating SDA degradation). Several reactions at $SiO_2/B_2O_3=8$ formed a stiff paste that was not amenable to pH measurement. These reactions were stopped after 45

days heating and filtered as for other reactions. All crude products were washed with water plus a small amount of acetone and methanol then dried at room temperature. N,N-dimethylformamide (DMF) extractions were performed on as-made materials using ~0.4g zeolite : 10mL DMF. Solutions were sealed inside PTFE autoclaves and heated at 150°C for 24 hours. The extracted product was filtered and washed extensively with water then dried at room temperature.

2.2.3: Product Characterization

Powder X-ray diffraction (XRD) patterns were collected on a Scintag XDS-2000 diffractometer using CuKα radiation or Siemens D-500 diffractometer. Thermogravimetric analysis (TGA) was performed with a Netzsch STA449C using 75 mL min^{-1} air plus 25 mL min^{-1} Argon at a heating rate of 5°C min^{-1}. Nitrogen adsorption/desorption isotherms were collected on a Micromeritics ASAP 2000 instrument at 77K. Micropore volumes were calculated using the t-plot method. Solid-state NMR spectra were collected using either Bruker Avance 200 MHz or Bruker DSX 500 MHz instruments. ^{29}Si Bloch Decay (BD) experiments on as made materials used 500s recycle delay. Scanning electron microscopy (SEM) was performed using a JEOL JSM-6700F instrument. Elemental analyses were performed by Galbraith Laboratories (Knoxville, TN).

2.2.4: Catalytic Testing

Catalytic activity of aluminum containing SSZ-70 (Al-SSZ-70) materials was evaluated through the Constraint Index test (CI test)[24]. Al-SSZ-70 synthesized using NaY as aluminum source was treated with 1N HCl at 95°C for 48 hours to neutralize any residual material that may affect catalytic activity[25]. SSZ-25 was synthesized as previously described[26]. All materials were calcined to 540°C at a heating rate of 1°C min^{-1} under flowing nitrogen with a small amount of air. Calcined materials were ion-exchanged with 1N NH$_4$NO$_3$ at 50°C then filtered and washed with distilled de-ionized water. The ammonium-exchanged materials were pelletized, crushed and sieved with the 20–40 mesh fraction collected. Sized material (typically 0.5 g) was loaded into a stainless steel reactor tube supported by glass wool and activated by heating under flowing Argon at 350°C for at least four hours. Reactions were performed at 350°C unless otherwise noted. Hydrocarbon cracking was performed by introducing an equimolar n-hexane/3-methylpentane mixture (both from Sigma-Aldrich, ≥99.9%) via syringe pump into a mixing assembly with 5% Ar in He sweep gas (Airliquide, 99.999%) (LHSV=1.67 hr^{-1}). Products were analyzed using online GC/MS (Agilent GC 6890/MSD 5973N) with a Plot-Q capillary column.

2.3: Results and Discussion

2.3.1: Results Overview

The phases obtained from the initial inorganic reaction screen at 150°C are presented in Tables 2.1–2.4. Pure silica fluoride results in Table 2.1 show a cluster of SSZ-70 with **5** and **7-10**. This was surprising as fluoride mediated reactions typically produce products with very few silanol defects yet here we have a layered material with a high density of Q_3 silicon atoms (verified by ^{29}Si MAS and ^{29}Si CP-MAS NMR). Beta and ZSM-12 (MTW) appear frequently, with beta particularly common at $H_2O/SiO_2=3.5$. Both of these observations are consistent with recent reports under similar inorganic conditions[2, 5]. Interestingly, no entry shows SSZ-70 across all dilutions. The entry for bis(cyclopentyl) SDA **7** at $H_2O/SiO_2=14.5$ displayed a transition from layered SSZ-70 plus EU-1 (EUO) at 52 days to EUO plus minor SSZ-70 upon further heating to 72 days. The intermediate dilution reaction was also heated to 72 days with only SSZ-70 present.

In addition to **1–3; 6, 13** and **15** produce the same product at all dilutions. These results extend the rare behavior of imidazolium SDAs in this chemistry where the organic influences nucleation selectivity to a greater extent than the fluoride anion. Previous reports with **3** and 1,2,3-trimethylimidazolium SDA showed product formation rates were influenced by dilution when the same product formed at all dilutions[5]. Similar trends were observed using **6**, **13** and **15** in the present study. Product formation tended to be slower than reported for the smaller imidazolium SDAs. For example, CFI and Beta, respectively, were observed after > 40 days heating at $H_2O/SiO_2=3.5$ using **15** and $H_2O/SiO_2=14.5$ using

13. In the low water to silica reactions fluoride is often found stabilizing double four ring (D4R) silicate units: none of the products obtained at $H_2O/SiO_2=3.5$ with known structures contain D4Rs (TON, MTT, BEA, MTW and CFI). The smaller 1,2,3- and 1,3,4-trimethylimidazolium SDAs make ITQ-12 (ITW) in the presence of fluoride or germanium[5, 27]. ITW contains linked D4R units forming cavities with 8MR openings. Larger imidazolium SDAs would not fit in the ITW cage thereby removing this as a potential host. In the case of fluoride stabilizing D4R units the compensating charge from the SDA must be located relatively close. For imidazolium SDAs the charge is located at the center with symmetrical groups on either side in the present study. This feature adds a periodicity restriction to D4R spacing and may explain why no Beta Polymorph C (BEC) was observed as a minor component (ITQ-10 or ITQ-14 type materials)[28].

Table 2.1: Phases obtained from pure silica fluoride reactions at 150°C

	H$_2$O/SiO$_2$		
SDA	3.5	7.5	14.5
1	ZSM-22	ZSM-22	ZSM-22
2	ZSM-22	ZSM-22	ZSM-22
3	ZSM-23	ZSM-23	ZSM-23
4	Beta	Beta	Amorphous
5	SSZ-70	SSZ-70	ZSM-12
6	ZSM-12	ZSM-12	ZSM-12
7	Beta	SSZ-70	SSZ-70→EU-1[a]
8	Beta	SSZ-70	SSZ-70
9	Beta	SSZ-70	SSZ-70
10	NR[b]	SSZ-70	NR
11	Beta	Beta	ZSM-12
12	Amorphous	Amorphous	Amorphous
13	Beta	Beta	Beta
14	Amorphous	Amorphous	Amorphous
15	CIT-5	CIT-5	CIT-5
16	Amorphous	NR	NR

[a] Initial product SSZ-70 plus EU-1 that transformed with extended heating to EU-1 plus SSZ-70

[b] NR indicates synthesis not run

Three molecules did not make any product in the pure silica reactions. These were bis(isooctyl) SDA **12**, bis(mesityl) SDA **14** and bis(diisopropylphenyl) SDA **16**. Gels using **14** and **16** became yellow while evaporating water and ethanol. No other gels showed similar behavior. Reported pK$_a$ values for 1,3-disubstituted imidazoliums in dimethylsulfoxide (DMSO) indicate phenyl substitution lowers C(2) proton pK$_a$ by approximately 2 units compared to alkyl and benzyl substitution[29]. In addition, kinetic H/D

exchange measurements in methanol gave significantly faster rates with mesityl and 2,6-diisopropylphenyl substitution[30]. These data suggest phenyl substituted imidazoliums may be unstable due to enhanced attack at the acidic C(2) position. In comparison, **12** should possess similar C(2) proton acidity to the remaining 13 SDAs and therefore the inability to nucleate a crystalline phase was due to other factors. With no success in pure silica fluoride reactions these three SDAs were omitted from the borosilicate fluoride and hydroxide reactions to preserve the relatively limited supply. Further experiments in aluminosilicate hydroxide reactions will be discussed below.

The results for borosilicate reactions presented in Tables 2.2 and 2.3 show SSZ-70 as a very common product. The only SSZ-70 absences occur for **1**, **2**, **4**, **13** & **15**. SDA **4** does not crystallize any products except under concentrated fluoride conditions. SDA **6** shows strong specificity to MTW products with only one instance of SSZ-70 under high boron substitution with fluoride. In the absence of fluoride no crystalline product was obtained at the boron-rich condition studied. Bis(cyclooctyl) SDA **13** did not give any SSZ-70 products, with Beta the only zeolite product. This sharp delineation between the bis(C7) substituted SDAs **9-11** and bis(C8) substituted **13** could indicate SSZ-70 contains a feature that cannot accommodate the larger cyclooctyl group. MWW contains a sinusoidal 10MR within the layers and this apparent size exclusion suggests a similar feature may be present in SSZ-70. However, caution must be exercised as kinetic rather than thermodynamic factors largely determine what product evolves. Layered phases other than SSZ-70 were observed in borosilicate hydroxide reactions. Kanemite was found in several reactions with characteristic XRD reflections at 20–23 (broad) and 36°2θ. In addition, an unidentified layered phase was observed with **15** with quite sharp XRD reflections less than

6°2θ and weaker reflections at higher diffraction angles. These reflections did not persist after calcination. Approximately 30 wt% mass loss >200°C was measured by TGA leading to the conclusion of a layered phase.

Table 2.2: Phases obtained from borosilicate fluoride reactions at 150°C

	SiO_2/B_2O_3	
SDA	36	11
1	NR	ZSM-22
2	NR	ZSM-5
3	Amorphous + SSZ-70	Amorphous
4	Amorphous	Amorphous
5	SSZ-70	SSZ-70
6	ZSM-12	SSZ-70[a]
7	SSZ-70	SSZ-70
8	SSZ-70	SSZ-70
9	SSZ-70	SSZ-70
10	NR	SSZ-70
11	SSZ-70	SSZ-70
13	Amorphous	Beta
15	CIT-5	Amorphous

[a] Low angle reflections shifted compared to typical SSZ-70 product.

In contrast to the fluoride reactions with bis(adamantyl) SDA **15**, no zeolite phases were obtained in borosilicate hydroxide reactions. The original CIT-5 synthesis used LiOH to suppress SSZ-24 formation[31], therefore, two further experiments were performed under pure silica and SiO_2/B_2O_3=100 conditions with NaOH replaced by LiOH. The reactions

were run statically at 165°C and CFI was obtained from both conditions (some layered material was present in the pure silica product). Boron rich fluoride and hydroxide reactions with **2** gave ZSM-5 (MFI). This SDA shows strong structure direction to TON materials under pure silica and aluminosilicate hydroxide conditions. Introducing sufficient boron to the gel induced a transition to three-dimensional MFI. Similarly, borosilicate reactions with **3** gave MTW at intermediate boron incorporation contrasting with SSZ-70 and MTT under boron rich and pure silica conditions, respectively.

Table 2.3: Phases obtained from borosilicate hydroxide reactions at 150°C

SDA	SiO$_2$/B$_2$O$_3$			
	8	**50**	**100**	∞
1	Amorphous	NR	NR	ZSM-22[3]
2	ZSM-5	NR	NR	ZSM-22[3]
3	SSZ-70[a]	ZSM-12	ZSM-12	ZSM-23[3]
4	Amorphous	Kanemite	Kanemite	Kanemite
5	SSZ-70	SSZ-70	SSZ-70	ZSM-12+SSZ-70
6	Amorphous	ZSM-12	ZSM-12	ZSM-12
7	SSZ-70	SSZ-70	SSZ-70	SSZ-70
8	SSZ-70	SSZ-70	SSZ-70	SSZ-70
9	SSZ-70	SSZ-70	SSZ-70	SSZ-70
10	NR	SSZ-70	NR	SSZ-70
11	SSZ-70 + Beta	SSZ-70	ZSM-12	ZSM-12
13	Beta	Beta	Beta	Quartz+Kanemite
15	Amorphous[b]	Layered[c]	Kanemite[d]	Layered[c,d]

[a] Reaction at 170°C

[b] SiO$_2$/B$_2$O$_3$=12

[b] Sharp XRD reflections <6°2θ that do not persist on calcination

[c] CFI obtained using LiOH instead of NaOH

The phases obtained from aluminosilicate reactions also reveal several SSZ-70 instances, again SDAs **5** & **7–10** show at least one occurrence for each reaction. Beta appears frequently throughout, with few instances of MTW. The first reaction with NaY as

aluminum source (y=0.25) shows Mordenite (MOR) appearing in all but one reaction. In an attempt to avoid MOR formation the lower NaOH condition was tried (y=0.05). Several interesting products were obtained with SSZ-70 observed using **7–10** and SSZ-16 (AFX) with the large bis(adamantyl) SDA **15**. Most reactions did not fully convert the NaY reagent with minor reflections visible by XRD. In comparison, the reactions using unstructured Reheis F-2000 show only three instance of SSZ-70. These data reinforce the subtle changes in nucleation selectivity brought about by inorganic reagent selection. An additional experiment using Reheis F-2000 at SAR=35 and $NaOH/SiO_2$=0.05 using **8** gave Beta.

Table 2.4: Phases obtained from aluminosilicate hydroxide syntheses at 150°C

SDA	SiO$_2$/Al$_2$O$_3$			
	35 (y=0.25)	35 (y=0.05)	50	100
3	ZSM-23	ZSM-23	ZSM-23	ZSM-23
4	MOR	Amorphous (NaY)	Amorphous	Amorphous
5	Beta (MOR)	ZSM-12 (NaY)	SSZ-70	SSZ-70
6	ZSM-12 (MOR)	ZSM-12 (NaY)	Amorphous	ZSM-12+amorphous
7	Beta	SSZ-70 + Beta	Beta	Beta+SSZ-70
8	Beta (MOR)	SSZ-70 (NaY/MOR)	Beta	Beta
9	Beta (MOR)	SSZ-70	Beta	Beta
10	NR[a]	SSZ-70 + Beta	NR	Beta
11	Beta+MOR (NaY)	ZSM-12 (NaY)	Beta	Beta
12	Magadiite (NaY)	Amorphous (NaY)[c]	NR	Amorphous
13	Beta (MOR)	Beta (NaY)	Beta	Beta
14	NR	Amorphous[c]	NR	NR
15	MOR	SSZ-16 (NaY)	Amorphous	SSZ-35
16	NR	Amorphous[c]	NR	NR

[a] Phases in parentheses indicate minor impurity.

[b] NR indicates reaction was not run.

[c] NaOH/SiO$_2$=0.10.

To investigate the possibility of SSZ kinetic metastability the reaction screen was repeated for several conditions using SDAs **5**, **8** and **9**. Pure silica fluoride reactions were

repeated at 175°C and hydroxide reactions at 170°C. Pure silica fluoride and hydroxide results are presented in Tables 2.5 and 2.6 respectively. Higher temperature narrowed the SSZ-70 window for **5** and **8** with MTW and EUO observed at $H_2O/SiO_2=7.5$ and 14.5 respectively. In addition, Beta and SSZ-70 were observed in the concentrated reaction using **5**. The borosilicate hydroxide reactions with **5** gave MTW in all cases in contrast to the 150°C results where SSZ-70 was observed with boron substitution. These data indicate additional thermal energy was sufficient in several cases to produce a fully four-connected host product.

Table 2.5: Phases obtained from pure silica fluoride syntheses at 175°C

SDA	H_2O/SiO_2		
	3.5	7.5	14.5
5	Beta + SSZ-70	ZSM-12	ZSM-12
8	Beta	SSZ-70	EU-1 (SSZ-70)[a]
9	Beta	SSZ-70	SSZ-70

[a] Phases in parentheses indicate minor impurity.

Table 2.6: Phases obtained from hydroxide syntheses at 170°C

SDA	SiO_2/B_2O_3			SiO_2/Al_2O_3	
	50	100	∞	35 (y=0.05)	50
5	ZSM-12	ZSM-12	ZSM-12	SSZ-70+ZSM-12	SSZ-70+amorphous
8	SSZ-70	SSZ-70	SSZ-70	Beta + SSZ-70	Beta
9	SSZ-70	SSZ-70	SSZ-70	SSZ-70	Beta

Finally, the above results indicated bis(isobutyl) SDA **5** to be the most selective to SSZ-70. A small number of aluminosilicate fluoride reactions were performed with H_2O/SiO_2=15.5 and SAR=30-70 at 150°C. SSZ-70 was obtained at SAR=30, 50 & 70 (minor impurity in SAR=70 product). Similar reactions using bis(cyclohexyl) SDA **8** at SAR=40 gave Beta, in accordance with the hydroxide reactions at SAR=50 and 100.

Several interesting trends were observed in the approximately 160 reactions detailed above. Producing the normally aluminum rich AFX with a large, hydrophobic SDA was surprising. Energy minimization calculations indicate the SDA nicely occupies the large AFT cage (not shown). As noted in the original SSZ-16 report, no organic is expected to occupy the smaller Gmelinite cage[32]. Another intriguing result was obtaining SSZ-35 (STF) with **15** in the SAR=100 reaction. STF contains 18 MR cages connected through 10MR windows suggesting the imidazolium sitting in the 10 MR with adamantyl groups occupying the larger cavities. This supports the observation of STF using a diquaternary tropane SDA in a recent study[23]. Furthermore, the tropane-C_4-tropane SDA was one of the original molecules reported to synthesize SSZ-16 so it appears these two molecules have certain similarities that enable structure direction to the same products. An important aspect was whether the **15** was intact within each host framework. If the SDA degraded to a fragment containing a mono-adamantyl moiety this could be the actual organic species occluded. Mono-adamantyl N,N,N-trimethyl-1-adamantanammonium can synthesize a variety of high silica phases[25] although no syntheses of CFI, AFX or STF using this SDA have been reported. Solid-state ^{13}C CP-MAS NMR was performed and all three products gave similar resonances. The alkyl carbon resonances were easily detected whereas the imidazolium resonances were broad and weak. All spectra agree with the

SDA chloride salt as shown in Figure 2.2. These data indicate the SDA was occluded intact within each host phase.
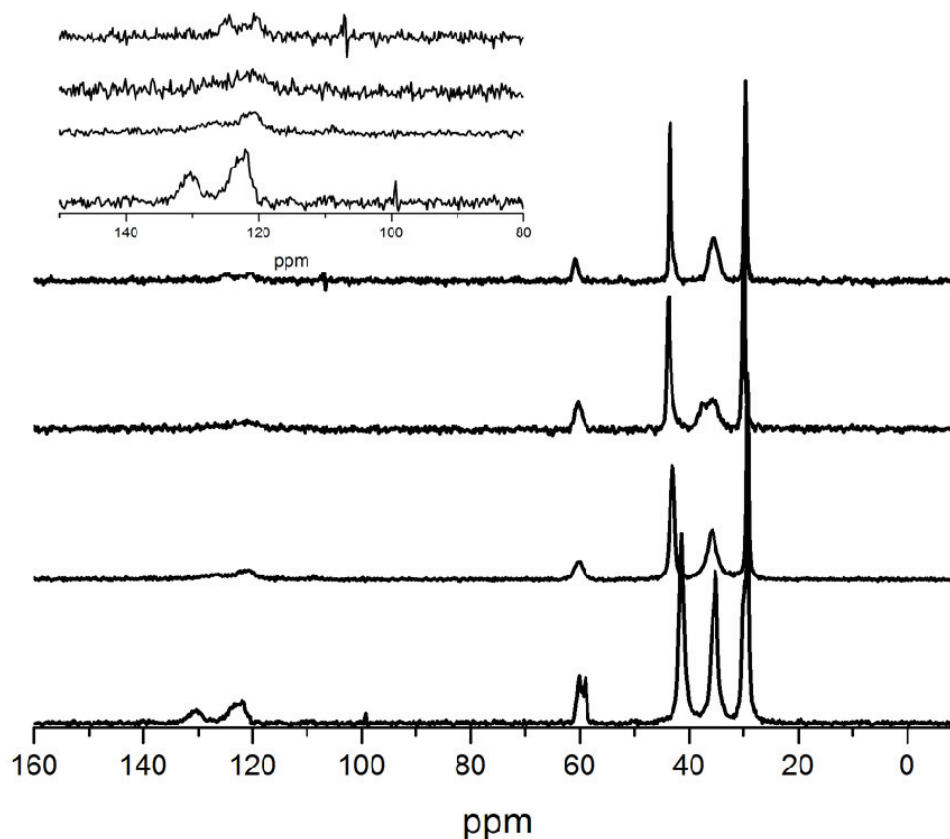
Figure 2.2: ^{13}C CP-MAS NMR of products obtained using 1,3-bis(1-adamantyl) imidazolium SDA **15**. Top to bottom=CIT-5, SSZ-35, SSZ-16 and SDA$^+$Cl$^-$. The inset enlarges the imidazolium region

Entries in Table 2.4 for **12**, **14** and **16** show no crystalline zeolite products in agreement with the previous pure silica fluoride results. Reactions with **14** and **16** rapidly discolored with viscous red oil appearing on the surface. Discoloration was attributed to degradation caused by the more acidic C(2) proton in these SDA and therefore no further reactions were performed. In addition, bis(*tert*-butyl) **4** only made MOR under sodium rich

NaY reaction conditions. MOR can be considered a default product given sufficient sodium and aluminum with nucleation and growth due to inorganic factors. Therefore, **4** should be included with **12** with both unable to direct the formation of any desirable phase. The inability of **4** to nucleate phases except under very narrow conditions of low water content was particularly puzzling. This SDA appeared an ideal candidate with intermediate hydrophobicity (Σ(C+N)=13) and similar periodicity to **3**. Additional NaY reactions and germanosilicate experiments were performed using **4**, **8**, **12** and **15** to gain further insight. The additional NaY reactions varied $NaOH/SiO_2$ to look for transitions to default products such as MOR. In addition, certain reactions looked at $NaOH/SiO_2$=0.10 and SDA^+OH^-/SiO_2=0.25. Here the total hydroxide content was higher and the SDA contributed a higher hydroxide ratio compared to silica. The results for these reactions are plotted in Figure 2.3 and show MOR appeared for all four SDAs. MOR was observed using **15** in the initial reaction screen so experiments at higher NaOH content were not performed. Layered Magadiite was observed with **12** for two reaction conditions with this eventually displaced by MOR at higher NaOH. Bis(cyclohexyl) SDA **8** shows four products with SSZ-70, Beta, MOR and NaP1 (GIS) forming from low to high NaOH content.
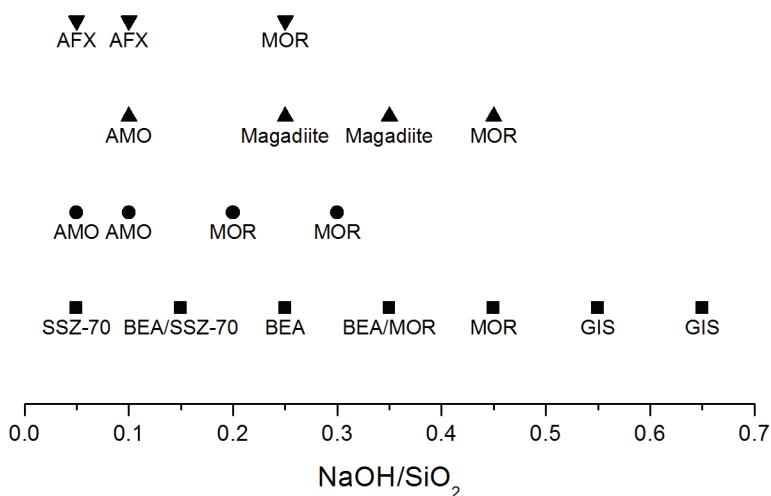
Figure 2.3: Phases obtained in NaY reactions as a function of NaOH/SiO$_2$ ratio for bis(cyclohexyl) SDA **8** (■), bis(*t*-butyl) SDA **4** (●), bis(isooctyl) SDA **12** (▲) and bis(adamantyl) SDA **15** (▼). AMO indicates amorphous and residual NaY is not shown

Germanosilicate reactions were investigated to see if D4R-rich structures could be produced. In this case a perturbation from the concentrated fluoride reaction results was anticipated. The results presented in Figure 2.4 show mostly amorphous material for **15** and **12** while **8** and **4** produced Beta, with ITQ-7 (ISV) visible for **4**. The gels for **12** and **15** formed solid masses that were difficult to probe. This was probably due to the low water content and hydrophobic SDAs. The smaller SDA **4** shows Beta plus ISV, with ISV containing D4R units, whereas regular Beta was observed with **8**. A possible explanation for these data is the smaller distance between adjacent charge centers in **4** compared to **8** as discussed earlier. Overall, the synthesis window for **4** was not enlarged and **12** did not succeed in nucleating a desirable crystalline phase. An insight to the relative inability of **4** and **12** to nucleate products was offered by crystallographic studies of NHC-Pd

complexes[33]. These studies examined the excluded or buried volume associated with each NHC ligand and found bis(adamantyl) and bis(*tert*-butyl) ligands the most sterically demanding (highest buried volume). The local environment of **4**, **12** and **15** adjacent to nitrogen is similar with quaternary carbons in all three suggesting **12** should display similar steric demands. The methyl groups projected into the imidazolium plane by **4** and **12** may inhibit interaction with hydrated silica species thereby giving few or no products. This was supported by concentrated conditions being required for **4** to nucleate a crystalline phase with organic and silica species presumably in intimate contact with minimal solvent (water) present.

The steric factors discussed above appear contrary to the results obtained with **15** where three crystalline phases were obtained. However, if steric demand at the charge center was solely responsible for structure direction, minimal differences should be observed between the cycloalkyl substituted **7**–**9** and **12**. While some overlap does occur there are clear differences suggesting space filling away from the charge center is equally important. In this context the bulky, rigid adamantyl groups of **15** are a distinguishing feature. The adamantyl group offers favorable silicate interactions demonstrated by the number of high silica phases synthesized with mono-adamantyl SDAs. Therefore, obtaining three phases with **15** may be largely due to silicate organization away from the charge center. Both STF and CFI feature undulation along the pore with this being particularly pronounced in STF. The corrugated pores may give favorable interactions with the boomerang-shaped **15**. Also, SSZ-16 was only obtained from the NaY reaction, no product was synthesized at SAR=50 using unstructured aluminum hydroxide gel. The

Faujasite reagent contains many six-rings and this might help specify AFX containing exclusively six-rings.
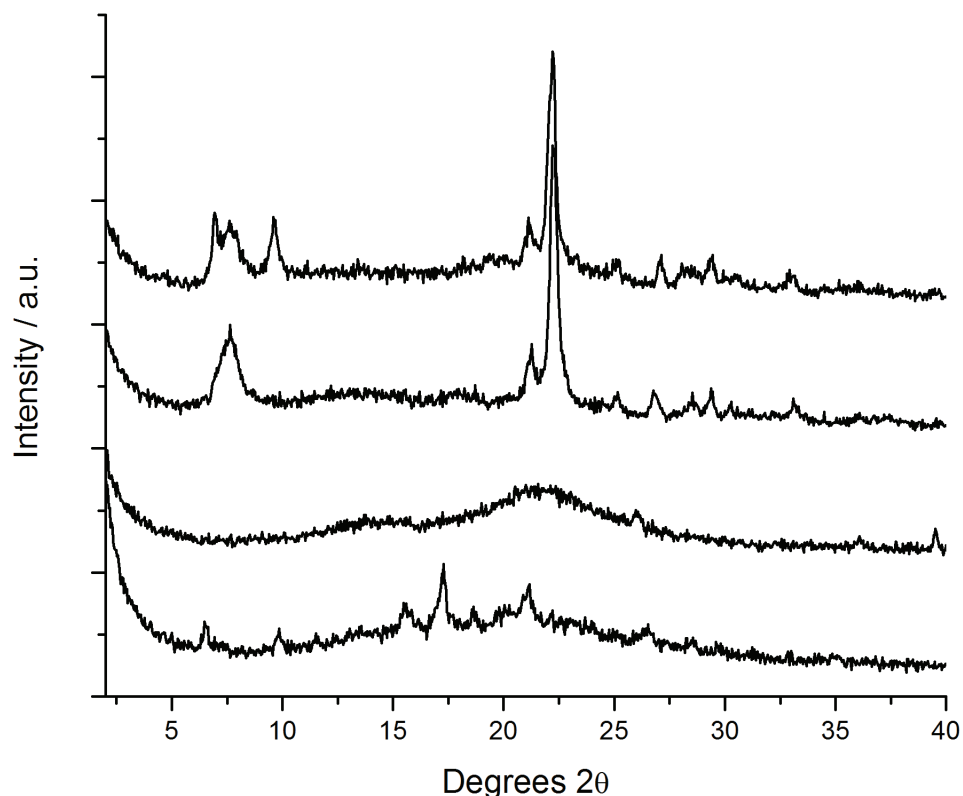
Figure 2.4: XRD patterns for germanosilicate reactions using **4**, **8**, **12** and **15**. Top to bottom=**4** (Beta+ISV), **8** (Beta), **12** (amorphous) and **15** (amorphous)

2.3.2: SSZ-70 Characterization

Powder XRD patterns are shown in Figures 2.5–2.7 for as-made and calcined SSZ-70. Preliminary inspection of the powder XRD pattern shows similarity to those of MWW precursor materials. Figure 2.5 shows XRD patterns for as-made Al-containing SSZ-70 synthesized in fluoride and hydroxide media using **5** (Al-SSZ-70(F) and Al-SSZ-70(OH)

respectively). Also included in Figure 2.5 is the XRD pattern of as-made SSZ-25 as a representative MWW material. Figure 2.6 enlarges the XRD patterns in the 2–12°2θ range. The as-made pattern shows one reflection with large d-spacing (~27Å) and several integer multiples are also present. The pattern for Al-SSZ-70(OH) is considerably broader than both SSZ-25 and Al-SSZ-70(F) with the low angle reflection appearing as a weak shoulder. Broad reflections in the hydroxide material were likely due to smaller crystal size. All three materials give quite sharp reflections at ~26.0°2θ indicating similar structural features may be present in both materials. Inspection of the low-angle features in Figure 2.6 reveals enlarged d-spacing compared to MWW materials, similar to ITQ-30. Comparing the hydroxide and fluoride patterns reveals the same d-spacing for all reflections except one broad reflection at ~8.7°2θ for the fluoride product whereas the hydroxide product gives two reflections at ~7.9 and 9.5°2θ. This diffraction intensity difference could be due to differences in crystal size as observed in DIFFaX simulations of MCM-22 and MCM-56[12]. Simulated diffraction patterns in this region were sensitive to the number of unit cells along the c-direction (orthogonal to layers) for 1–3 repeat units.
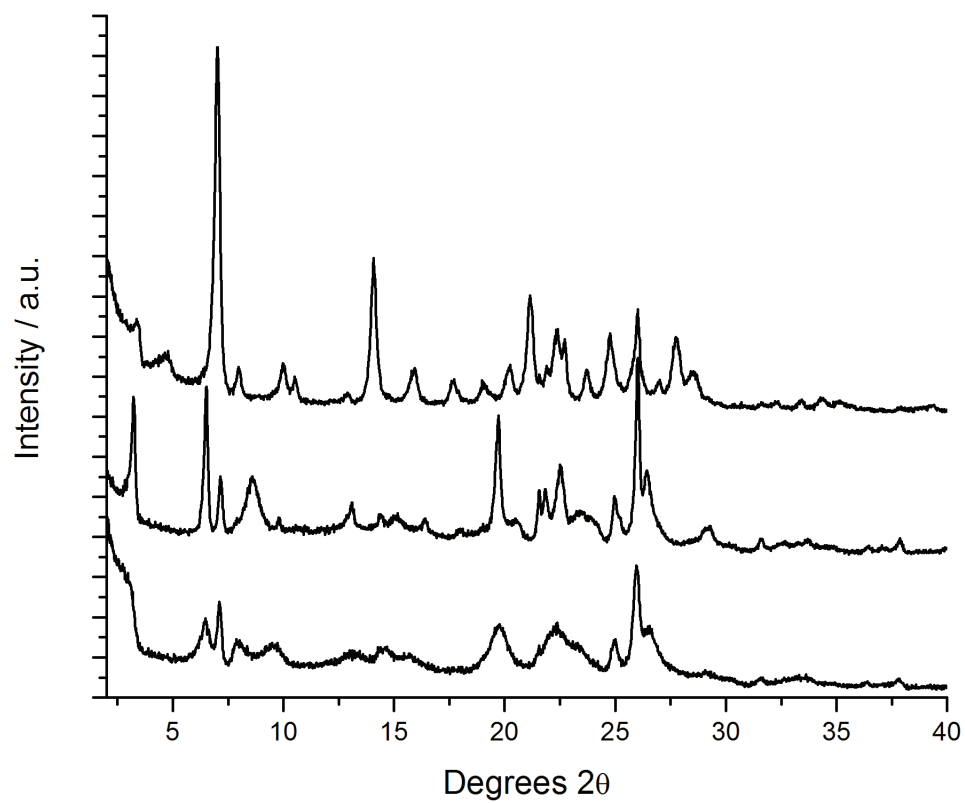
Figure 2.5: XRD patterns for top to bottom; SSZ-25, Al-SSZ-70 (F) and Al-SSZ-70 (OH)
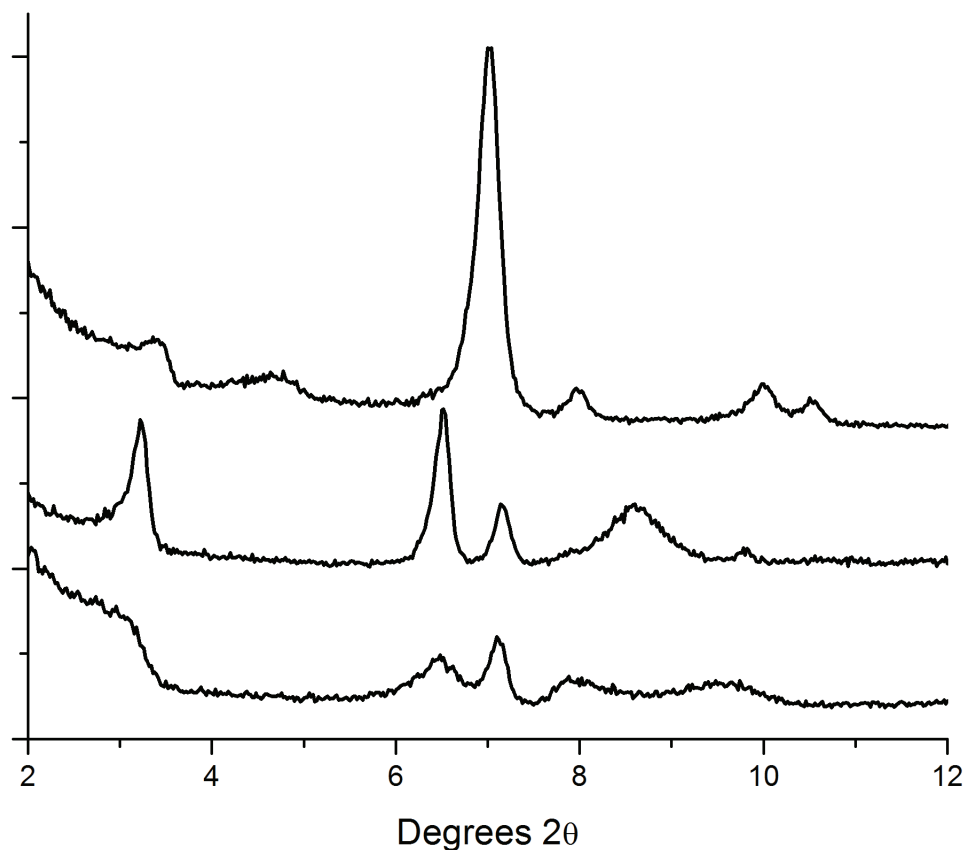
Figure 2.6: XRD patterns from 2–12°2θ for top to bottom; SSZ-25, Al-SSZ-70 (F) and

Al-SSZ-70 (OH)

Figure 2.7 shows XRD patterns for calcined SSZ-70 materials synthesized in fluoride media using **5**. Shown are pure silica (Si-SSZ-70(F)), borosilicate (B-SSZ-70(F)) and aluminosilicate (Al-SSZ-70(F)) materials. For both Si-SSZ-70(F) and Al-SSZ-70(F) the two low-angle reflections present in the as-made material are absent or appear with reduced intensity after calcination. The first significant reflection occurs at 7.0°2θ (~12.5Å) in both materials. In contrast, the low-angle reflections persist after calcination for B-SSZ-70(F) albeit with lower relative intensity. Both low-angle reflections were not observed after calcining B-SSZ-70(OH).
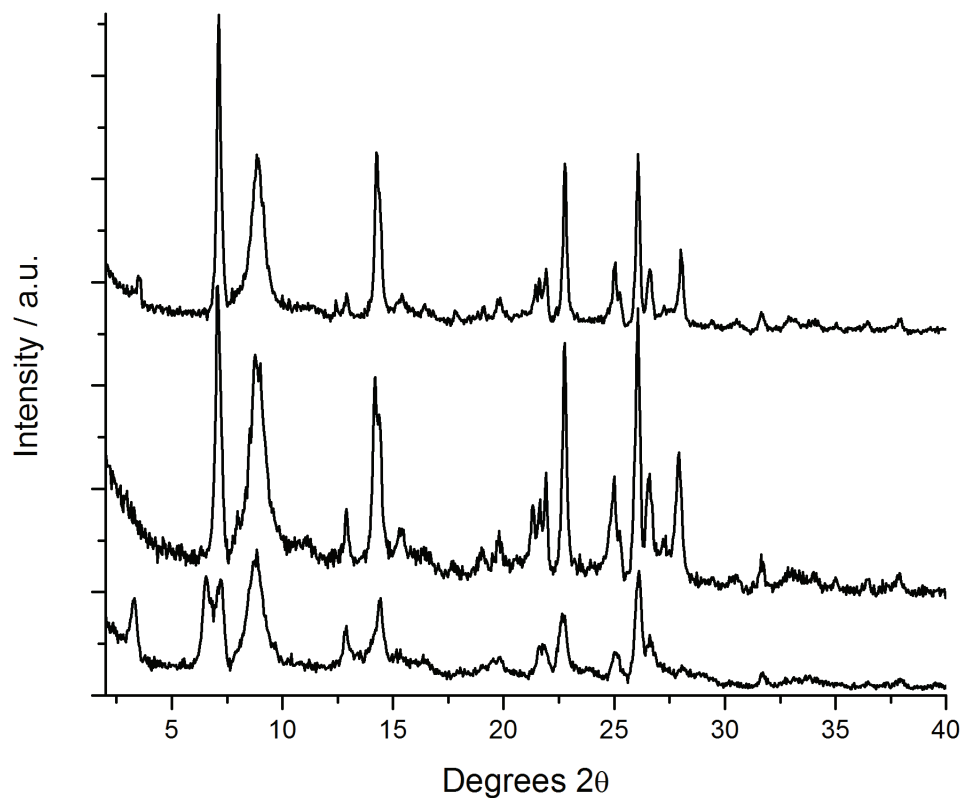
Figure 2.7: XRD patterns of calcined SSZ-70 products. Top to bottom; Si-SSZ-70(F),

Al-SSZ-70 (F) and B-SSZ-70 (F)

Solid-state ^{29}Si NMR was performed on Si-SSZ-70 from fluoride and hydroxide

reactions. Spectra were collected on samples obtained using bis(cycloheptyl) **9**. Figure 2.8

shows cross-polarization magic angle spinning (CP MAS) and Bloch decay (BD MAS)

spectra on as-made Si-SSZ-70 samples. Both as-made spectra show significant Q^3[2] silica

content (-94 ppm resonance). A comparison of the CP and BD spectra show higher relative

intensity for the -116 and -120 ppm resonances under CP conditions (2 ms contact time)

---

[2] $Q^n=Si(OSi)_n(OH)_{4-n}$

and relative decrease for the -106 ppm resonance. This change in relative intensity suggests SDA molecules do not reside in close proximity to the silicon resonating at -106 ppm. The resonances in the fluoride sample are well defined and span a similar chemical shift range to those reported for ITQ-1[34, 35]. The calcined spectrum shown in Figure 2.9 shows six well resolved resonances with a small amount of Q^3 silica still present. Tables 2.7 and 2.8 list the observed resonances for each sample studied as well as those reported for ITQ-1.

Table 2.7 gives the observed chemical shifts for as-made Si-SSZ-70 materials. Relative intensity was determined by integration of the BD MAS spectra. In general the resonances for Si-SSZ-70 samples were not as well resolved as those for ITQ-1. This was particularly true for the hydroxide sample. No attempt was made to deconvolute the spectra as the limited resolution did not warrant this. Therefore, fewer chemical shifts were included in the table. Inspecting the relative intensities shows a significant population of Q^3 silica species in both hydroxide and fluoride samples. The resonance <-100 ppm for each sample can be assigned as Q^3 but there was some ambiguity regarding the resonances near-105 ppm. The calcined spectrum for Si-SSZ-70(F) shown in Figure 2.9 clearly shows the -105 ppm resonance, whereas the -95 ppm one was significantly diminished. This suggests the -105 ppm resonance to be Q^4 to give a relative Q^3 abundance of ~10% in the as-made material. The broad resonance centered at -104 ppm for the hydroxide material could not be conclusively assigned to either Q^3 or Q^4 giving an estimated relative Q^3 population of ~22–28%. The upper estimate for Q_3 content in the hydroxide sample was in general agreement with those reported for ITQ-1 (29–33%). For Si-SSZ-70(F) there was

no analogous material to compare the relative Q^3 population as fluoride reactions generally

produce materials with very low defects (low Q^3).
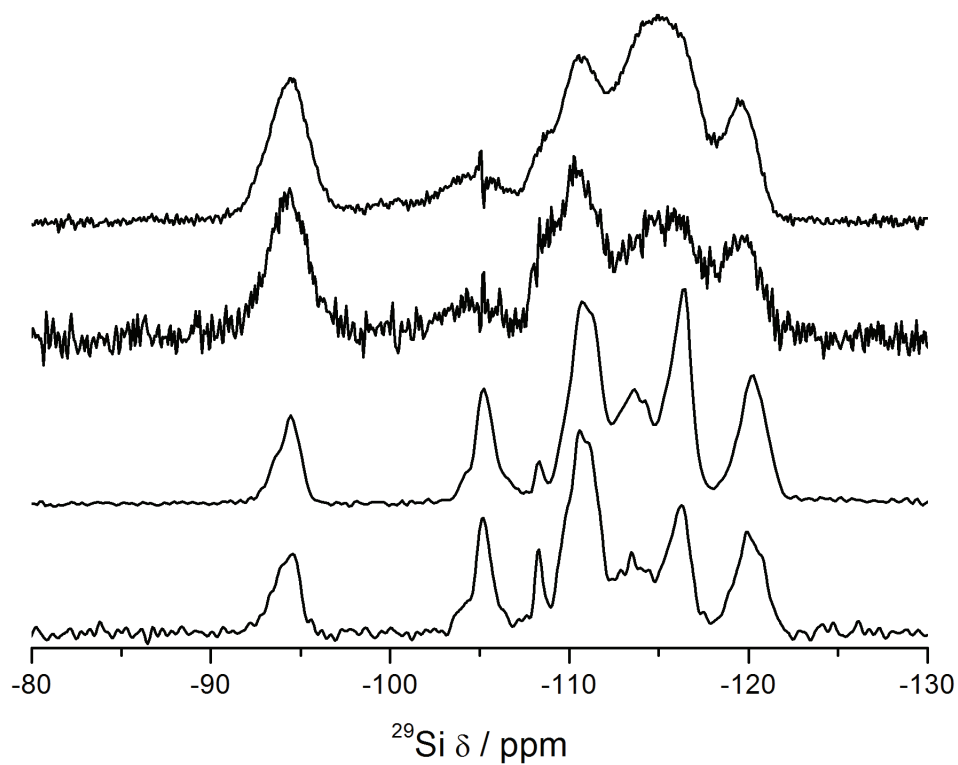
Figure 2.8: Solid-state ^{29}Si NMR spectra of Si-SSZ-70. Top to bottom: Si-SSZ-70(OH)

CP-MAS, Si-SSZ-70(OH) BD-MAS, Si-SSZ-70(F) CP-MAS and Si-SSZ-70(F) BD-

MAS
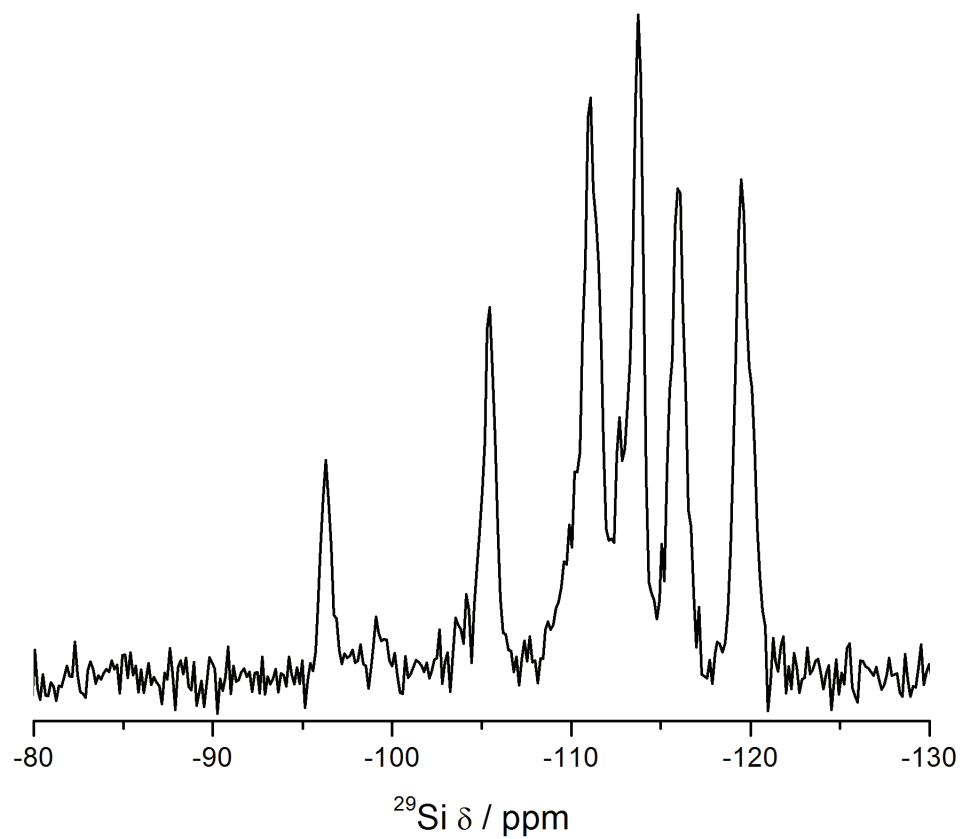
Figure 2.9: Solid-state ^{29}Si BD-MAS NMR of calcined Si-SSZ-70(F)

Table 2.7: ^{29}Si chemical shifts and relative intensities for as-made Si-SSZ-70(OH), Si-SSZ-70(F) and ITQ-1

Si-SSZ-70 (OH)		Si-SSZ-70 (F)		ITQ-1		
δ / ppm	I / %	δ / ppm	I / %	δ / ppm	Assignment	I / %
				-92.6	Q^3	12.0
-94.1	22.1	-94.6	10.5	-94.1	Q^3	19.0
-104.3	6.4	-105.2	11.5	-103.7	Q^3	1.9
-110.4	30.1	-108.3	4.9	-105.0	Q^4	2.8
-115.6	27.9	-110.6	30.5	-108.3	Q^4	1.7
-119.7	13.5	-113.5	12.1	-110.1	Q^4	27.8
		-116.3	15.6	-112.4	Q^4	2.5
		-119.9	14.8	-114.7	Q^4	10.7
				-116.7	Q^4	10.1
				-119.8	Q^4	11.5

Table 2.8: ^{29}Si chemical shifts and relative intensities for calcined Si-SSZ-70(F) and ITQ-1

Si-SSZ-70 (F)		ITQ-1		
δ / ppm	I / %	δ / ppm	Assignment	I / %
-96.3	4.6			
-105.4	11.5	-105.9	Q^4	15.1
-111.0	25.9	-111.2	Q^4	15.1
-113.7	23.1	-111.8	Q^4	4.9
-116.0	17.3	-112.6	Q^4	7.6
-119.5	17.6	-113.9	Q^4	19.0
		-116.5	Q^4	18.9
		-120.3	Q^4	19.4

The chemical shifts and relative intensities for calcined Si-SSZ-70(F) shown in Table 2.8 show several differences. As mentioned above, calcination did not completely remove all Q^3 species. In addition, the as-made resonance at -108.3 ppm was not visible in the calcined spectrum. It would appear unlikely that this resonance was from a silanol defect as the observed chemical shift is in the general range for Q^4 silica. Also, ^{29}Si resonances of pentacoordinated silicon with fluorine are found in the -120 to -150 ppm range so the resonance should not arise from fluoride incorporation[36]. This was supported by the weak shoulder at ~-108 ppm in the hydroxide spectra. The observed chemical shifts and relative intensities show similarity to those of ITQ-1.

SEM images of Si-SSZ-70(F) are shown in Figure 2.10. Thin hexagonal plates were visible in the as-made and calcined material. MWW materials form crystals with similar habit. The observed crystal habit supports the similarity to MWW materials as demonstrated by XRD and ^{29}Si NMR. Figure 2.11 shows a TEM image of B-SSZ-70 with the layers clearly observed. Images at higher magnification did not show pore features as observed for MCM-22[10] and SSZ-25[37].
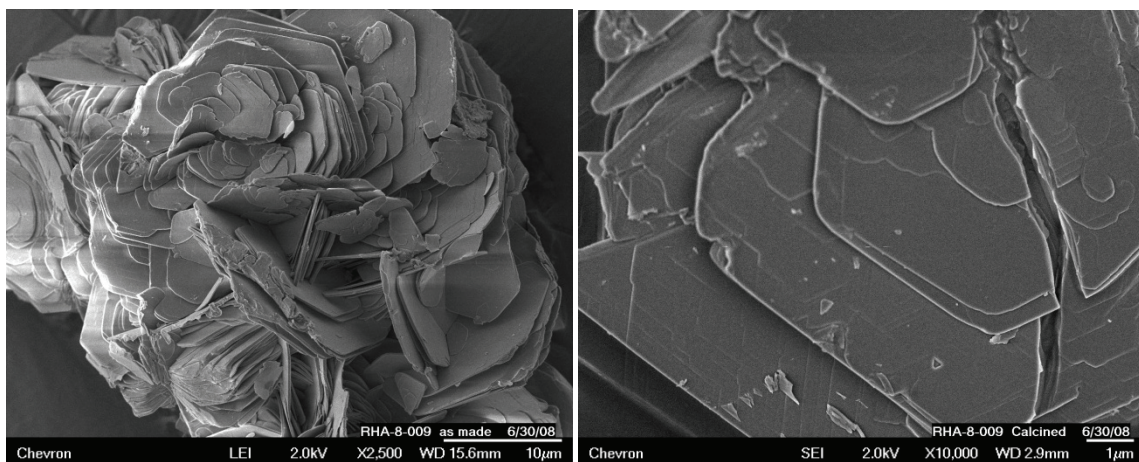
Figure 2.10: SEM images of as-made Si-SSZ-70 (left) and calcined Si-SSZ-70 (right)
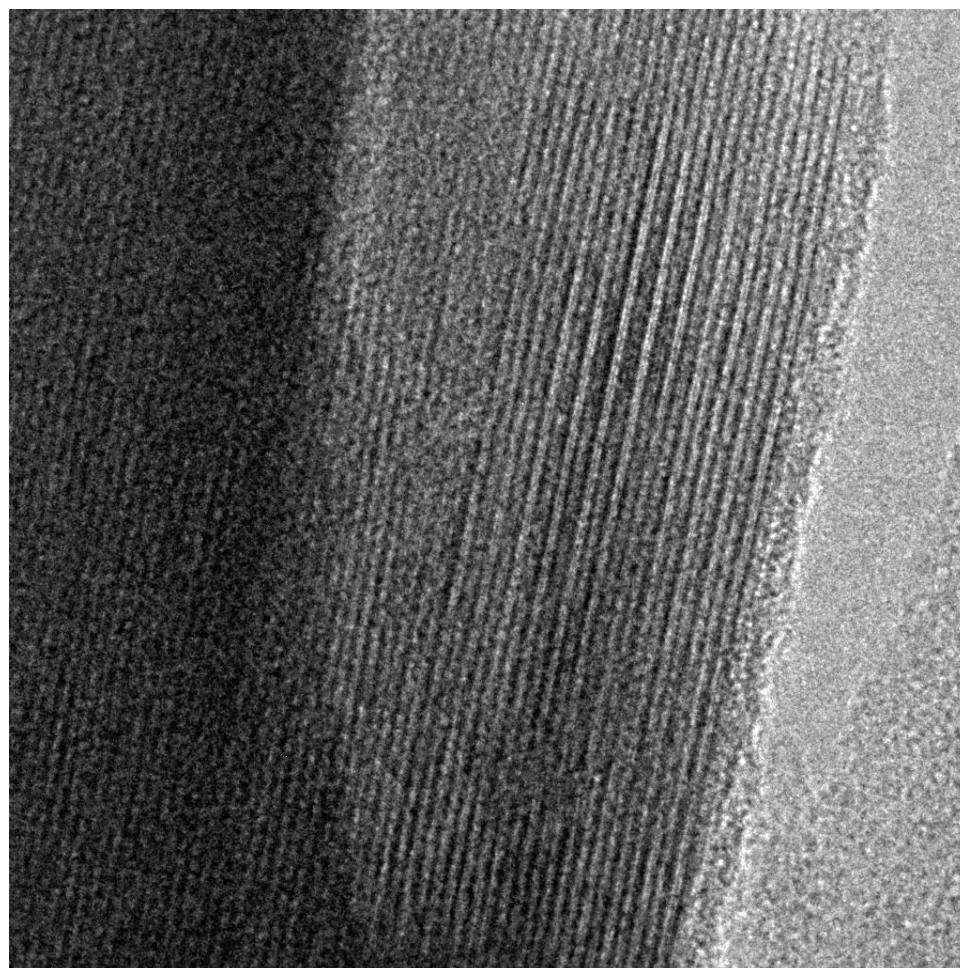
SIZ16489 SSZ-70a
BC6Ebb 200kx

20 nm

Figure 2.11: TEM image of B-SSZ-70

Chemical analysis was performed on several products to gain further insight into SSZ-70. The majority of the chemical analysis was performed on SSZ-70 materials using **5**. One aspect of particular interest was the amount of fluoride incorporated into SSZ-70 materials. This was investigated through studying pure silica products as a function of water to silica ratio for **5**, **6** and **11**. These SDAs were chosen as **5** gave two instances of SSZ-70 plus MTW, **6** gave MTW under all three water to silica ratios and **11** transitioned

from Beta to MTW with increasing dilution. The phases for the nine products analyzed are restated in Table 2.9 for convenience.

Table 2.9: Phase summary for chemical analysis of pure-silica fluoride products using **5**, **6** and **11**

SDA	H_2O/SiO_2=3.5	H_2O/SiO_2=7.5	H_2O/SiO_2=14.5
5	SSZ-70	SSZ-70	MTW
6	MTW	MTW	MTW
11	Beta	Beta	MTW

Tables 2.10 and 2.11 present chemical analysis for pure silica fluoride products. The carbon and nitrogen data in Table 2.10 show less organic occluded within one-dimensional MTW compared to three-dimensional Beta. The measured organic content for SSZ-70 falls between these two boundaries. Calculated carbon to nitrogen ratios agree with those expected for the parent SDAs except **11** at H_2O/SiO_2=14.5 where 8.5 was observed (expected 7.3). This sample gave the lowest nitrogen content of all samples and therefore might contain higher relative error (0.5 wt% detection limit). Fluoride analysis for the same products is shown in Table 2.11. Calculated fluoride to nitrogen values is also included. All F/N ratios can be compared to the theoretical F/N value for the SDA^+F^- salt (0.68 for all imidazolium SDAs studied). This value corresponds to a neutral product with no connectivity defects. The two SSZ-70 products show significantly lower fluoride content and F/N ratios compared to the other seven products. Fluoride absence means organic charge must be balanced by silanol defects[38] as observed by ^{29}Si NMR above. The remaining materials show F/N values very close to the theoretical value for defect-free

material. Two samples gave slightly higher ratios (0.83 and 0.86) with the 0.86 ratio

calculated for the same MTW product using **11** that showed low nitrogen content above.

Interestingly, the fluoride content of MTW products using **6** did not show a significant

trend with water content. Previous studies using **3** found higher fluoride incorporation in

MTT products with increasing water content[5]. Analysis reveals slightly higher fluoride

content at H_2O/SiO_2=3.5 (~1.4 wt% and F/N=0.83) than the two other products (~1.0 wt%

F and F/N=0.7). The H_2O/SiO_2=3.5 MTW product using **6** also shows slightly higher

carbon and nitrogen content. The higher carbon, nitrogen and fluorine content suggest

amorphous SiF_x species with occluded SDA might be present in small amounts (~1.7 wt%

additional C+N).

Table 2.10: Carbon and nitrogen content for pure-silica fluoride products using **5**, **6** and

11

SDA	H_2O/SiO_2=3.5			H_2O/SiO_2=7.5			H_2O/SiO_2=14.5		
	C/wt%	N/wt%	C/N	C/wt%	N/wt%	C/N	C/wt%	N/wt%	C/N
5	11.91	2.41	4.9	13.65	2.79	4.9	6.94	1.43	4.9
6	9.71	1.67	5.8	8.14	1.39	5.9	8.17	1.43	5.7
11	15.46	1.99	7.8	13.72	1.74	7.9	7.28	0.86	8.5

Table 2.11: Fluoride content for pure-silica fluoride products using **5**, **6** and **11**

SDA	H_2O/SiO_2=3.5		H_2O/SiO_2=7.5		H_2O/SiO_2=14.5	
	F/wt%	F/N	F/wt%	F/N	F/wt%	F/N
5	0.69	0.29	0.83	0.30	1.06	0.74
6	1.38	0.83	0.99	0.71	1.02	0.71
11	1.46	0.73	1.25	0.72	0.74	0.86

Chemical analysis of B-SSZ-70(F), Al-SSZ-70(F) and Al-SSZ-70(OH) products synthesized using **5** in Table 2.12 show very similar organic content across the seven products. Carbon to nitrogen ratios were between 4.8 and 5.0 agreeing very well with the expected ratio of 4.7. Slightly higher fluorine content was measured in the borosilicate samples compared to the pure silica and aluminosilicate samples. With trivalent lattice substitution (B or Al) framework charge is introduced and fluoride is no longer required to balance the cation charge. However, the values calculated show little variation with lattice substitution for both boron and aluminum incorporation. In addition, the ratios for all three aluminosilicate samples were almost the same as the pure silica products. One report on MCM-22 synthesis using hexamethyleneimine with alkali fluoride salts showed varying amounts of fluoride incorporated in the aluminosilicate product[39]. Under the approximately neutral reaction conditions the secondary amine should be protonated and similar cation/framework charge arguments must hold. Additional work is required to elucidate the exact nature of fluoride species present in B-SSZ-70(F) and Al-SSZ-70(F).

Inspecting the Si/B and Si/Al ratios measured in the as-made products reveals less boron incorporation than present in the reactions gel. Aluminosilicate fluoride and hydroxide products showed Si/Al ratios almost identical to the reaction gel. These data agree with reports in hydroxide reactions comparing boron and aluminum reactions using the same SDA[18]. Chemical analysis for both hydroxide products shows some sodium incorporation. The measured values correspond to ~0.25 and 0.11 Na/Al for Si/Al=50 and Si/Al=25, respectively. This indicates framework charge was predominantly compensated by SDA rather than alkali. This suggests organic occupies most of the void space within

SSZ-70 in contrast to SSZ-25 where the bulky adamantyl SDA was not expected to fit in the sinusoidal 10MR[26].

Table 2.12: Chemical analysis of B-SSZ-70(F), Al-SSZ-70(F) and Al-SSZ-70(OH) products synthesized using **5**

	Gel composition						
	Si/B=18	**Si/B=5.5**	**Si/Al=35**	**Si/Al=25**	**Si/Al=15**	**Si/Al=50**	**Si/Al=25**
C/wt%	13.67	13.51	12.23	13.07	13.54	13.62	13.37
N/wt%	2.80	2.77	2.57	2.71	2.70	2.82	2.81
F/wt%	1.16	1.04	0.70	0.64	0.82	-	-
F/N	0.41	0.38	0.27	0.24	0.30	-	-
Na/wt%	-	-	-	-	-	0.17	0.14
Si/B	21.7	13.7	-	-	-	-	-
Si/Al	-	-	34.1	25.5	16.6	44.4	22.2

In addition to chemical analysis, TGA was performed on SSZ-70 products. Figure 2.12 compares the TG profiles for Si-SSZ-70(F) synthesized using **5** and **8**. Both materials show very similar mass loss between 200 and 620°C (19.3% for **5** and 20.4% for **8**) yet the mass loss profiles were distinct. Smaller bis(isobutyl) **5** shows one mass loss starting at approximately 250°C whereas two mass losses can be seen for the larger bis(cyclohexyl) **8**. The first mass loss starts around 250°C as per **5** with an inflection point at ~425°C followed by another mass loss. Observing two mass loss regions with the larger SDA indicates two distinct organic environments. With SSZ-70 being a layered material the first mass loss was assigned to organic occluded between layers and the second mass loss attributed to organic occluded within the layers. Observing one mass loss with the smaller SDA was likely due to weaker fit within the framework offering lower thermal protection.

Several post-synthesis experiments were performed on an Al-SSZ-70 sample synthesized using **8** to gain insight into the relative contribution of each organic environment. The sample was obtained from the SAR=35 NaY reaction and treated with 1N HCl to neutralize residual FAU species as described in the experimental section. The first experiment explored SDA removal by DMF extraction. Similar experiments with SSZ-25 showed organic removal and significant changes in the XRD pattern after DMF extraction[26]. No organic removal was detected by TGA after extraction for the Al-SSZ-70 material studied. In addition, the XRD pattern was identical to the parent material. This suggested an organic/framework environment similar to traditional zeolites where extraction does not typically remove organic.

The second experiment thermally treated the as-made material to remove the low-temperature organic material. Inspecting the TGA profiles indicated 350°C was sufficient to remove the first organic environment and should be ~75°C below the mass loss onset of the second environment. After heating at 350°C for five hours in air all organic below 425°C was removed and the XRD pattern showed clear differences. TGA profiles and XRD patterns are shown in Figures 2.13 and 2.14, respectively. The XRD pattern resembled calcined Al-SSZ-70(OH) even though ~7 wt% organic remained occluded. This heat treated material was ammonium-exchanged and assessed for micropore volume and catalytic activity as described below.
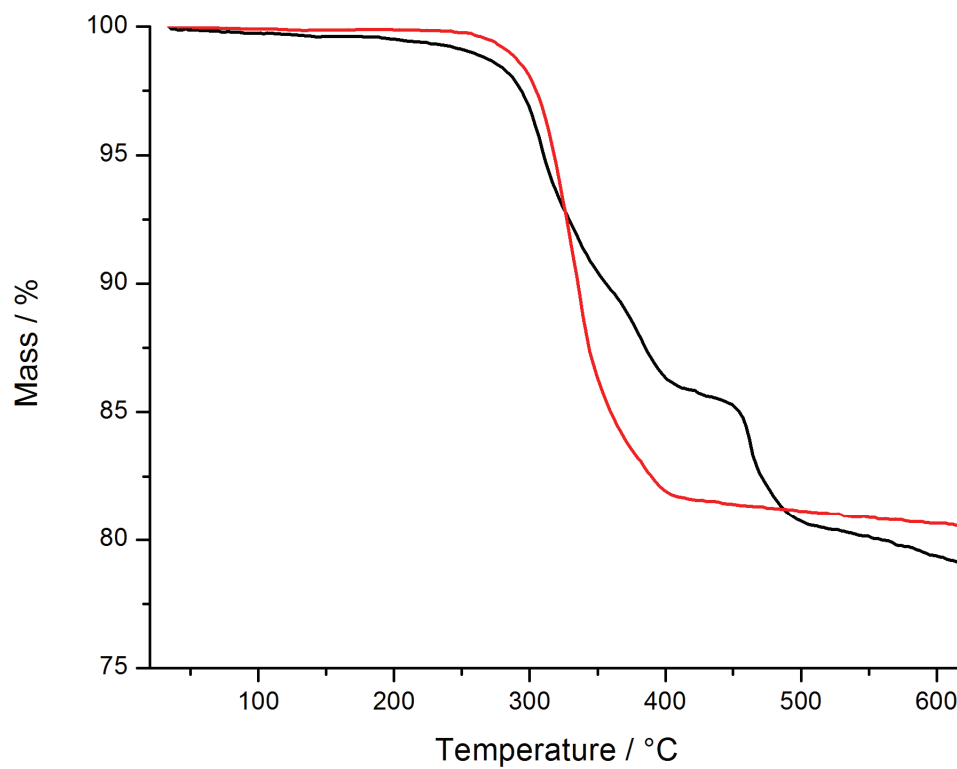
Figure 2.12: TGA of Si-SSZ-70(F) synthesized using **5** (red) and **8** (black)
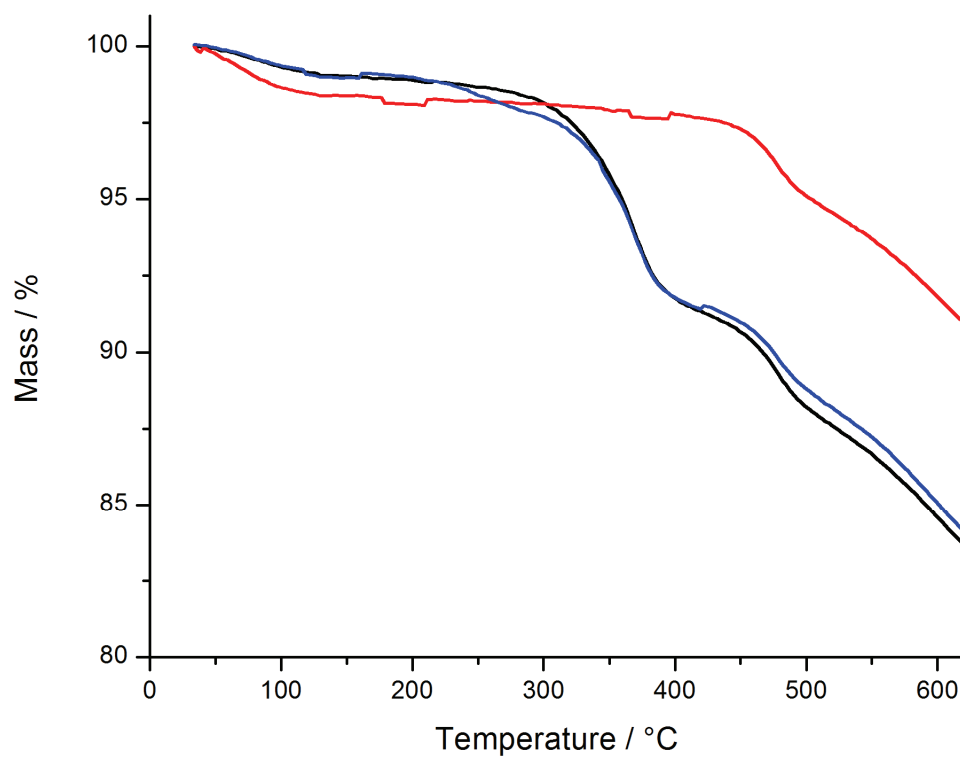
Figure 2.13: TGA of post-synthesis treatments for Al-SSZ-70(OH) synthesized using **8**.

Black=parent material, blue=DMF extracted and red=350°C treated
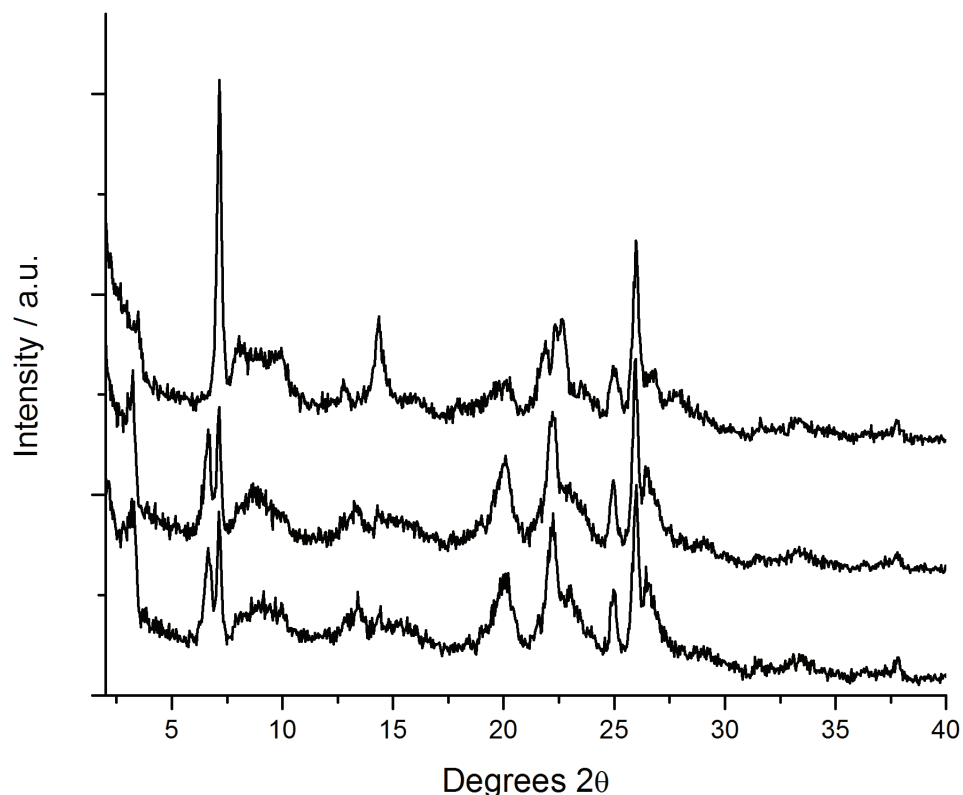
Figure 2.14: XRD patterns of post-synthesis treatments for Al-SSZ-70(OH) synthesized

using **8**. Bottom to top: parent material, DMF extracted and 350°C treated

Finally, textural properties of SSZ-70 products were examined using nitrogen adsorption. All SSZ-70 samples examined were synthesized using **5** except Si-SSZ-70(OH) that used **9** and the Al-SSZ-70(OH) 350°C treated sample synthesized using **8**. Table 2.13 lists micropore volume and external surface areas for each SSZ-70 material. These data show a clear distinction between the fluoride and hydroxide products with 0.20 cm^3 g^{-1} micropore volume observed for all three fluoride products and 0.09–0.14 cm^3 g^{-1} observed for the hydroxide products. The micropore volumes for the fluoride products are similar to those reported for MWW materials (0.17–0.18 cm^3 g^{-1}). External surface areas typical of zeolites were observed for all products except the two Al-SSZ-70(OH) products.

These materials returned ~190 and 100 m^2 g^{-1} external surface area possibly indicating some delamination occurred during heat treatment. The observed external surface areas were significantly lower than those reported for delaminated and exfoliated ITQ-2 (~700 m^2 g^{-1} external surface area)[14]. The 350°C treated material shows ~2/3 the micropore volume of the calcined Al-SSZ-70(OH) material. Assuming this organic resides in interlayer regions this gives a similar contribution as reported for SSZ-25 where ~0.12 cm^3 g^{-1} micropore volume was attributed to the large cages formed between layers.

Table 2.13: Textural properties of SSZ-70 products

SSZ-70 Product	Micropore volume / cm^3 g^{-1}	External surface area / m^2 g^{-1}
Si-SSZ-70 (F)	0.20	9
B-SSZ-70 (F)	0.20	37
Al-SSZ-70 (F)	0.20	46
Si-SSZ-70 (OH)	0.09	56
B-SSZ-70 (OH)	0.12	45
Al-SSZ-70 (OH)	0.14	189
Al-SSZ-70 (OH) 350°C treated	0.09	96

2.3.3: Catalytic Activity

Catalytic activity used the constraint index (CI) test as a model acid-catalyzed hydrocarbon reaction. In this reaction the relative cracking rates of n-hexane and 3-methylpentane are used to calculate the constraint index given by the following equation:

$$CI = \frac{\log(\text{n-hexane conv.})}{\log(\text{3-methylpentane conv.})}$$

Four Al-SSZ-70 materials were tested: Al-SSZ-70(F, Si/Al=26) and Al-SSZ-70(OH, Si/Al=22) synthesized using **5** plus Al-SSZ-70(OH) and the 350°C treated material synthesized using **8**. The characterization outlined above showed similarity to MWW materials so SSZ-25 was included for comparison (the SSZ-25 cracking reaction was performed at 330°C). Figure 2.15 shows cracking rate as a function of time on stream (TOS). The three SSZ-70 materials show slight differences in initial cracking rate then converge with increasing TOS. The deactivation with TOS follows a similar path to SSZ-25. The 350°C treated material shows the same deactivation trend although the initial rate was significantly lower than for all other materials owing to lower number of active sites. These data again suggest strong similarity to MWW materials; however, the CI versus TOS shown in Figure 2.16 presents clear distinction. All materials show initial CI values < 1 with SSZ-25 giving a rapid increase as previously described[40]. In contrast, all SSZ-70 materials show CI values < 1.2 throughout. In noting the anomalous SSZ-25 behavior with TOS it was postulated the deactivation rates of the two independent pore systems were different giving rise to changing CI. Both pore systems contribute to initial reactivity, with the more accessible MWW cage dominating over the sinusoidal pore system. The high

initial activity from active sites located within the cages masks the sinusoidal pore reactivity. As active sites in the cages deactivated due to fouling, the sinusoidal pores accounted for relatively higher reactivity resulting in a CI increase to the range expected for medium pore materials (1 < CI < 12). All SSZ-70 materials show similar cracking rate deactivation suggesting the presence of a similar cavity, but the absence of increasing CI as the material deactivates suggests a second pore system distinct to the sinusoidal 10MR pore found in MWW. Additional catalytic tests and adsorption studies[41, 42] might offer insight into the structure of SSZ-70; however, a structural model should be the ultimate aim.
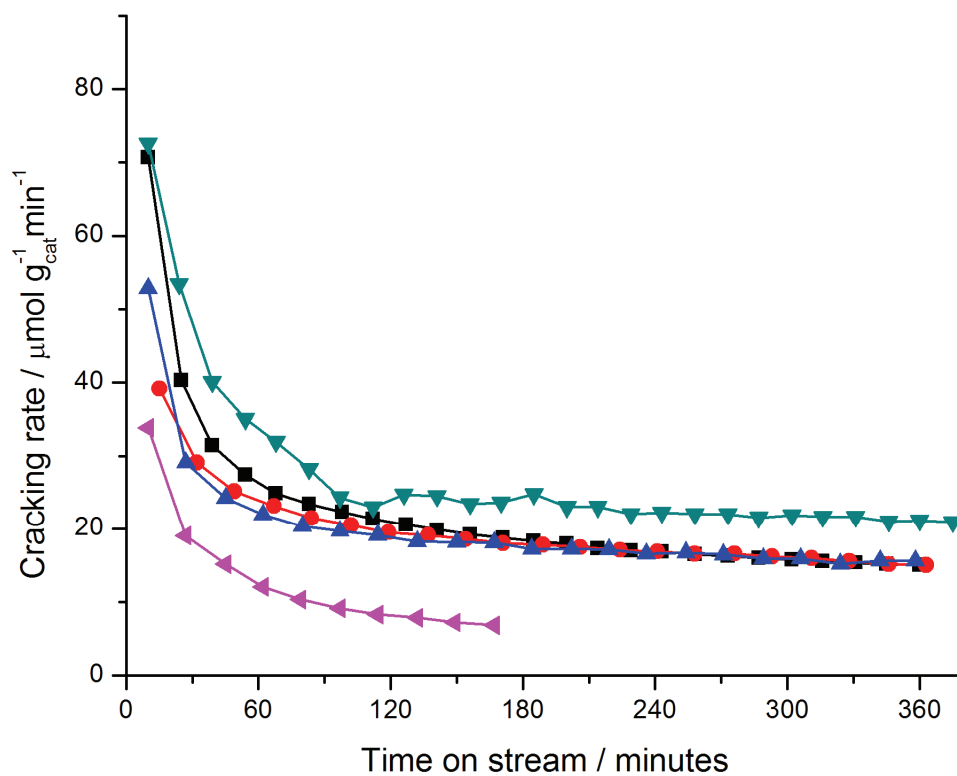
Figure 2.15: CI test cracking rate vs. time on stream for Al-SSZ-70 materials. SSZ-25(▼), Al-SSZ-70(F)(●), Al-SSZ-70(OH-**5**)(▲), Al-SSZ-70(OH-**8**)(■) and Al-SSZ-70(OH-**8** 350°C treated)(◄)
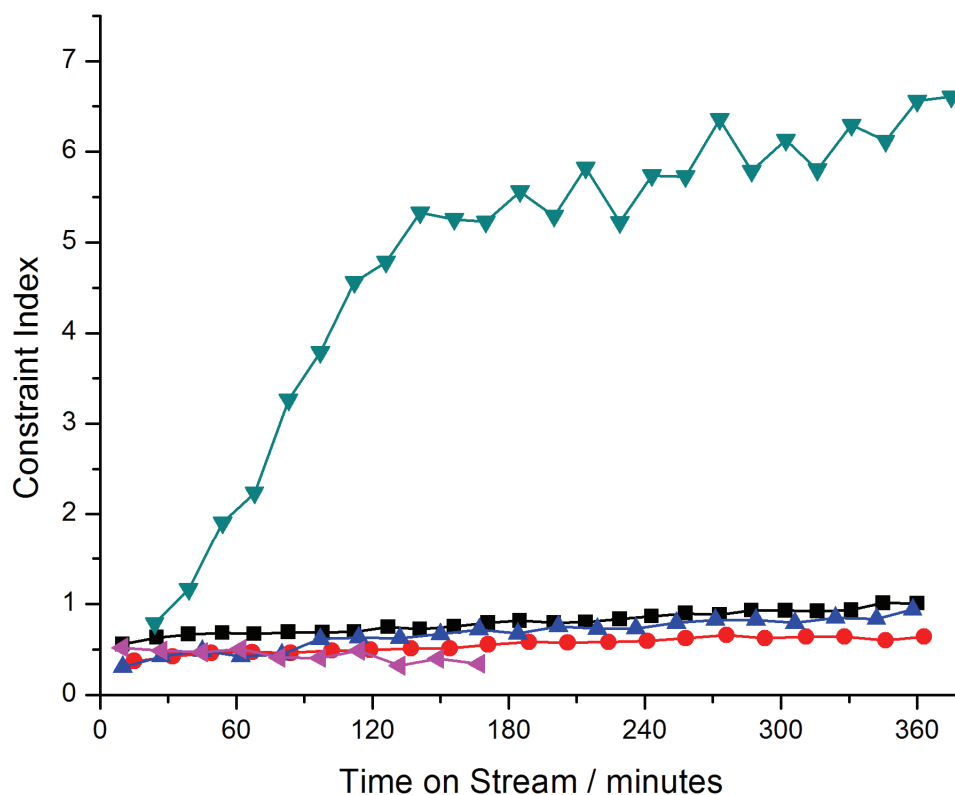
Figure 2.16: Constraint index vs. time on stream for Al-SSZ-70 materials. SSZ-25(▼),

Al-SSZ-70(F)(●), Al-SSZ-70(OH-**5**)(▲), Al-SSZ-70(OH-**8**)(■) and Al-SSZ-70(OH-**8**

350°C treated)(◄)

2.4: Conclusions

Investigating guest/host relationships for a library of 16 imidazolium SDAs found eight guest molecules synthesized SSZ-70. The original synthesis under boron-rich conditions using **3** was expanded to pure-silica and aluminosilicate SSZ-70 under both fluoride and hydroxide conditions. Characterization by XRD, ^{29}Si MAS NMR, electron microscopy and nitrogen adsorption showed similarity to MWW materials. Catalytic tests on Al-SSZ-70 revealed active catalytic behavior with distinct differences to SSZ-25.

2.5: Acknowledgments

2.6: References

1. S. I. Zones and A. W. Burton, US Patent No. 7,108,843 (2006).

2. S. I. Zones, R. J. Darton, R. Morris and S. J. Hwang, Journal of Physical Chemistry B **109** (1), 652–661 (2005).

3. S. I. Zones, Zeolites **9** (6), 458–467 (1989).

4. A. W. Burton, Journal of the American Chemical Society **129** (24), 7627–7637 (2007).

5. S. I. Zones, S. J. Hwang, S. Elomari, I. Ogino, M. E. Davis and A. W. Burton, Comptes Rendus Chimie **8** (3–4), 267–282 (2005).

6. S. I. Zones, US Patent No. 4,483,835 (1984).

7. J. March and M. B. Smith, *March's Advanced Organic Chemistry: Reactions, Mechanisms, and Structure*, 5th ed. (Wiley-Interscience, 2001).

8. A. J. Arduengo, R. L. Harlow and M. Kline, Journal of the American Chemical Society **113** (1), 361–363 (1991).

9. A. J. Arduengo, Accounts of Chemical Research **32** (11), 913–921 (1999).

10. M. E. Leonowicz, J. A. Lawton, S. L. Lawton and M. K. Rubin, Science **264** (5167), 1910–1913 (1994).

11. A. Corma, M. J. Díaz-Cabanas, M. Moliner and C. Martínez, Journal of Catalysis **241** (2), 312–318 (2006).

12. G. G. Juttu and R. F. Lobo, Microporous and Mesoporous Materials **40** (1–3), 9–23 (2000).

13. W. J. Roth, C. T. Kresge, J. C. Vartuli, M. E. Leonowicz, A. S. Fung and S. B. McCullen, Catalysis by Microporous Materials **94**, 301–308 (1995).

14. A. Corma, V. Fornes, S. B. Pergher, T. L. M. Maesen and J. G. Buglass, Nature **396** (6709), 353–356 (1998).

15. C. Y. Chen, S. I. Zones, S. J. Hwang, A. W. Burton and A. J. Liang, in *Studies in Surface Science and Catalysis (From Zeolites to Porous MOF Materials— the 40th Anniversary of International Zeolite Conference)*, edited by R. R. Xu, Z. Gao, J. Chen and W. Yan (Elsevier 2007), Vol. 170.

16. T. Ikeda, Y. Akiyama, Y. Oumi, A. Kawai and F. Mizukami, Angewandte Chemie-International Edition **43** (37), 4892–4896 (2004).

17. C. Y. Chen and S. I. Zones, in *Studies in Surface Science and Catalysis (Zeolites and Mesoporous Materials at the Dawn of the 21st Century: Proceedings of the 13th International Zeolite Conference)*, edited by A. Galarneau, F. Di Renzo, F. Fajula and J. Vedrine (Elsevier, 2001), Vol. 135.

18.   S. I. Zones and S.-J. Hwang, Microporous and Mesoporous Materials **58** (3), 263–277 (2003).

19.   S. I. Zones, M. M. Olmstead and D. S. Santilli, Journal of the American Chemical Society **114** (11), 4195–4201 (1992).

20.   W. A. Herrmann, V. P. W. Bohm, C. W. K. Gstottmayr, M. Grosche, C. P. Reisinger and T. Weskamp, Journal of Organometallic Chemistry **617** (1), 616–628 (2001).

21.   W. A. Herrmann, C. Kocher and L. J. Goossen, US Patent No. 6,025,496 (2000).

22.   A. K. Burrell, R. E. Del Sesto, S. N. Baker, T. M. McCleskey and G. A. Baker, Green chemistry **9** (5), 449–454 (2007).

23.   A. Jackowski, S. I. Zones, S.-J. Hwang and A. W. Burton, Journal of the American Chemical Society **131** (3), 1092–1100 (2009).

24.   V. J. Frillette, W. O. Haag and R. M. Lago, Journal of Catalysis **67** (1), 218–222 (1981).

25.   S. I. Zones, Y. Nakagawa, G. S. Lee, C. Y. Chen and L. T. Yuen, Microporous and Mesoporous Materials **21** (4–6), 199–211 (1998).

26.   S. I. Zones, S. J. Hwang and M. E. Davis, Chemistry—a European Journal **7** (9), 1990–2001 (2001).

27.   X. B. Yang, M. A. Camblor, Y. Lee, H. M. Liu and D. H. Olson, Journal of the American Chemical Society **126** (33), 10403–10409 (2004).

28.   M. A. Camblor, P. A. Barrett, M.-J. Díaz-Cabañas, L. A. Villaescusa, M. Puche, T. Boix, E. Pérez and H. Koller, Microporous and Mesoporous Materials **48** (1–3), 11–22 (2001).

29. Y. Chu, H. Deng and J. P. Cheng, Journal of Organic Chemistry **72** (20), 7790–7793 (2007).

30. T. Fahlbusch, M. Frank, J. Schatz and D. T. Schuhle, Journal of Organic Chemistry **71** (4), 1688–1691 (2006).

31. P. Wagner, M. Yoshikawa, M. Lovallo, K. Tsuji, M. Taspatsis and M. E. Davis, Chemical Communications (22), 2179–2180 (1997).

32. R. F. Lobo, S. I. Zones and R. C. Medrud, Chem. Mater. **8** (10), 2409–2411 (1996).

33. N. M. Scott and S. P. Nolan, European Journal of Inorganic Chemistry (10), 1815–1828 (2005).

34. M. A. Camblor, A. Corma, M. J. Diaz-Cabanas and C. Baerlocher, J. Phys. Chem. B **102** (1), 44–51 (1998).

35. M. A. Camblor, C. Corell, A. Corma, M.-J. Diaz-Cabanas, S. Nicolopoulos, J. M. Gonzalez-Calbet and M. Vallet-Regi, Chemistry of Materials **8** (10), 2415–2417 (1996).

36. H. Koller, A. Wolker, L. A. Villaescusa, M. J. Diaz-Cabanas, S. Valencia and M. A. Camblor, Journal of the American Chemical Society **121** (14), 3368–3376 (1999).

37. I. Y. Chan, P. A. Labun, M. Pan and S. I. Zones, Microporous Materials **3** (4–5), 409–418 (1995).

38. H. Koller, R. F. Lobo, S. L. Burkett and M. E. Davis, Journal of Physical Chemistry **99** (33), 12588–12596 (1995).

39. R. Aiello, F. Crea, F. Testa, G. Demortier, P. Lentz, M. Wiame and J. B. Nagy, Microporous and Mesoporous Materials **35–36**, 585–595 (2000).

40. S. I. Zones and T. V. Harris, Microporous and Mesoporous Materials **35–36**, 31–46 (2000).

41. C. Y. Chen and S. I. Zones, Microporous and Mesoporous Materials **104** (1–3), 39–45 (2007).

42. S. I. Zones, C. Y. Chen, A. Corma, M. T. Cheng, C. L. Kibby, I. Y. Chan and A. W. Burton, Journal of Catalysis **250** (1), 41–54 (2007).

Chapter Three: Guest/Host Relationships using Chiral Imidazolium Structure Directing Agents in Molecular Sieve Synthesis

3.1: Introduction

The results presented in Chapter Two showed 42 instances of Beta across seven imidazolium SDA. Beta was favored as the SDAs became larger with bis(cyclooctyl) SDA **13** only making Beta. This apparent strong specificity for Beta lead to an additional guest/host study using chiral imidazolium SDAs.

Zeolite Beta was discovered in the 1960s by workers at Mobil using tetraethylammonium hydroxide as SDA[1]. Indirect characterization methods using probe molecule adsorption and catalytic testing suggested a large pore multi-dimensional structure. The exact structure remained unknown until the late 1980s when it was independently solved by workers at Exxon[2, 3] and Mobil[4]. The proposed structure is an intergrowth of two pure end-members denoted polymorphs A and B. Lateral shifts along a and b between adjacent layers determine the structure. The basic Beta layer is shown in Figure 3.1 together with representations for three ordered polymorphs. Details of the possible stacking sequences leading to the various end members are available online from the Database of Zeolite Structures[5].
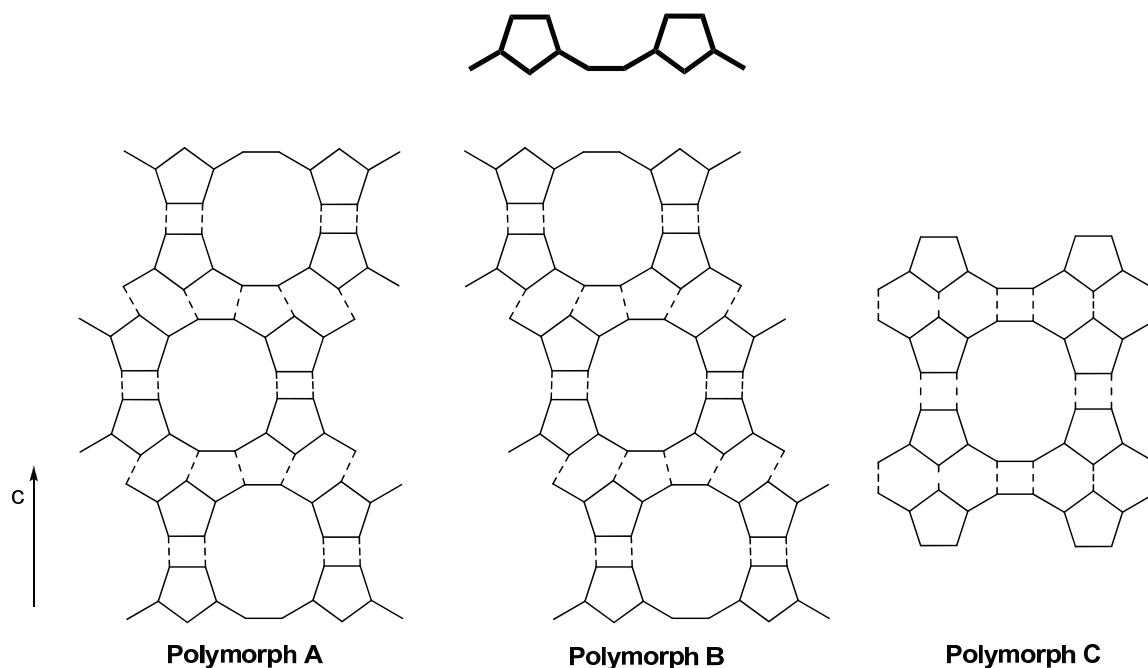
Figure 3.1: Beta building layer and representations of Polymorphs A, B and C. For clarity oxygen atoms have been omitted. Solid lines connect neighboring silicon atoms in each layer unit and dashed lines connect silicon atoms in adjacent layers

Tetragonal polymorph A contains two enantiomorphs with $P4_122$ or $P4_322$ symmetry. Monoclinic polymorph B is achiral with symmetry C2/c (often lowered to P(-1) for comparison with other polymorphs). Traditional Beta products are achiral with equal amounts of "right-" and "left-handed" polymorph A intergrown with polymorph B. The possibility of synthesizing a chiral Beta material has been actively pursued by many groups since publication of the structure. Potential applications of an enantiopure zeolite could include chiral catalysis and separations. Examples of chiral frameworks in compositions other than high-silica exist and have been recently discussed[6]. Many of the reported materials are phosphate-based with reduced hydrothermal stability. Two recent reports of

chiral germanosilicates SU-32 ($P6_122/P6_522$)[7] and ITQ-37 ($P4_132/P4_332$)[8] also noted limited hydrothermal stability compared to high-silica molecular sieves. Neither material employed chiral organic molecules in their synthesis.

Additional polymorphs were predicted from the *BEA layer elucidated in the aforementioned references. One stacking sequence (0a, 0b) forms a structure rich in double four rings (D4R, a cube) and is denoted polymorph C[2]. This subunit appears frequently in germanosilicate materials with Ge preferentially occupying sites in the D4R[9] subunits. Beta polymorph C (BEC) was synthesized as a pure germanium dioxide material (FOS-5)[10] and germanosilicate (ITQ-17)[11]. Recently, germanium free ITQ-17 has been synthesized using Diels-Alder derived SDAs[12, 13]. The germanium free syntheses required fluoride to stabilize the D4R subunits. Another stacking sequence forms an ordered intergrowth of polymorphs A and B that is denoted polymorph C_H (polymorph C-Higgins)[4]. A material denoted SSZ-63[14] exhibits X-ray diffraction (XRD) reflections more closely resembling Polymorph C_H than those expected for typical Beta (random polymorph A/B intergrowth).

Structural differences brought about by different stacking sequences manifest in changes to XRD patterns. Diffraction patterns for faulted materials can be simulated using software programs such as DIFFaX[15]. Simulated diffraction patterns can be generated for a series of fault probabilities that can be compared to experimental patterns. The relative contribution of polymorphs A and B to Beta was estimated using this process. This also provides a valuable tool for this study as experimental XRD patterns can be compared to those expected for increasing polymorph A content. Figure 3.2 presents simulated XRD patterns for polymorphs A and B. In the context of enriched polymorph A two features should appear in the XRD pattern. The first is separation of the broad, almost symmetrical

reflection between 7 and 8°2θ into two resolved reflections with appropriate intensity. The

second feature is the appearance of a reflection at ~9.7°2θ with increasing polymorph A

content. This second feature does not overlap with any reflections from polymorph B

making it valuable in assessing polymorph A enrichment.
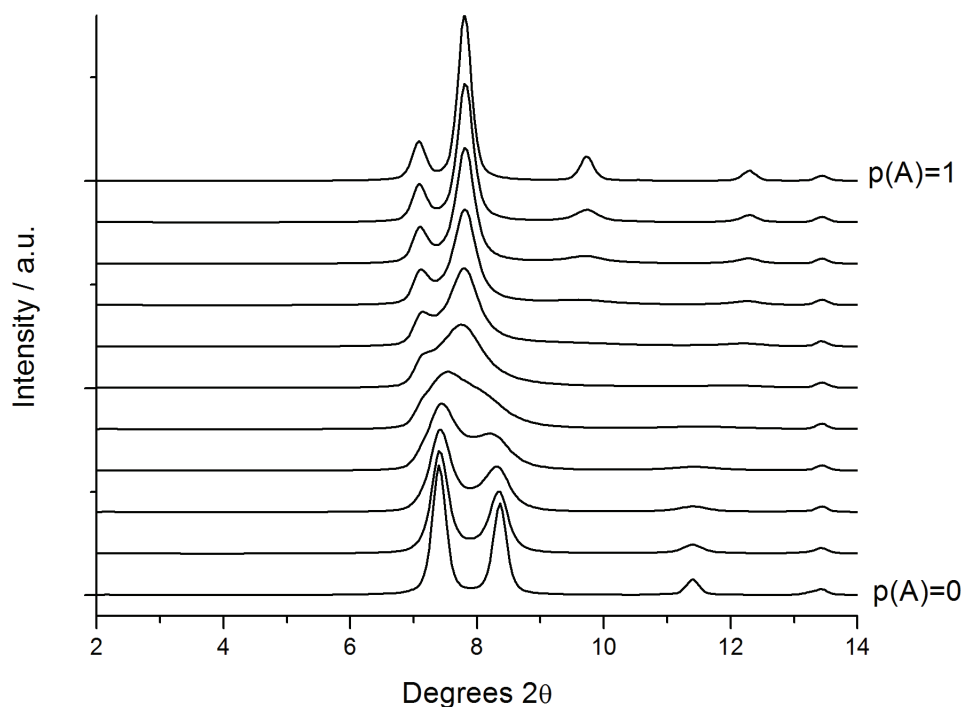
Figure 3.2: Simulated XRD patterns for Beta polymorphs A and B. Bottom to top=100%

polymorph B (p(A)=0) to 100% polymorph A (p(A)=1))

In the wider context of rational design of molecular sieves, Davis and Lobo

proposed several criteria considered necessary to synthesize pure polymorph A[16]. The

proposed criteria envisioned the use of a true template molecule. A hypothetical

template/chiral zeolite composite would have lower energy compared to all other silicate

structures. Therefore, this molecule would strictly specify the formation of Polymorph A.

Additional constraints were as follows:

(i) The molecule must be chiral.

(ii) The molecule must be > 10Å in length.

(iii)The molecule must be stable under synthesis conditions.

Previous studies with imidazoliums have not shown any true templates although

several show strong specificity to a given product. Therefore, exploring chiral imidazolium

SDAs might offer a chance to synthesize enriched polymorph A. Chiral imidazolium salts

have been synthesized as precursors to chiral N-heterocyclic carbene (NHC) ligands in

organometallic complexes[17–20]. NHC compounds have also been applied in asymmetric

organocatalysis[21, 22]. The synthetic methods for these C_2-symmetric imidazoliums are

identical to those used in Chapter Two with chiral primary amines the chiral source. Figure

3.3 shows the chiral imidazolium SDAs used in the present study. The chiral SDA library

covers a similar C/N^+ range to the SDAs found to make Beta in Chapter Two. Four of the

five SDAs contain a chiral carbon adjacent to nitrogen, whereas the remaining one derives

chirality from the pinene-precursor. Although the ability to direct a specific product is not

known *a priori*, all five were expected to meet the additional constraints listed above.

17

18

19

20

21
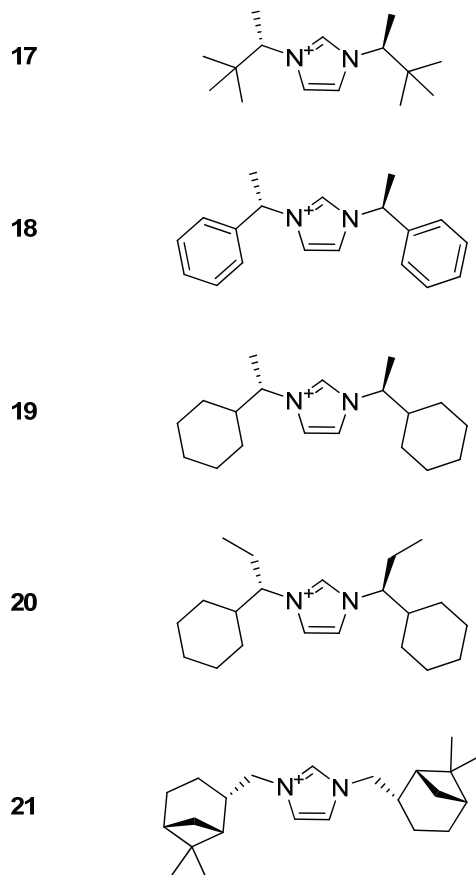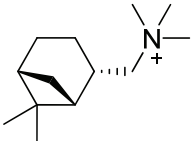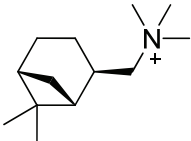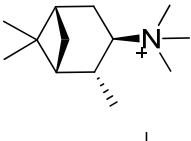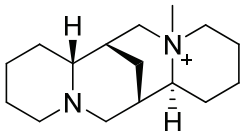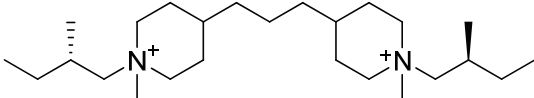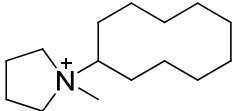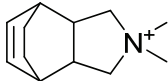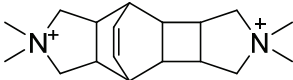
Figure 3.3: Chiral imidazolium SDAs studied

Selected examples of chiral SDAs reported in molecular sieve synthesis are given in Table 3.1. Also included in Table 3.1 are three SDAs that have given Beta products enriched in certain Polymorphs. SDAs **I-III** derive chirality from the pinene skeleton and all three produce achiral products. Additional pinene-derived SDAs were investigated with MTW the only additional phase[23]. (-)-sparteine derived SDA **IV** has been used to synthesize four high-silica phases. In all cases the product phases are achiral. Other sparteine-derived SDAs have been investigated with CFI the only phase obtained[24, 25]. SDA **V** was reported to synthesize MTW+Beta with this the only apparent report of a

chiral organocation synthesizing any Beta material. It should be noted that a report of slight polymorph A enrichment has appeared, although no details of the organic were reported[16].

Table 3.1: Examples of chiral SDAs used in molecular sieve synthesis and SDAs used to synthesize enriched Beta products

SDA	Structure	Product	Reference
I		CIT-1 (CON)	26
II		CIT-1 (CON)	26
III		SSZ-31 (*STO)	26
IV		SSZ-24 (AFI), CIT-5 (CFI), ITQ-21, ITQ-30	27–30
V		ZSM-12 (MTW)+Beta	31
VI		SSZ-63 (enriched Polymorph C$_H$)	14
VII		Pure-silica Beta C, enriched Polymorph B	12, 32
VIII		Pure-silica Beta C	13

The three remaining SDA give Beta products enriched in various polymorphs. Both **VII** and **VIII** require fluoride to synthesize pure-silica BEC using the cooperative effect of fluoride stabilized D4Rs. Reactions using **VII** also required KOH with K_2SiF_6 buffering deemed necessary to form BEC. The report regarding enriched Polymorph C_H using **VI** noted boron under hydroxide conditions was required for ordering. These reports indicate a variety of inorganic conditions in both fluoride and hydroxide conditions must be screened in attempts to synthesize enriched products.

In addition to the enriched Beta examples above other reports of Beta products enriched in various polymorphs have appeared. A series of materials denoted NCL-5, NCL-6 and NCL-7 claim polymorph B enrichment[33, 34]. These materials were synthesized using tetraethylammonium fluoride with perchloric acid added as a nucleation promoter, although a recent publication argued that the experimental evidence was consistent with BEC enrichment instead[32]. Another report used tetraethylammonium hydroxide and chiral Rhodium complexes or alkaloids under acidic fluoride conditions (pH~4) to "recrystallize" Beta. The authors deconvoluted the broad low angle reflection shown in Figure 3.2 to calculate relative polymorph A/B ratios and claimed partial polymorph A enrichment[35]. The authors noted that no products gave a reflection at ~9.7°2θ that would provide clear evidence of polymorph A.

3.2: Experimental Section

3.2.1: Structure Directing Agent Synthesis

All reagents were purchased from commercial vendors and were used as received. SDAs were synthesized according to published procedures[17, 19] and purified using the methodologies outlined in Chapter Two. Specific optical rotation measurements were performed using a Jasco P-2000 Polarimeter. Liquid NMR spectra were recorded on 300 MHz Varian Mercury spectrometers. Combustion analysis was performed at the Chevron Energy Technology Center (Richmond, CA) using a Carlo-Erba Combustion Elemental Analyzer. All SDAs were exchanged to the hydroxide form using Dowex Monosphere 550A UPW hydroxide resin (Supelco). Final hydroxide concentration was determined by titration with 0.01N HCl solution to a phenolphthalein end point.

1,3-bis((S)-3,3-dimethylbutan-2-yl)imidazolium chloride (**17**): Using (S)-3,3-dimethyl-2-butylamine (2x121 mmol; Alfa-Aesar, 99+%, ee 99+%) and activated carbon purification, 8.81 g white solids (32.3 mmol, 27% yield) were obtained. ^{1}H NMR (300 MHz, DMSO-d$_6$): 9.77, 7.94, 4.39, 1.49, 0.87. ^{13}C NMR (75 MHz, DMSO-d$_6$): 136.0, 121.7, 64.3, 34.5, 25.9, 14.7. Analysis calculated for C$_{15}$H$_{29}$ClN$_2$: C, 66.03; H, 10.71; N, 10.27 (C/N=6.43). Observed C, 64.24; H, 10.72; N, 10.07 (C/N=6.38). $[\alpha]_D^{25}$ = -5.33 (c=14.4, H$_2$O) (after ion-exchange to the hydroxide form).

1,3-bis((S)-1-phenylethyl)imidazolium tetrafluoroborate (**18**): Using (S)-(-)-1-phenylethylamine (2x73 mmol; Alfa-Aesar, 99+%, ee 99.5%) followed by recrystallization from ethyl acetate/dichloromethane to give 13.93g off-white solids (38.3

mmol, 52% yield). ^{1}H NMR (300 MHz, DMSO-d$_6$): 9.71, 7.96, 7.44–7.37, 5.81, 1.90.

^{13}C NMR (75 MHz, DMSO-d$_6$): 139.6, 134.8, 129.1, 128.7, 126.6, 121.6, 58.9, 20.4.

Analysis calculated for C$_{19}$H$_{21}$BF$_4$N$_2$: C, 62.66; H, 5.81; N, 7.69 (C/N=8.15). Observed

C, 64.68; H, 6.21; N, 7.99 (C/N=8.10). $[\alpha]_D^{25}$ = -17.5 (c=1.18, CHCl$_3$). $[\alpha]_D^{20}$ = +18.5

(c=0.96, CHCl$_3$) reported for 1,3-bis-((R)-1-phenylethyl)imidazolium tetrafluoroborate[19].

1,3-bis((S)-1-cyclohexylethyl)imidazolium tetrafluoroborate (**19**): Using (S)-(+)-

1-cyclohexylethylamine (2x98 mmol, Alfa-Aesar, 98%, ee 97+%) followed by

recrystallization from ethyl acetate to give 14.65g pale tan crystals (38.9 mmol, 40%

yield). ^{1}H NMR (300 MHz, DMSO-d$_6$): 9.27, 7.90, 4.26, 1.74–1.63, 1.49, 1.22–1.04,

0.97–0.81. ^{13}C NMR (75 MHz, DMSO-d$_6$): 134.5, 121.2, 60.9, 42.4, 28.6, 28.4, 25.6,

25.3, 25.1, 17.4. Analysis calculated for C$_{19}$H$_{33}$BF$_4$N$_2$: C, 60.65; H, 8.84; N, 7.44

(C/N=8.15). Observed C, 61.09; H, 8.64; N, 7.45 (C/N=8.20). $[\alpha]_D^{25}$ = -7.90 (c=1.01,

CHCl$_3$). $[\alpha]_D^{22}$ = +11.2 (c=1.0, CHCl$_3$) reported for 1,3-bis((R)-1-cyclohexylethyl)

imidazolium chloride[21].

1,3-bis((S)-1-cyclohexylpropyl)imidazolium bromide (**20**): (S)-1-

cyclohexylpropylamine was obtained via hydrogenation of (S)-(-)-1-phenylpropylamine

(187.2 mmol, Alfa-Aesar, 99+%, ee 99%) using a Parr shaker apparatus[36, 37]. Partial

hydrogenation was observed using 5% Rh/Al$_2$O$_3$ under acidic aqueous conditions (pH~1)

at 50 psi H$_2$ over approximately 40 hours at room temperature[3]. The catalyst was filtered

off and the aqueous solution made basic with sodium hydroxide. The basic solution was

extracted with diethyl ether, dried over Na$_2$SO$_4$ filtered and concentrated by rotary

evaporation. The crude phenyl + cyclohexyl mixture was further hydrogenated using

---

[3] No reaction was observed under 1 atmosphere H$_2$ in contrast to the report in Reference 4.

PtO_2 in acetic acid at 50 psi H_2 in approximately 12 hours. After careful catalyst separation via filtration, 6N sodium hydroxide solution was added to pH>12. The aqueous phase was extracted with diethyl ether (3x100 mL). The combined organic extracts were washed with brine, dried over Na_2SO_4, filtered and concentrated by rotary evaporation to give 25.2 g clear, colorless (S)-1-cyclohexylpropylamine (178.6 mmol, 95% yield). ^{1}H NMR (300 MHz, $CDCl_3$): 2.29, 1.67–1.65, 1.62–1.52, 1.39, 1.18–1.09, 1.07–0.90, 0.81. ^{13}C NMR (75 MHz, $CDCl_3$): 57.5, 43.3, 29.7, 27.8, 27.3, 26.6, 26.5, 26.4, 10.8.

Imidazolium synthesis was performed using (S)-1-cyclohexylpropylamine from above (2x85.0 mmol). The crude product was recrystallized in several crops from 1:1 methanol/ethyl acetate at -18°C using just enough diethyl ether to give a cloudy solution. The combined crops gave 19.35 g white to off-white crystals (48.7 mmol, 57% yield). ^{1}H NMR (300 MHz, $CDCl_3$): 10.80, 7.38, 4.32, 3.43, 2.07–2.01, 1.94–1.63, 1.25–0.92, 0.78. ^{13}C NMR (75 MHz, $CDCl_3$): 138.0, 120.3, 68.4, 42.2, 30.0, 29.0, 25.9, 25.8, 25.7, 25.0, 10.5. Analysis calculated for $C_{21}H_{37}BrN_2$: C, 63.46; H, 9.38; N, 7.05 (C/N=9.00). Observed C, 62.94; H, 9.57; N, 7.07 (C/N=8.90). $[\alpha]_D^{25}$ = -22.42 (c=1.21, $CHCl_3$).

1,3-bis(((1S,2S,5R)-6,6-dimethylbicyclo[3.1.1]heptan-2-yl)methyl)imidazolium tetrafluoroborate (**21**) (1,3-bis(cis-Myrtanyl)imidazolium tetrafluoroborate): The procedure for bis(cyclopentyl) SDA **7** in Chapter Two was adapted using (-)-cis-Myrtanylamine (2x32.6 mmol, Sigma-Aldrich, 98%). The crude reaction layers were separated after adding 50 mL diethyl ether and 10 mL saturated $KHCO_3$ solution plus 20 mL water. The aqueous layer plus oily residue were extracted with chloroform (3x35 mL). Organic extracts were combined and washed with brine (50 mL), dried over

MgSO$_4$, filtered and stripped down by rotary evaporation to obtain a dark, viscous oil. Further drying under high vacuum yielded a waxy residue. Ethyl acetate (30 mL) was added to the residue and sonication (2x15 minutes) separated a small quantity of pale solids. Diethyl ether (~50 mL) was slowly added until the supernatant became cloudy then the flask was moved to a 4°C refrigerator. Filtration and subsequent drying under high-vacuum gave 9.51 g pale tan solids (22.2 mmol, 68% yield). ^{1}H NMR (300 MHz, DMSO-d$_6$): 9.58, 8.01, 4.29, 3.50, 2.72–2.66, 2.05–1.95, 1.87, 1.72 – 1.69, 1.34, 1.25, 1.06. ^{13}C NMR (75 MHz, CDCl$_3$): 136.3, 122.6, 54.0, 42.6, 41.0, 40.5, 38.2, 32.3, 27.5, 25.2, 22.9, 18.2. Analysis calculated for C$_{23}$H$_{37}$BF$_4$N$_2$: C, 64.49; H, 8.71; N, 6.54 (C/N=9.86). Observed C, 66.09; H, 8.62; N, 6.66 (C/N=9.93). $[\alpha]_D^{25}$ = -13.44(c=1.15, CHCl$_3$).

3.2.2: Inorganic Reactions

All reactions were performed in 23mL PTFE-lined stainless steel autoclaves (Parr Instruments). Hydroxide mediated reactions were tumbled at approximately 40 rpm using spits built into convection ovens. Fluoride mediated reactions were not tumbled. Silica sources were tetraethylorthosilicate (TEOS, Sigma-Aldrich, 98%) for fluoride reactions and Cab-O-Sil M5 fumed silica (Cabot) for hydroxide reactions. Boric acid (J.T. Baker, ACS Reagent) was used for borosilicate reactions and Reheis F-2000 aluminum hydroxide gel (50–53 wt% Al$_2$O$_3$) or NaY zeolite (Tosoh HSZ-320NAA) was used in aluminosilicate reactions. All reactions were performed at 150°C unless otherwise noted. B-Beta was provided by S.I. Zones (Chevron Energy Technology Company, Richmond, CA) and

calcined under nitrogen with a small amount of air to minimize boron hydrolysis. Germanosilicate reactions used TEOS and germanium dioxide (Alfa-Aesar, 99.98%). Silicoaluminophosphate (SAPO) reactions used Cab-O-Sil M5, Reheis F-2000 and 85wt% phosphoric acid (Fisher, ACS Reagent) as silicon, aluminum and phosphorus sources respectively. SAPO gels were prepared by combining silica with SDA^+OH^- solution then adding to the aluminophosphate gel. The combined gel was homogenized then aged overnight at room temperature.

3.2.3: Molecular Modeling

Cerius^2 (Molecular Simulations Inc./Accelrys Software Inc.) was used for molecular modeling. Inorganic frameworks built into the software were used without modification. Framework atom positions and unit cell dimensions were fixed during energy minimizations. All energy minimizations employed the Burchart-Universal Force-Field[38, 39]. Coulombic interactions between the silicate framework and SDA were not included[40]. Reported stabilization energies represent the computed energy difference between the free SDA and the SDA occluded within the silicate framework, normalized by the number of tetrahedral atoms. In general, several SDA starting locations were tried for each guest/host pair although no attempt was made to exhaustively search for global energy minima.

3.2.4: Product Characterization

Powder X-ray diffraction (XRD) patterns were collected on a Scintag XDS-2000 diffractometer equipped with scintillation detector using CuKα radiation. Thermogravimetric analysis (TGA) was performed using a Netzsch STA449C instrument under 75 mL min^{-1} air plus 25 mL min^{-1} Argon at a heating rate of 5°C min^{-1}. Solid-state NMR spectra were collected using either Bruker Avance 200MHz or Bruker DSX 500 MHz instruments. Scanning electron microscopy (SEM) was performed using a JEOL JSM-6700F instrument. Elemental analyses were performed by Galbraith Laboratories (Knoxville, TN).

3.3: Results and Discussion

To investigate the synthesis of zeolite Beta enriched in polymorph A an initial reaction screen was performed using all five chiral SDAs. Three water to silica ratios in pure silica fluoride reactions were performed for all SDAs and at least one boron or aluminum rich hydroxide reaction was attempted. Similar reaction conditions studied in Chapter Two yielded many instances of Beta. Not all hydroxide conditions were studied for each SDA due to reduced SDA quantity. The phases obtained in pure silica fluoride reactions are reported in Table 3.2 while borosilicate and aluminosilicate reaction results are presented in Table 3.3.

Results from pure silica fluoride reactions in Table 3.2 only show five instances of crystalline products. The crystalline products were obtained with two SDAs (**17** and **19)**.

Pleasingly, three of these five contained Beta as the major product. Discovering two chiral SDAs capable of synthesizing Beta was promising as published studies using chiral SDAs only showed one instance of Beta as discussed in Section 3.1. The two remaining instances showed Beta and EU-1 (EUO) using **17**. The XRD pattern of the Beta product obtained using **17** at H_2O/SiO_2=3.5 showed distinct differences in the low angle reflection compared with a typical Beta pattern. The distinct asymmetry in the low angle reflection did not correspond to any simulated XRD patterns for polymorph A/polymorph B intergrowths. Figure 3.4 shows the XRD patterns for Beta products obtained using **17** and **19** at H_2O/SiO_2=3.5.

The phases obtained from hydroxide reactions presented in Table 3.3 again show crystalline products were limited to **17** and **19**. Beta was the major product in four of the five reactions that gave crystalline products. Two unusual Beta XRD patterns were observed using **19** with boron and aluminum lattice substitution. In contrast to the pure silica fluoride reactions the one Beta instance using **17** gave a regular Beta pattern. EU-1 was observed as the major product under borosilicate conditions using **17** and as an impurity under aluminosilicate conditions. Figure 3.5 shows XRD patterns for borosilicate products obtained using **17** and **19**.

Table 3.2: Phases obtained in pure silica fluoride reactions using chiral imidazolium

SDAs

SDA	H_2O/SiO_2		
	3.5	7.5	14.5
17	Beta (odd)[a]	Beta + EU-1 [a]	EU-1 (Beta) [a]
18	Amorphous	Amorphous	Amorphous
19	Beta	Beta	Amorphous
20	Amorphous [a]	Amorphous [a]	Amorphous [a]
21	Amorphous	Amorphous	Amorphous

[a] Reaction performed at 175°C

The odd Beta XRD patterns obtained using **17** and **19** were investigated further and close inspection of the XRD patterns presented in Reference 41(top pattern in Figure 3 and lower patterns in Figure 4) shows clear similarities to the patterns obtained above and those reported for SDA labeled "MBABO[+]" (6-benzyl-1,3,3,6-tetramethyl-6-azoniabicyclo[3.2.1]octane) and several described as Beta/SSZ-31 intergrowths. The authors grouped the distinct Beta product with typical Beta products as additional ^{19}F NMR analysis showed no evidence of resonances typical of fluoride residing in D4R cages. The product obtained from the concentrated fluoride reaction with **17** was analyzed by ^{19}F MAS NMR and a small resonance at -37.0 ppm was visible in addition to the dominant resonance at -70.6 ppm (relative intensity 1.0:18.1). The -37 ppm resonance is characteristic of fluoride residing in D4Rs and therefore this material probably contains some BEC. This could partially explain the observed diffraction pattern, although the quantity of D4Rs indicated by ^{19}F MAS NMR was lower than those reported to show changes in XRD

patterns. For the odd Beta patterns from hydroxide reactions ^{19}F NMR was not possible

and therefore a clear signature was not available to conclusively assign the intergrowth.
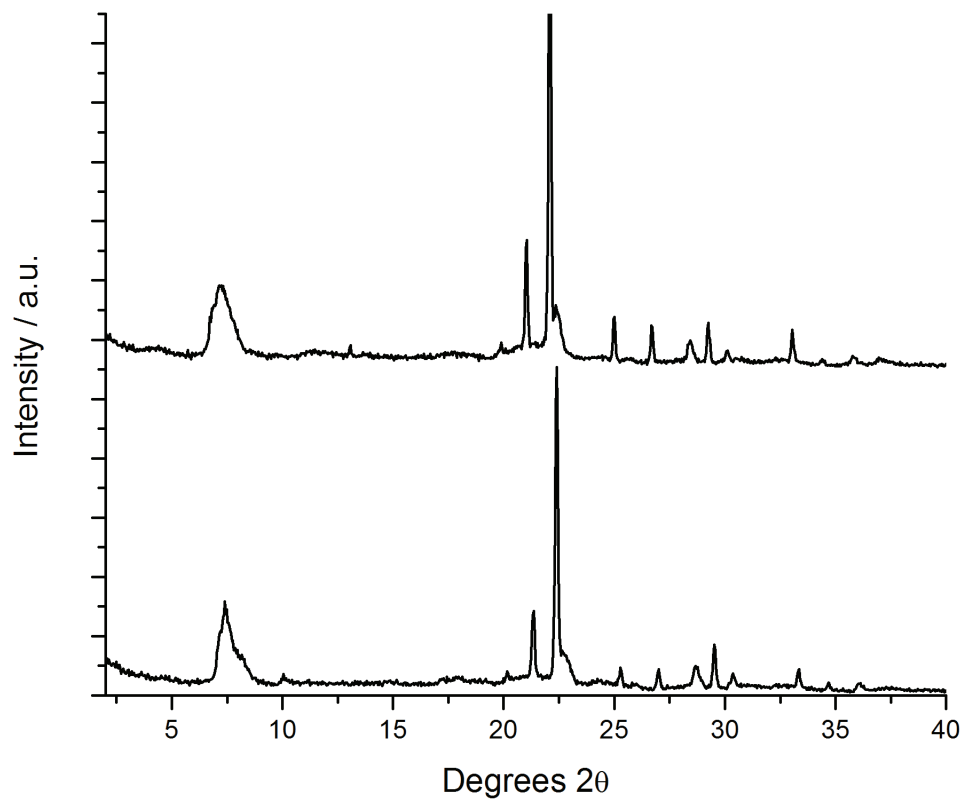
Figure 3.4: XRD patterns of pure silica Beta products using **17** and **19** at H_2O/SiO_2=3.5.

Top=regular Beta obtained with **19** and bottom=odd Beta pattern using **17** with distinct

asymmetry in the low angle reflection

Table 3.3: Phases obtained in aluminosilicate and borosilicate hydroxide reactions using

chiral imidazolium SDAs

SDA	$SiO_2/Al_2O_3=35$ (NaY reaction)	$SiO_2/Al_2O_3=50$	$SiO_2/B_2O_3\leq30$
17	NR	Beta (EU-1)	EU-1 (layered)
18	Amorphous	Amorphous	Amorphous
19	Beta	Beta (odd)	Beta (odd)
20	NR	Amorphous	Amorphous
21	Amorphous (FAU)	NR	NR

NR indicates reaction not run
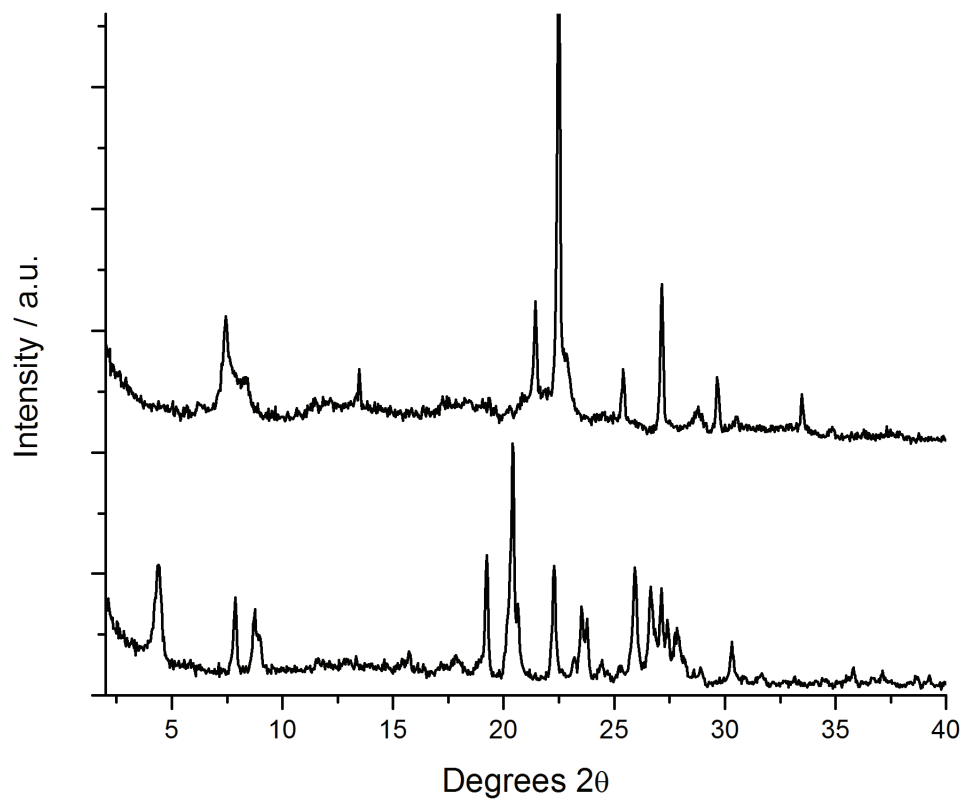
Figure 3.5: Borosilicate hydroxide XRD patterns. Top=Beta with asymmetry in the low

angle reflection using **19** and bottom shows EU-1 plus minor layered using **17**

The initial inorganic reaction matrix gave very promising results with **17** and **19** while the remaining three SDAs gave no crystalline products. This was particularly perplexing in the case of **18** as the SDA was almost identical to **19** that exhibited strong specificity to Beta materials. The inability of **20** and **21** to form products could be due to higher hydrophobicity. Although bis(adamantyl) SDA **15** studied in Chapter Two produced three crystalline phases, it could be argued that this arose from the unique properties of the adamantyl groups (bulky, rigid and hydrothermally stable). Therefore, while it was possible to synthesize crystalline products using **15** with $\Sigma(C+N)=25$ this may represent an exceptional case. In light of this, no additional reactions were attempted with **20** and **21** while independent studies were undertaken using **18** and **19**. The additional reactions using **18** were aimed at producing any crystalline phase, whereas those with **19** were aimed at perturbing the reaction environment such that polymorph A enriched Beta might be obtained.

Table 3.4 summarizes additional reactions performed with **19** in attempts to obtain polymorph A enriched Beta. The first group was additional fluoride reactions (Entries 1–5). Entries 1–4 added aluminum or boron to the gel to probe the role framework charge might have on the product phase. The aluminosilicate and borosilicate hydroxide reactions with this SDA gave several instances of the odd Beta pattern in contrast to pure silica reactions that did not. Therefore, it was hypothesized that framework charge introduced by aluminum or boron substitution might be responsible for the observed XRD patterns. These reactions gave amorphous products for all aluminosilicate reactions while regular Beta was obtained with boron addition. Entries 1–3 were particularly intriguing as aluminum addition completely suppressed product formation at all water to silica ratios.

The H_2O/SiO_2=3.5 reaction was particularly surprising as low water content and aluminum introduction separately favor formation of open structures with low framework density, with Beta being particularly common. Entry 5 used the inorganic conditions Cantín et al. employed to synthesize pure silica BEC using Diels-Alder SDA **VII**[12]. Under these conditions only K_2SiF_6 was observed.

Entries 6-13 were aluminosilicate or borosilicate hydroxide reactions with perturbations to the gel composition. The first group (6–10) employed seeding in attempts to induce polymorph A nucleation and growth. Seeding often increases product formation rate as suitable nuclei for crystal growth are introduced into the reaction gel. In addition, seeding can improve product purity by suppressing growth of competing phases. In this regard, polymorph B and one polymorph A intergrowth could be viewed as competing phases to the desired enantiopure polymorph A structure. All five entries gave Beta, and all four borosilicate reactions gave the odd Beta pattern presented in Figures 3.4 and 3.5. Interestingly, no asymmetry was observed in the seeded aluminosilicate reaction (Entry 10). Seeded reactions at 150°C gave faster product formation, e.g., Entry 6 showed nice phase separation after four days whereas the unseeded reaction required 18 days. Entries 6–8 also explored seeded reactions at different temperatures to investigate if lower thermal energy could lead to polymorph A enrichment. The results showed the same XRD pattern at each temperature. Similarly, substituting KOH for NaOH did not alter the product XRD pattern.

The final subset added chiral amino alcohols to perturb the reaction gel. Gel compositions were modeled after those employed to synthesize SSZ-25 using a mixed quaternary ammonium/amine system[42]. Leucine- and proline-derived amino alcohols (S)-

leucinol and (S)-1-methyl-2-pyrrolidinemethanol were used as chiral additives. No effect was observed in the aluminosilicate reaction whereas quartz and quartz plus minor Beta were obtained under borosilicate conditions. This approach did not have any positive effect so was not investigated further.

The final reactions undertaken were aimed at synthesizing a one dimensional product that could have a helical pore. The two reactions were at $SiO_2/Al_2O_3=100$ and ∞ respectively. The SAR=100 gave Beta while the pure silica reaction gave quartz. These results are in agreement with those observed using bis(cyclooctyl) SDA **13** in Chapter Two where Beta was observed under all conditions except pure silica hydroxide. With no trivalent lattice substitution both SDAs were unable to crystallize Beta.

Table 3.4: Summary of additional inorganic reaction attempts using **19**

Entry	Gel Composition	Phase
1	$1.0SiO_2$:$0.02Al_2O_3$:$0.5SDA^+OH^-$:$0.5HF$:$3.0H_2O$	Amorphous
2	$1.0SiO_2$:$0.02Al_2O_3$:$0.5SDA^+OH^-$:$0.5HF$:$7.0H_2O$	Amorphous
3	$1.0SiO_2$:$0.02Al_2O_3$:$0.5SDA^+OH^-$:$0.5HF$:$14.0H_2O$	Amorphous
4	$1.0SiO_2$:$0.05B_2O_3$:$0.5SDA^+OH^-$:$0.5HF$:$7.0H_2O$	Beta
5	$1.0SiO_2$:$0.5SDA^+OH^-$:$0.25KOH$:$0.5HF$:$7.25H_2O$	K_2SiF_6
6	$1.0SiO_2$:$0.03B_2O_3$:$0.2SDA^+OH^-$:$0.1NaOH$:$50.0H_2O$[a]	Beta (odd)
7	$1.0SiO_2$:$0.03B_2O_3$:$0.2SDA^+OH^-$:$0.1NaOH$:$50.0H_2O$[a,b]	Beta (odd)
8	$1.0SiO_2$:$0.03B_2O_3$:$0.2SDA^+OH^-$:$0.1NaOH$:$50.0H_2O$[a,c]	Beta (odd)
9	$1.0SiO_2$:$0.03B_2O_3$:$0.2SDA^+OH^-$:$0.1KOH$:$50.0H_2O$[a]	Beta (odd)
10	$1.0SiO_2$:$0.02Al_2O_3$:$0.2SDA^+OH^-$:$0.1KOH$:$40.0H_2O$[d]	Beta
11	$1.0SiO_2$:$0.03B_2O_3$:$0.1SDA^+OH^-$:$0.1NaOH$:$0.2amine$[e]:$50.0H_2O$[a]	Quartz
12	$1.0SiO_2$:$0.03B_2O_3$:$0.1SDA^+OH^-$:$0.1NaOH$:$0.2amine$[f]:$50.0H_2O$[a]	Quartz (Beta)
13	$1.0SiO_2$:$0.02Al_2O_3$:$0.1SDA^+OH^-$:$0.1NaOH$:$0.2amine$[e]:$50.0H_2O$[d]	Beta
14	$1.0SiO_2$:$0.01Al_2O_3$:$0.15SDA^+OH^-$:$0.1KOH$:$40.0H_2O$[g]	Beta
15	$1.0SiO_2$:$0.00Al_2O_3$:$0.15SDA^+OH^-$:$0.1KOH$:$40.0H_2O$[g]	Quartz

[a]Added calcined B-Beta seeds

[b]Reaction performed at 135°C

[c]Reaction performed at 115°C

[d]Added calcined Beta seeds

[e]Added (S)-1-methyl-2-pyrrolidinemethanol as chiral amine

[f]Added (S)-leucinol as chiral amine

[g]Performed at 160°C

The combined results presented in Tables 3.2–3.4 show many instances of Beta using SDAs **17** and **19** and several show asymmetry in the low angle XRD reflection. Further analysis was performed on the solid products in attempts to gain insight into the differences in XRD patterns. Thermogravimetric analysis (TGA) was performed on solids

obtained from reactions discussed above. Nine products were selected encompassing amorphous, Beta and Beta with asymmetric low angle reflections ("odd" Beta). Table 3.5 presents the mass loss between 200 and 620°C. This temperature range broadly measures the organic content occluded within the silicate host. Any mass loss below 200°C was assigned to bound water with many pure silica fluoride products showing negligible mass loss < 200°C (<0.5 wt%).

The organic content for both aluminosilicate fluoride reactions using **19** at H_2O/SiO_2=3.5 and 7.5 was low at 6.6 and 6.5 wt% respectively. The reported mass loss also includes any fluorine bonded to silica. The low organic content suggests aluminum addition created unfavorable organic/silicate interactions thereby preventing nucleation. In comparison, the eight reactions yielding Beta show mass loss ranging from 22.1 to 17.5 wt%. The measured mass loss for the four fluoride reactions includes fluorine bonded to silica. This complicates the analysis as 1–2 wt% fluorine was expected based on elemental analyses presented in Chapter Two. The remaining Beta products contain no fluorine and show subtle differences in organic content. Products with odd Beta XRD patterns show slightly higher organic content compared to the normal Beta product. This suggests the odd XRD pattern may result from slightly higher organic content in certain Beta products.

Table 3.5: Thermogravimetric analysis of inorganic reaction products using **17** and **19**

Phase	SDA	Notes	Mass loss / wt%
Amorphous	**19**	Aluminosilicate fluoride, H_2O/SiO_2=3.5	6.6
Amorphous	**19**	Aluminosilicate fluoride, H_2O/SiO_2=7.5	6.5
Beta (odd)	**17**	Pure silica fluoride, H_2O/SiO_2=3.5	22.1
Beta	**17**	Aluminosilicate hydroxide, NaOH	18.4
Beta	**19**	Pure silica fluoride, H_2O/SiO_2=3.5	21.1
Beta	**19**	Pure silica fluoride, H_2O/SiO_2=7.5	20.6
Beta	**19**	Borosilicate fluoride, H_2O/SiO_2=7.5	19.0
Beta (odd)	**19**	Borosilicate hydroxide, seeded, NaOH	18.4
Beta (odd)	**19**	Borosilicate hydroxide, seeded, KOH	19.3
Beta	**19**	Aluminosilicate hydroxide, seeded, KOH	17.5

In addition, solid-state NMR analysis was performed to ensure the occluded organic was intact. Figures 3.6 and 3.7 show ^{13}C cross-polarization magic-angle spinning (CP-MAS) NMR of Beta products obtained using **19** and **17** respectively. Both figures include the ^{13}C liquid NMR spectra of the parent salt recorded in deuterated dimethyl sulfoxide. Both figures show evidence of imidazolium carbon resonances at ~135 and 120 ppm and alkyl carbons between 65 and 10 ppm. The imidazolium resonances are broad due to less efficient cross-polarization and/or constrained motion. These spectra are in agreement with the parent SDA spectra. The top spectrum in Figure 3.6 shows two resonances at 125 and 121 ppm whereas the other spectra do not show this. The ~120 ppm resonance in liquid ^{13}C spectra arises from the C(4) and C(5) carbons of the imidazolium ring. Observing apparent splitting suggests these carbons may reside in different environments within the host framework. A similar observation was noted for 1,4-diazabicyclo[2.2.2]octane-

derived quaternary polymer molecules residing in gmelinite (GME)[43]. In contrast to the apparent splitting observed for **19**, one resonance at ~121 ppm was observed for **17**. The spectrum for **17** occluded within Beta shows relatively sharp imidazolium resonances compared to those for **19**. This could be due to greater mobility within the channels for the smaller SDA **17**.
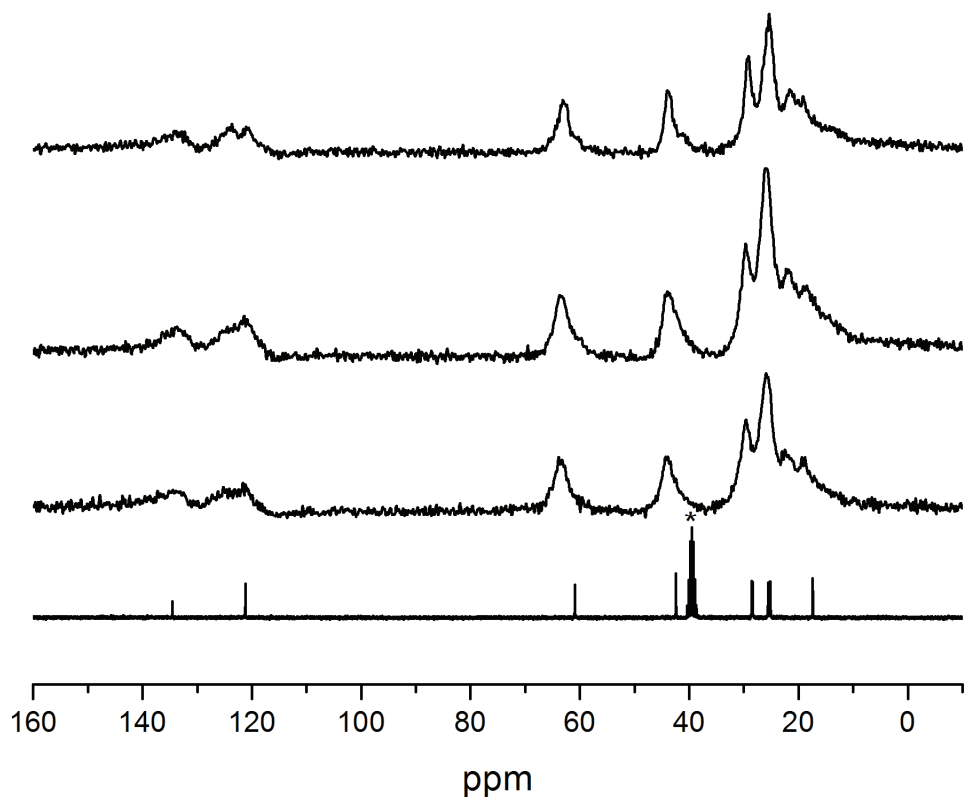
Figure 3.6: ^{13}C CP-MAS NMR of Beta products using **19**. Top to bottom: Pure silica fluoride at H_2O/SiO_2=3.5, aluminosilicate hydroxide (SAR=50), borosilicate hydroxide (seeded) and liquid ^{13}C NMR of tetrafluoroborate salt (asterisk denotes NMR solvent resonances)
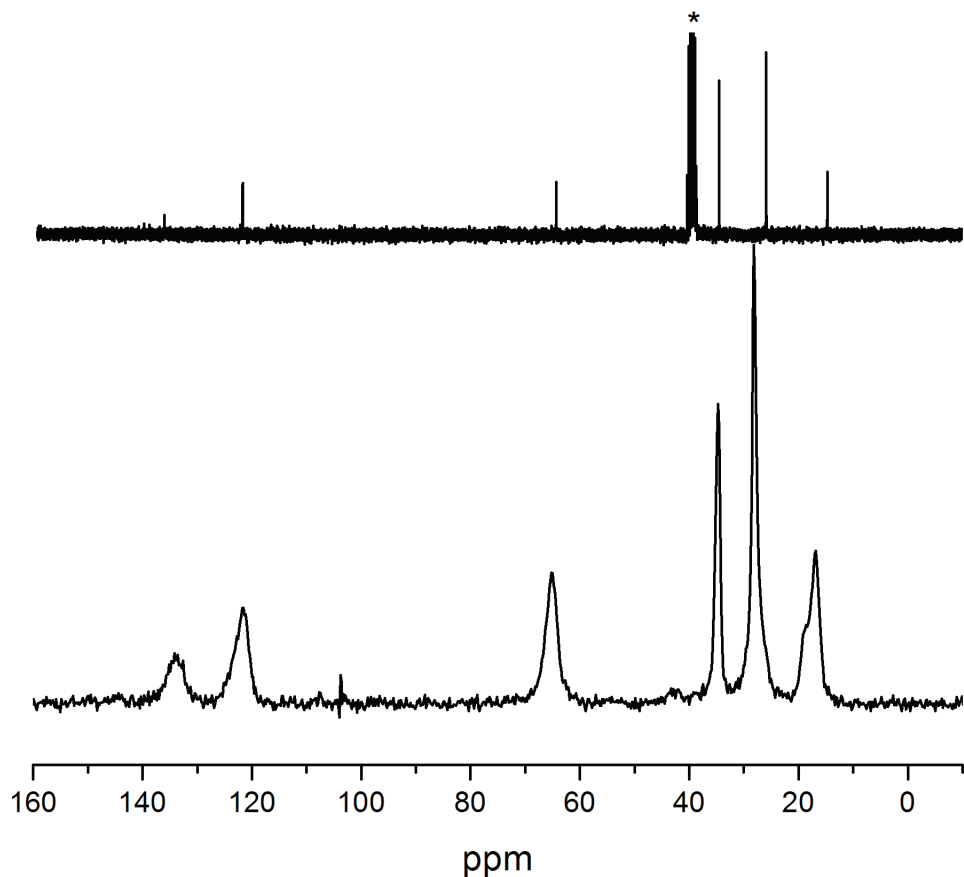
Figure 3.7: ^{13}C CP-MAS NMR of Beta products using **17**. Top spectra shows liquid ^{13}C NMR of chloride salt (asterisk denotes NMR solvent resonances) and bottom shows ^{13}C CP-MAS NMR of Beta product

Table 3.6 presents the additional inorganic reactions attempted using **18**. Entries 1 and 2 used calcined boron-Beta (B-Beta) either as the entire source of tetrahedral atoms (Si and B, 1) or as seed material (2). The gel composition for the B-Beta transformation was based on reported conditions where rapid transformations to a variety of products occurred[44] while the seeded reaction was as reported in Table 3.4. Beta was observed by XRD after 39 days at 150°C for the B-Beta reaction. This implied the SDA occupied the

void volume within the framework thereby preventing dissolution. TGA of the recovered product gave 17.7 wt% mass loss between 200 and 620°C confirming organic occlusion. In contrast, the addition of B-Beta seeds to an unstructured borosilicate gel resulted in layered product formation. This was in stark contrast to the entries in Table 3.4 using **19** where seeded reactions yielded rapid Beta formation.

A collection of reactions with varying aluminum content was considered next (Entries 3–5). Entry 3 repeated the NaY reaction reported in Table 3.2 but with additional NaOH (NaOH/SiO$_2$=0.4 *cf* 0.1 in Table 3.2). Entries 4 and 5 used the same gel compositions as Entries 14 and 15 in Table 3.4 in a similar attempt to synthesize one-dimensional products. The three reactions gave Mordenite (MOR), layered and quartz respectively. As discussed in Chapter Two, MOR appears very frequently in NaY reactions with increasing Na$^+$ content and can be considered the default product. Obtaining layered material and quartz from the low aluminum reactions also suggests unfavorable organic/silicate interactions with both phases undesirable.

The final reaction collection explored germanosilicate reactions as germanium incorporation has lead to the discovery of many new materials. Germanium inclusion often directs the formation of small cages, with D4Rs very common. Fluoride addition to germanosilicate gels has been shown to accelerate product formation through cooperative stabilization of D4Rs[9]. Three germanosilicate reactions were investigated at Si/Ge≤10 and low water content (H$_2$O/SiO$_2$≤3.5)[45]. The two germanosilicate fluoride reactions (Entries 6 and 7) also included aluminum at (SiO$_2$+GeO$_2$)/Al$_2$O$_3$=75 to further enhance the prospect of synthesizing open framework structures. All three reactions yielded amorphous products, with weak AlPO$_4$-16 (AST) reflections visible in the hydroxide reaction. AST is

a clathrate phase constructed entirely of connected D4Rs. The AST cages are not large enough to occlude an intact SDA suggesting minor organic degradation may occur under the synthesis conditions.

Table 3.6: Summary of additional inorganic reaction attempts using **18**

Entry	Gel Composition	Phase
1	$1.0SiO_2:0.03B_2O_3:0.15SDA^+OH^-:0.1NaOH:30.0H_2O$[a]	Beta
2	$1.0SiO_2:0.03B_2O_3:0.2SDA^+OH^-:0.1NaOH:50.0H_2O$[b]	Layered
3	$1.0SiO_2:0.029Al_2O_3:0.25SDA^+OH^-:0.4NaOH:30.0H_2O$[c]	Mordenite
4	$1.0SiO_2:0.01Al_2O_3:0.15SDA^+OH^-:0.1KOH:40.0H_2O$[d]	Layered
5	$1.0SiO_2:0.00Al_2O_3:0.15SDA^+OH^-:0.1KOH:40.0H_2O$[d]	Quartz
6	$1.0SiO_2:0.2GeO_2:0.016Al_2O_3:0.6SDA^+OH^-:0.6HF:3.6H_2O$	Amorphous
7	$1.0SiO_2:0.1GeO_2:0.015Al_2O_3:0.55SDA^+OH^-:0.55HF:3.3H_2O$	Amorphous
8	$1.0SiO_2:0.11GeO_2:0.50SDA^+OH^-:3.5H_2O$[e]	Amorphous(AST)

[a]Calcined B-Beta used as Si and B source

[b]Added calcined B-Beta seeds

[c]NaY reaction at $SiO_2/Al_2O_3=35$

[d]Performed at 160°C

[e]Performed at 170°C

From the combined inorganic reactions presented above using **18** it was very clear that this SDA was not likely to synthesize a zeolite phase. This shows that very subtle changes to an SDA can effect profound changes on the products obtained. In this case, replacing the cyclohexyl groups of **19** with the phenyl groups of **18** transforms a SDA selective to Beta to one that did not direct the formation of any product. The alkyl-substituted imidazoliums studied by others and presented in Chapter Two were stable under

synthesis conditions while the bis(aryl) SDAs **14** and **16** studied in Chapter Two appeared to degrade significantly faster. For these aryl-substituted imidazoliums, hydroxide attack at the more acidic C(2) proton[46] may have lead to faster degradation. However, reported acidities of benzyl-substituted imidazolium and benzimidazolium salts do not show significantly lower pKa values compared to alkyl substituted salts[46, 47]. To check that the SDA remained intact under synthesis conditions elemental analysis and ^{13}C CP-MAS NMR were performed.

The amorphous products from pure-silica fluoride reactions using **18** were subjected to elemental analysis for carbon, nitrogen and fluorine. Table 3.7 shows very low organic incorporation for the reactions at higher water to silica ratios. The entry for the concentrated reaction does show ~14 wt% combined carbon, nitrogen and fluorine. In addition, the measured carbon to nitrogen ratio of 7.7 was close to the expected ratio of 8.2. The calculated carbon to nitrogen ratio for the intermediate dilution product was substantially lower than expected for the parent SDA (3.2 *cf* 8.2). This indicates organic degradation occurred for the intermediate dilution reaction, whereas the organic remained substantially intact in the concentrated reaction. These data suggest the SDA was stabilized by the surrounding silicate species under concentrated conditions whereas at higher water dilution the SDA/silicate interaction was not favorable and therefore the SDA was exposed to degradation. In addition, the fluorine/nitrogen weight ratio for the concentrated reaction was 1.51. This was more than double the value expected for SDA$^+$F$^-$ (wt% F/wt% N=0.68) suggesting fluorine-rich silicon species may be present (e.g., $[SiF_6]^{2-}$). The unusually high fluorine content could explain why no tetrahedral SiO_2 framework was obtained in any reaction.

Table 3.7: Carbon, Nitrogen and Fluorine content of amorphous products from pure silica

fluoride reactions **18**

H$_2$O/SiO$_2$	Carbon / wt%	Nitrogen / wt%	Fluorine / wt%	C/N
3.5	10.81	1.40	2.11	7.7
7.5	3.30	1.02	1.52	3.2
14.5	1.44	<0.50	0.91	N/A

In addition to chemical analysis, ^{13}C CP-MAS NMR was performed on two products using **18**. These were the concentrated pure silica fluoride reaction that showed organic incorporation by elemental analysis and the B-Beta reaction product. Figure 3.8 shows the liquid ^{13}C NMR of the parent tetrafluoroborate salt in addition to the ^{13}C CP-MAS NMR spectra for each product. Aromatic and alkyl resonances are visible for each product and agree with those of the parent SDA. This confirms the SDA did not degrade significantly under these two reaction conditions.
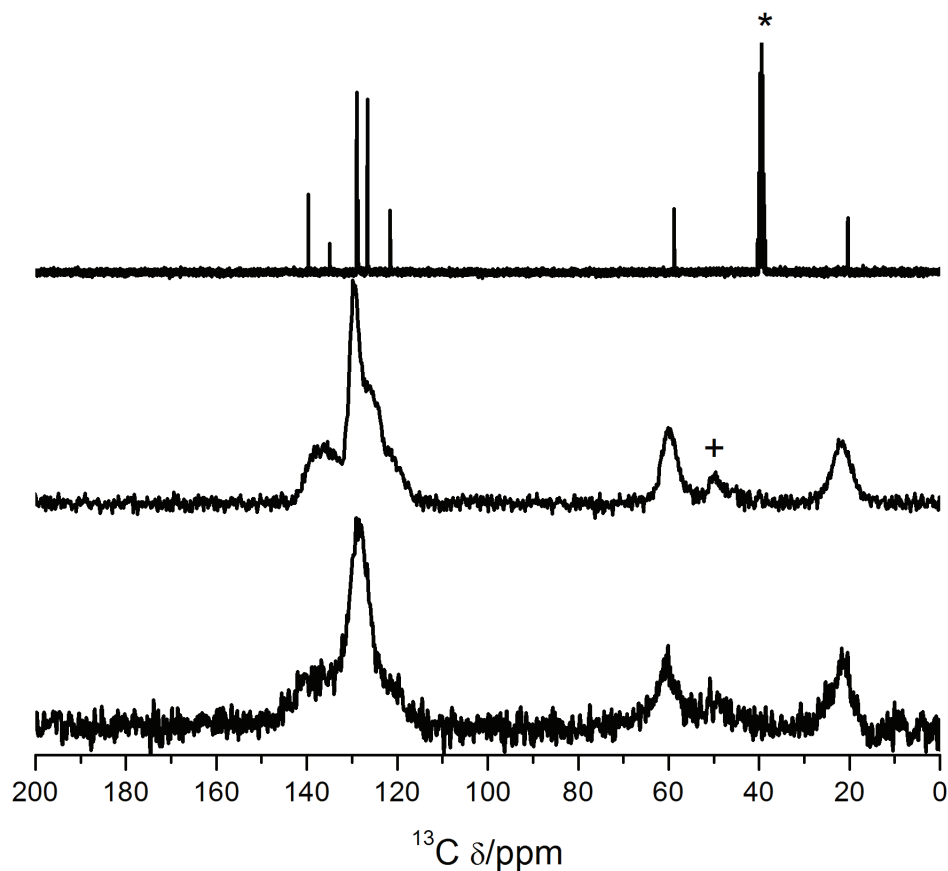
Figure 3.8: Liquid ^{13}C NMR of SDA **18** and ^{13}C CP-MAS NMR of products using **18**.
Top to bottom=liquid NMR spectrum, B-Beta reaction product and pure-silica product at
H_2O/SiO_2=3.5. * denotes resonances from the NMR solvent and + indicates spinning
side-band.

The additional investigations with **19** did not reveal instances of polymorph A
enriched Beta. Without any success in crystallizing an enriched chiral product in high
silica chemistry, silicoaluminophosphate (SAPO) reactions were explored using **17** and **19**.
In contrast to the inorganic reactions presented above, SAPO reactions occur under acidic
conditions and this may offer alternative guest/host interactions. The gel compositions

used were: 1.0 Al_2O_3:1.0 P_2O_5:0.2 SiO_2:0.3 SDA^+OH^-:0.3 HX:55.0 H_2O, where X was Cl or F (HCl or HF). SAPO products reflect aluminophosphate (AlPO) frameworks and therefore contain even numbered rings exclusively[48]. Therefore, Beta would not be possible in these reactions as all polymorphs contain 5 MRs. Table 3.8 gives the phases obtained from SAPO reactions using **17** and **19**. Only $AlPO_4$-5 (AFI) and an unknown dense phase were observed. AFI has a one-dimensional large pore structure and is commonly observed in AlPO reactions. The organic stabilizes the growing crystal in an analogous manner to high silica zeolite reactions. This indicates both **17** and **19** reside in the straight pores of AFI. The straight pores in Beta polymorphs A and B are approximately the same diameter as in AFI and this suggests both SDAs may reside in these channels rather than the desired [001] sinusoidal channel of polymorph A. As a default phase was obtained in the initial SAPO reactions additional experiments were not performed as AFI was expected to dominate.

Table 3.8: Phases obtained from silicoaluminophosphate (SAPO) inorganic reactions

using **17** and **19**

SDA	SDA^+OH^- + HCl	SDA^+OH^- + HF
18	AFI[a]	AFI
20	Dense	AFI[a]

[a]Minor impurity present

The experimental results discussed above show two SDAs capable of synthesizing Beta but no detectable enrichment in polymorph A was observed. To gain further insight

into why no enrichment occurred molecular modeling was performed. Molecular modeling gives an estimated thermodynamic fit for a given guest/host pair plus a visual representation of possible organic conformations within the host. The modeling investigated guest/host interactions of **17** in *BEA ($P4_122$) and EUO, and **19** in *BEA ($P4_122$). No additional phases were considered for **19** as the experimental results presented above showed this SDA only synthesized Beta in high silica reactions.

SDA **17** was investigated first as two product phases were obtained allowing a comparison of the respective stabilization energies. The EUO pores consist of 10MR channels with deep side pockets delimited by 12MR openings. The SDA was found to nicely occupy the side pockets with calculated stabilization of -7.0 kJ mol^{-1} T_d atom. The SDA size and location agrees with those found through single crystal diffraction techniques for dibenzyldimethylammonium derived SDAs in ZSM-50 (EUO)[49].
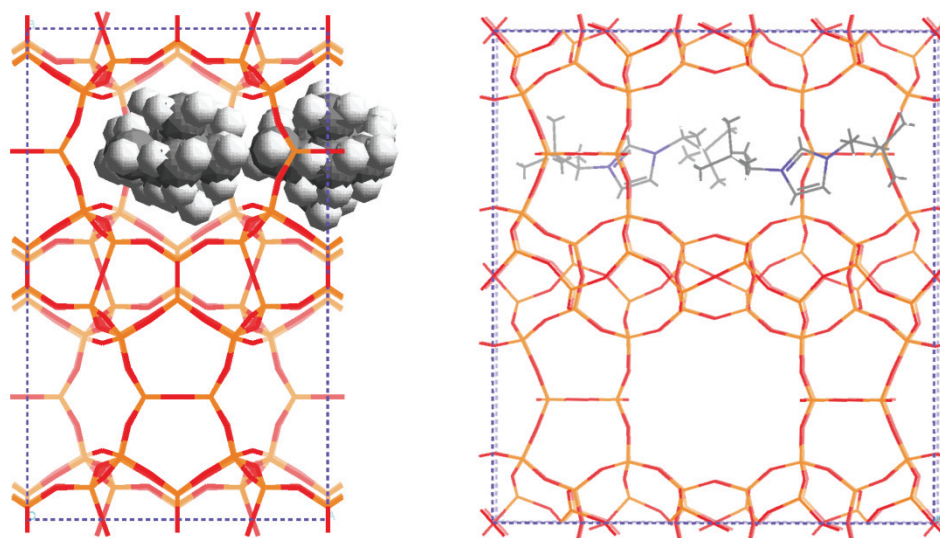
Figure 3.9: Energy-minimized location of **17** in EUO. Left panel shows [001] view

perpendicular to [100] 10MR pore, right panel shows [100] view along 10MR pore

In contrast to EUO, *BEA contains intersecting 12MR pores in all three crystallographic directions and several packing arrangements could be envisioned. Initial organic positions were investigated with molecules occupying the [100]/[010] pores exclusively as shown in Figure 3.10. The SDA molecules were accommodated in the straight pores with calculated stabilization of -10.2 kJ mol^{-1} T_d atom. The stabilization energy was lower than reported for **VI** in each Beta polymorph (-11 to -12 kJ mol^{-1} T_d atom). The slightly higher stabilization offered by the pyrrolidinium SDA **VI** could explain why greater ordering was observed compared to the present case. The calculated stabilization energies suggest more favorable interactions in *BEA yet EUO was observed under several conditions underscoring the importance of kinetic factors. In addition to the calculated stabilization energy, the organic content was checked. The cell shown in Figure

3.10 contains 8 SDA molecules and 128 Si atoms. This corresponds to 19.8 wt% organic content as a fraction of the total cell mass. This agrees with the TGA data given in Table 3.4. In this configuration the SDA molecule does not project any "handedness" across the fault planes along [001]. To accommodate one SDA along [001] an adjacent SDA running perpendicular was impeded. To avoid overlap the adjacent SDA must be removed; however, this would lower the organic content and not agree with the observed TGA data.
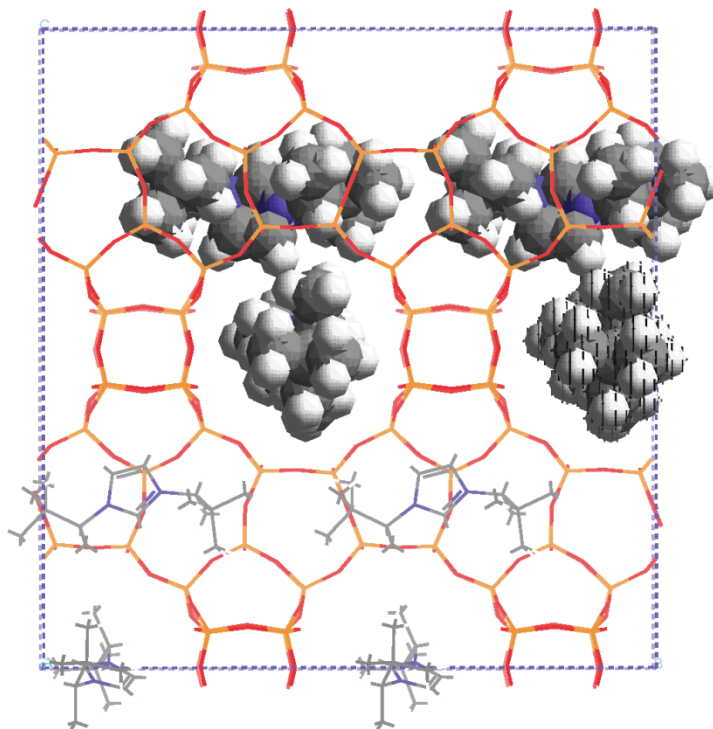
Figure 3.10: Energy-minimized location of **17** in *BEA

For **19** in *BEA a similar initial arrangement of [100]/[010] placement was implemented. In this case the larger SDA could be accommodated within the 12MR but with only one in each direction (the simulation cell was deeper compared to above). Figure

3.11 shows an energy minimized configuration for this case. This configuration did not fill the entire void volume efficiently with attempts to enlarge the cell further resulting in very slow energy minimizations. The cell as shown contains 8 SDA molecules and 256 Si atoms corresponding to 13.1 wt% organic content as a fraction of the total cell mass. Stabilization calculations gave -5.5 kJ mol^{-1} T_d atom. While both are lower than reported for **17** the SDA does appear to fit within the straight 12MR pores again explaining why minimal ordering was observed. Rotating one SDA to align with the [001] pore gave overlap as described above.
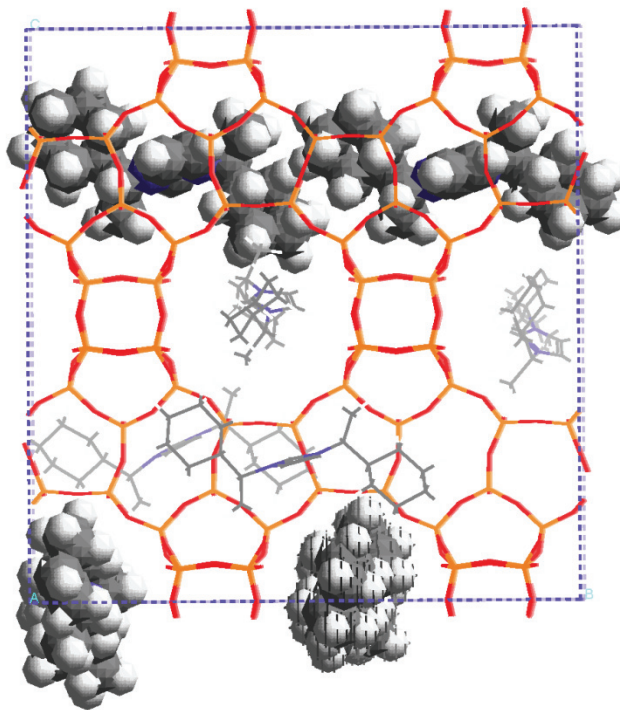
Figure 3.11: Energy minimized location of **19** in *BEA

These simulations show careful consideration must be given to filling the entire available void volume while still trying to project chirality across the [001] fault planes. In this regard large SDA molecules have the length necessary to span a fault plane; however, efficiently filling the void volume becomes unlikely.

3.4: Conclusions

Guest/host relationships were investigated for a series of five chiral imidazolium SDAs aimed at synthesizing Beta polymorph A or another chiral product. 1,3-bis((S)-3,3-dimethylbutan-2-yl)imidazolium synthesized Beta and EUO, while 1,3-bis((S)-1-cyclohexylethyl)imidazolium only made Beta. XRD patterns for many products using both SDAs showed distinct differences by XRD to regular Beta, although this did not correspond to polymorph A enrichment. Molecular modeling combined with TGA indicated both molecules occupy the straight 12MR [100] and [010] pores of Beta polymorphs A and B. In this conformation no significant chirality was projected across the [001] fault planes explaining why no enrichment was observed. The remaining three SDAs did not direct the formation of any crystalline phases. Increased hydrophobicity for 1,3-bis((S)-1-cyclohexylpropyl)imidazolium and 1,3-bis(cis-Myrtanyl)imidazolium was likely responsible for not obtaining crystalline products. No similar argument could be made for 1,3-bis((S)-1-phenylethyl)imidazolium as it has the same $\Sigma(C+N)$ as 1,3-bis((S)-1-cyclohexylethyl)imidazolium that successfully made Beta.

3.5: References

1.   R. L. Wadlinger, G. T. Kerr and E. J. Rosinski, US Patent No. 3,308,069 (1967).

2.   J. M. Newsam, M. M. J. Treacy, W. T. Koetsier and C. B. Degruyter, Proceedings of the Royal Society of London Series A—Mathematical Physical and Engineering Sciences **420** (1859), 375–405 (1988).

3.   M. M. J. Treacy and J. M. Newsam, Nature **332** (6161), 249–251 (1988).

4.   J. B. Higgins, R. B. Lapierre, J. L. Schlenker, A. C. Rohrman, J. D. Wood, G. T. Kerr and W. J. Rohrbaugh, Zeolites **8** (6), 446–452 (1988).

5.   http://www.iza-structure.org/databases/.

6.   J. H. Yu and R. R. Xu, Journal of Materials Chemistry **18** (34), 4021–4030 (2008).

7.   L. Tang, L. Shi, C. Bonneau, J. Sun, H. Yue, A. Ojuva, B.-L. Lee, M. Kritikos, R. G. Bell, Z. Bacsik, J. Mink and X. Zou, Nat Mater **7** (5), 381–385 (2008).

8.   J. Sun, C. Bonneau, A. Cantin, A. Corma, M. J. Diaz-Cabanas, M. Moliner, D. Zhang, M. Li and X. Zou, Nature **458** (7242), 1154–1157 (2009).

9.   T. Blasco, A. Corma, M. J. Diaz-Cabanas, F. Rey, J. Rius, G. Sastre and J. A. Vidal-Moya, Journal of the American Chemical Society **126** (41), 13414–13423 (2004).

10.   T. Conradsson, M. S. Dadachov and X. D. Zou, Microporous and Mesoporous Materials **41** (1–3), 183–191 (2000).

11.   A. Corma, M. T. Navarro, F. Rey, J. Rius and S. Valencia, Angewandte Chemie International Edition **40** (12), 2277–2280 (2001).

12. Á. Cantín, A. Corma, M. J. Díaz-Cabaña, J. L. Jordá, M. Moliner and F. Rey, Angewandte Chemie International Edition **45** (47), 8013–8015 (2006).

13. M. Moliner, P. Serna, A. Cantin, G. Sastre, M. J. Diaz-Cabanas and A. Corma, The Journal of Physical Chemistry C **112** (49), 19547–19554 (2008).

14. A. W. Burton, S. Elomari, I. Chan, A. Pradhan and C. Kibby, The Journal of Physical Chemistry B **109** (43), 20266–20275 (2005).

15. M. M. J. Treacy, J. M. Newsam and M. W. Deem, Proceedings of the Royal Society of London: Mathematical and Physical Sciences **433** (1889), 499–520 (1991).

16. M. E. Davis and R. F. Lobo, Chem. Mater. **4** (4), 756–768 (1992).

17. W. A. Herrmann, L. J. Goossen, G. R. J. Artus and C. Kocher, Organometallics **16** (11), 2472–2477 (1997).

18. A. Alexakis, Caroline L. Winn, F. Guillen, J. Pytkowicz, S. Roland and P. Mangeney, Advanced Synthesis & Catalysis **345** (3), 345–348 (2003).

19. C. L. Winn, F. Guillen, J. Pytkowicz, S. Roland, P. Mangeney and A. Alexakis, Journal of Organometallic Chemistry **690** (24–25), 5672–5695 (2005).

20. M. C. Perry and K. Burgess, Tetrahedron—Asymmetry **14** (8), 951–961 (2003).

21. Y. Suzuki, K. Muramatsu, K. Yamauchi, Y. Morie and M. Sato, Tetrahedron **62** (2–3), 302–310 (2006).

22. T. Kano, K. Sasaki and K. Maruoka, Organic Letters **7** (7), 1347–1349 (2005).

23. Y. Kubota, M. M. Helmkamp, S. I. Zones and M. E. Davis, Microporous Materials **6** (4), 213–229 (1996).

24. K. Tsuji, P. Wagner and M. E. Davis, Microporous and Mesoporous Materials **28** (3), 461–469 (1999).

25. I. Ogino and M. E. Davis, Microporous and Mesoporous Materials **67** (1), 67–78 (2004).

26. R. F. Lobo and M. E. Davis, Journal of the American Chemical Society **117** (13), 3764–3779 (1995).

27. Y. Nakagawa, US Patent No. 5,271,922 (1993).

28. M. Yoshikawa, P. Wagner, M. Lovallo, K. Tsuji, T. Takewaki, C. Y. Chen, L. W. Beck, C. Jones, M. Tsapatsis, S. I. Zones and M. E. Davis, Journal of Physical Chemistry B **102** (37), 7139–7147 (1998).

29. A. Corma, M. J. Diaz-Cabanas, J. Martinez-Triguero, F. Rey and J. Rius, Nature **418** (6897), 514–517 (2002).

30. A. Corma, M. J. Diaz-Cabanas, M. Moliner and C. Martinez, Journal of Catalysis **241** (2), 312–318 (2006).

31. K. Tsuji and M. E. Davis, Microporous Materials **11** (1–2), 53–64 (1997).

32. A. Corma, M. Moliner, A. Cantin, M. J. Diaz-Cabanas, J. L. Lorda, D. L. Zhang, J. L. Sun, K. Jansson, S. Hovmoller and X. D. Zou, Chemistry of Materials **20** (9), 3218–3223 (2008).

33. M. D. Kadgaonkar, M. W. Kasture, D. S. Bhange, P. N. Joshi, V. Ramaswamy, N. M. Gupta and R. Kumar, Microporous and Mesoporous Materials **105** (1–2), 82–88 (2007).

34. M. D. Kadgaonkar, M. W. Kasture, D. S. Bhange, P. N. Joshi, V. Ramaswamy and R. Kumar, Microporous and Mesoporous Materials **101** (1–2), 108–114 (2007).

35. Y. Takagi, T. Komatsu and Y. Kitabata, Microporous and Mesoporous Materials **109** (1–3), 567–576 (2008).

36. M. Strotmann and H. Butenschon, Synthetic Communications **30** (22), 4173–4176 (2000).

37. W. J. McGahren and M. P. Kunstmann, The Journal of Organic Chemistry **37** (6), 902–906 (1972).

38. E. D. Burchart, V. A. Verheij, H. Vanbekkum and B. Vandegraaf, Zeolites **12** (2), 183–189 (1992).

39. A. K. Rappe, C. J. Casewit, K. S. Colwell, W. A. Goddard and W. M. Skiff, Journal of the American Chemical Society **114** (25), 10024–10035 (1992).

40. A. W. Burton, Journal of the American Chemical Society **129** (24), 7627–7637 (2007).

41. M. A. Camblor, P. A. Barrett, M.-J. Díaz-Cabañas, L. A. Villaescusa, M. Puche, T. Boix, E. Pérez and H. Koller, Microporous and Mesoporous Materials **48** (1–3), 11–22 (2001).

42. S. I. Zones, S. J. Hwang and M. E. Davis, Chemistry—a European Journal **7** (9), 1990–2001 (2001).

43. M. E. Davis and C. Saldarriaga, Journal of the Chemical Society—Chemical Communications (14), 920–921 (1988).

44. S. I. Zones, Y. Nakagawa, G. S. Lee, C. Y. Chen and L. T. Yuen, Microporous and Mesoporous Materials **21** (4–6), 199–211 (1998).

45. D. J. Earl, A. W. Burton, T. Rea, K. Ong, M. W. Deem, S.-J. Hwang and S. I. Zones, J. Phys. Chem. C **112** (24), 9099–9105 (2008).

46.   Y. Chu, H. Deng and J. P. Cheng, Journal of Organic Chemistry **72** (20), 7790–7793 (2007).

47.   T. L. Amyes, S. T. Diver, J. P. Richard, F. M. Rivas and K. Toth, Journal of the American Chemical Society **126** (13), 4366–4374 (2004).

48.   A. W. Burton, Zeitschrift Fur Kristallographie **219** (12), 866–880 (2004).

49.   M. Arranz, J. Perez-Pariente, P. A. Wright, A. M. Z. Slawin, T. Blasco, L. Gomez-Hortiguela and F. Cora, Chem. Mater. **17** (17), 4374–4385 (2005).

Chapter Four: Supramolecular Structure Directing Agents *via* Adamantyl/Cyclodextrin Inclusion Complexes

4.1: Introduction

The results presented in Chapter Two using 1,3-bis(1-adamantyl)imidazolium hydroxide **15** as Structure Directing Agent (SDA) showed three crystalline phases were obtained (CIT-5 (CFI), SSZ-16 (AFX) and SSZ-35 (STF)). These results were unusual for a large, hydrophobic SDA as previous studies indicated decreasing phase diversity with increasing SDA size in high-silica reactions[1]. In addition, high silica reactions using SDAs with $\Sigma(C+N) \geq 17$ have typically given one-dimensional large or extra-large pore products with relatively high framework density, e.g., SSZ-24 (AFI)[2], CIT-5 (CFI)[3-5], SSZ-53 (SFH), SSZ-59 (SFN)[6] and UTD-1 (DON)[7]. Synthesizing cage-based structures SSZ-16 and SSZ-35 added further distinction to the phase behavior of the bis(adamantyl) SDA. Cage-based structures are characterized by narrow windows opening into larger cavities. These materials exhibit lower framework densities compared to materials with comparable pore windows and straight pores. In addition to AFX and STF, CFI contains an undulating extra-large one dimensional pore topology with internal pockets approximately 1 nm in diameter. The apparent affinity for cage-based structures provided motivation to search for larger lobes through non-covalent assembly. If larger lobes could be created on the SDA, frameworks with increased void volume may result. Larger cycloalkyl groups were not likely to give sufficient water solubility therefore alternative SDA structure was required.

Supramolecular assemblies were created using adamantyl/β-cyclodextrin (β-CD) association complexes. CDs are cyclic oligosaccharides containing α-1,4-D-glucopyranoside linked moieties. Common examples include α-, β-, and γ-CD containing six, seven and eight glucose residues respectively. Larger oligomers are possible but will not be discussed here. All CDs present a hydrophilic exterior surface with primary hydroxyl groups on one face and secondary hydroxyls on the other. Scheme 4.1 shows the structure of β-CD (n=7) plus a pictorial description of the three-dimensional structure. The "cup" dimensions are ~0.8 nm high (primary hydroxyl face to secondary hydroxyl face) and 1.46 (α-CD)-1.75 (γ-CD) nm diameter at the secondary hydroxyl face[8]. With all hydroxyl groups on the two planar faces CDs are water soluble and a hydrophobic cavity is created. The cavity diameter ranges from ~0.5 (α-CD) to ~0.78 (γ-CD) nm with the primary hydroxyl face narrower than the secondary hydroxyl face. CD size is of similar magnitude to the cavity diameter in FAU (~1.2 nm) and pore diameters of 18 MR structures VPI-5 (VFI) and ITQ-33 (~1.2 nm)[9, 10]. Therefore, supramolecular assemblies containing CDs could offer exciting structures with high void volume and pore diameter.
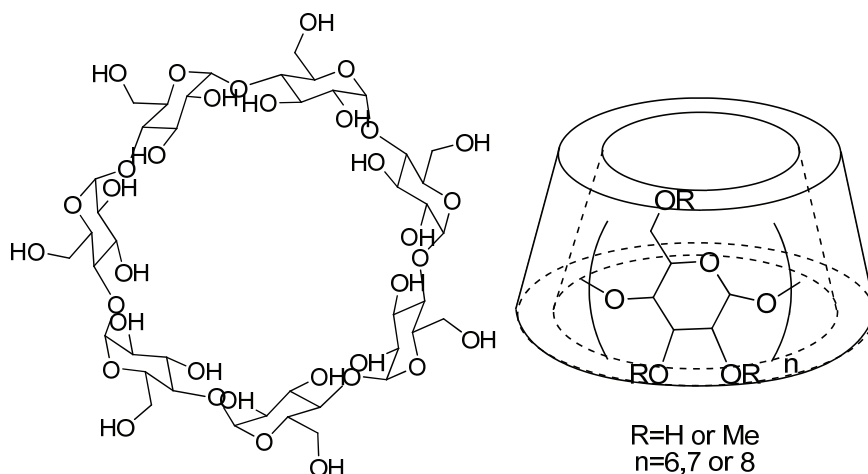
Scheme 4.1: β-cyclodextrin structure and three-dimensional pictorial description

The hydrophobic cavity within each CD offers an attractive environment for inclusion complex formation. The internal diameters of β- and γ-CD are appropriate for many small molecule drugs[8]. Inclusion complex formation with hydrophobic drugs offers an attractive solution to limited solubility for active pharmaceutical candidates. In this context of assembling supramolecular SDAs, β-CD was chosen based on the strong affinity for adamantane. Scheme 4.2 illustrates the proposed 2:1 inclusion complex formed between b-CD and 1,3-bis(1-adamantyl)imidazolium **15**. In addition to β-CD, randomly methylated β-CD (Me-O-β-CD) was chosen for investigation. This commercially available β-CD derivative contains random methoxy (CH_3-O-) groups in place of hydroxyls on both faces. This derivative shows significantly higher water solubility and should offer different interactions with silicate species.
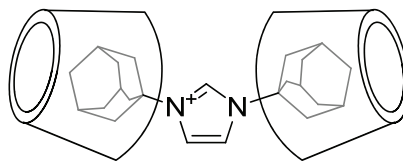
Scheme 4.2: Proposed 2:1 inclusion complex between β-CD and 1,3-bis(1-

adamantyl)imidazolium **15**

Examples of supramolecular SDAs in high-silica molecular sieve synthesis are not common. The majority of organic molecules used in molecular sieve synthesis contain nitrogen; either as an amine or quaternary ammonium moiety. Many small cyclic amines form clathrasil products such as Nonasil (NON) due to favorable van der Waals interactions. In spite of this, several novel materials were discovered using amines in conjunction with alkali hydroxide, e.g., MCM-22 (MWW) and MCM-35 (MTF) using hexamethyleneimine (homopiperidine). Water solubility/miscibility places an upper limit on the useful size of an amine for high-silica molecular sieve synthesis. In addition, alkali hydroxide incorporation to obtain sufficient silicate solubility creates competitive nucleation in solution with quartz or layered phases often produced with sufficient alkali content. In contrast, quaternary ammonium moieties convey significant water solubility and require less alkali hydroxide to obtain equivalent silicate solubility. An important consideration as the SDAs get larger (represented by C/N^+) is where the charge is located within the molecule. Researchers at Mobil investigated increasing alkyl chain length with N,N,N-trimethylammonium headgroups and discovered the novel MCM-41S family of mesoporous silica materials[11]. Here was an example of supramolecular assembly leading to ordered as opposed to crystalline materials. A schematic of MCM-41 synthesis is shown

in Scheme 4.1. In light of this discovery aggregation prevention was deemed necessary as

SDAs became more hydrophobic due to reduced hydrophobic hydration sphere overlap[12].
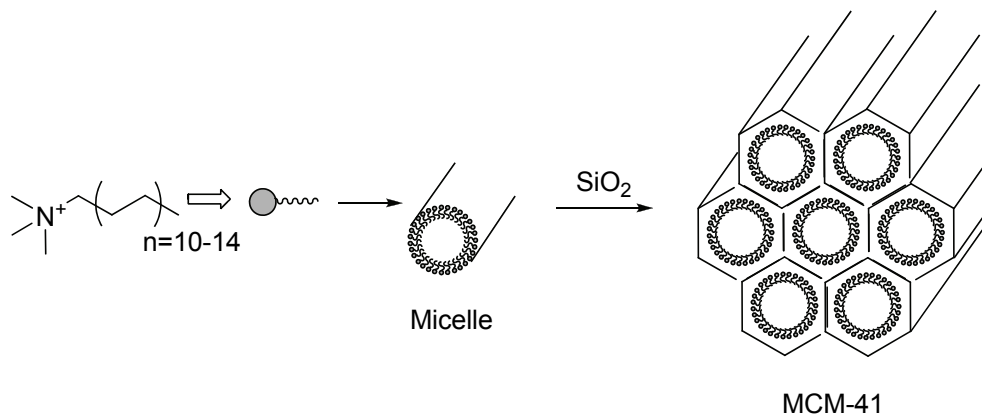
Scheme 4.3: MCM-41 formation schematic

The discussion above on avoiding uncontrolled aggregation does not preclude

controlled assembly as a viable structure direction method.   This was elegantly

demonstrated in the recent synthesis of pure-silica Linde Type A (LTA) denoted ITQ-29[13].

Typical LTA materials have Si/Al~1 and the high aluminum content limits hydrothermal

and acid stability. ITQ-29 synthesis uses an SDA that forms dimers in solution through

aromatic π-π interactions, with the SDA dimer occluded within the host product. Scheme

4.2 shows the SDA and model of the SDA dimer. This unique synthesis demonstrated

controlled supramolecular assembly though non-covalent bonds as a viable tool in

searching for new frameworks or novel compositions of known frameworks.
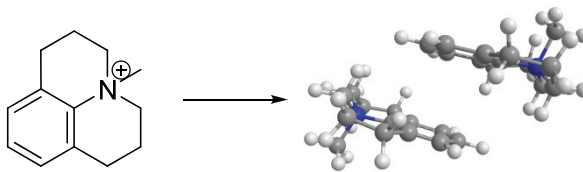
Scheme 4.4: Supramolecular SDA used to synthesize pure-silica LTA (ITQ-29)

Another example of supramolecular assembly occurs in the use of oligo-ether macrocycles (crown-ethers) with alkali cations (shown in Scheme 4.3). For this class of complex stoichiometry is restricted to one crown-ether per alkali metal cation. Gels containing 1,4,7,10,13,16-hexaoxacylooctadecane (18-crown-6) were used to synthesize EMC-2 (EMT), a structural polymorph of FAU[14]. Further studies investigated alkali metal/crown ether complex structure direction for FAU/EMT and concluded ion/dipole interactions directed assembly in the aluminosilicate gel[15]. A further example of crown-ether complex structure direction came in the synthesis of MCM-61 (MSO)[16]. MSO synthesis requires potassium/18-crown-6 complex as SDA. Structure solution revealed MSO contained 18 MR cavities with one crown-ether complex per cavity[17]. The above crown-ether-derived supramolecular SDAs are distinct from the earlier ITQ-29 dimer as ionic interactions dominate (as opposed to hydrophobic hydration interactions). This difference in structure direction does not diminish the potential application of carefully designed supramolecular assemblies in molecular sieve synthesis.
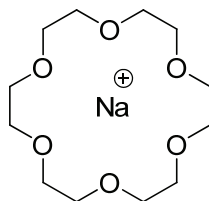
Scheme 4.5: Sodium/18-crown-6 complex

4.2: Experimental

1,3-bis(1-adamantyl)imidazolium hydroxide was synthesized as described in Chapter 2. In addition, 1,3-bis(1-adamantyl)imidazolium chloride was purchased from Strem Chemicals ($\geq$97%, Newburyport, MA) and was used as received. β-cyclodextrin (β-CD, Cavamax W7), randomly-methylated β-cyclodextrin (Me-O-β-CD, Cavasol W7 M Pharma) and γ-cyclodextrin (γ-CD, Cavamax W8 Pharma) were purchased from Wacker Chemical Corporation (Adrian, MI) and used as received. α-cyclodextrin (α-CD) was purchased from Amaizo and used as received. Tetraethylammonium hydroxide (TEAOH, 35wt% aqueous solution) and polyethylene glycol (M_w=400 and 3350) were purchased from Sigma-Aldrich and used as received. Inorganic reagents were used as described in Chapter Two. All inorganic reactions were performed at 150°C unless otherwise noted.

Inorganic reactions with adamantyl/cyclodextrin complexes were performed at CD:adamantyl molar ratios of 0.0-1.0. For example, two gels were created using 1,3-bis(1-adamantyl)imidazolium hydroxide and β-CD with composition 1.0 SiO_2:0.029 Al_2O_3:0.20 SDA$^+$OH$^-$:x CD:0.25 NaOH:30.0 H_2O where x = 0.0 or 0.40.

Isothermal Titration Calorimetry (ITC) was performed using a MicroCal MCS instrument (Northampton, MA). Titrations were performed at 30.0°C using 1x Dulbecco's Phosphate Buffered Saline (PBS) for both guest (adamantyl) and host (cyclodextrin) solutions. Concentrations were 2.475 mM in syringe (cyclodextrin solution) and 0.1006 mM in cell (adamantyl solution). A typical experiment used 1x2 µL injection then 10x24 µL injections with the first 2 µL injection discarded[18]. Blank experiments were performed by injecting 1xPBS into a solution of 1,3-bis(1-adamantyl)imidazolium chloride and also injecting β-CD solution into 1xPBS. The heat of dilution associated with each experiment was small compared to the binding enthalpy measured during the experiments, therefore, the heat of dilution was not included in the analysis. Binding stoichiometry (n), association equilibrium constant (K_a) and enthalpy (ΔH) were calculated using manufacturer supplied software. A review of the thermodynamic analysis relevant to ITC experiments using MicroCal instruments has been reported[19].

N,N,N-trimethyl-1-adamantanammonium hydroxide was synthesized by quaternizing 1-adamantylamine with iodomethane using the method previously described for SDA with $10 \leq C/N^+ \leq 14$[20]. The crude iodide salt was recrystallized from hot methanol. Ion exchange to the hydroxide form was performed with Bio-Rad AG1-X8 hydroxide resin (Bio-Rad Laboratories, Hercules, CA).

4.3: Results and Discussion

ITC was performed using 1,3-bis(1-adamantyl)imidazolium chloride and β-CD. Binding stoichiometry of two cyclodextrins per bis(adamantyl)imidazolium was expected. The results are presented in Table 4.1 and a typical isotherm is presented in Figure 4.1. The results in Table 4.1 show the expected 2:1 inclusion complex was observed. The binding equilibrium constant was approximately one order of magnitude lower than reported for 1:1 adamantane/β-CD guest/host complexes such as 1-adamantanecarboxylic acid/β-CD[19]. The statistical analysis assumed a single binding site model with no difference between the first and second binding events. Repeating the analysis with a two site model with n=1 for each site did not improve the statistical fit to the experimental data (not shown).

Table 4.1: β-cyclodextrin/1,3-bis(1-adamantyl)imidazolium binding stoichiometry, equilibrium constant and enthalpy

n	K_a / M^{-1}	ΔH / kJ mol^{-1}
2.04±0.09	13900±2000	-23.6±1.6
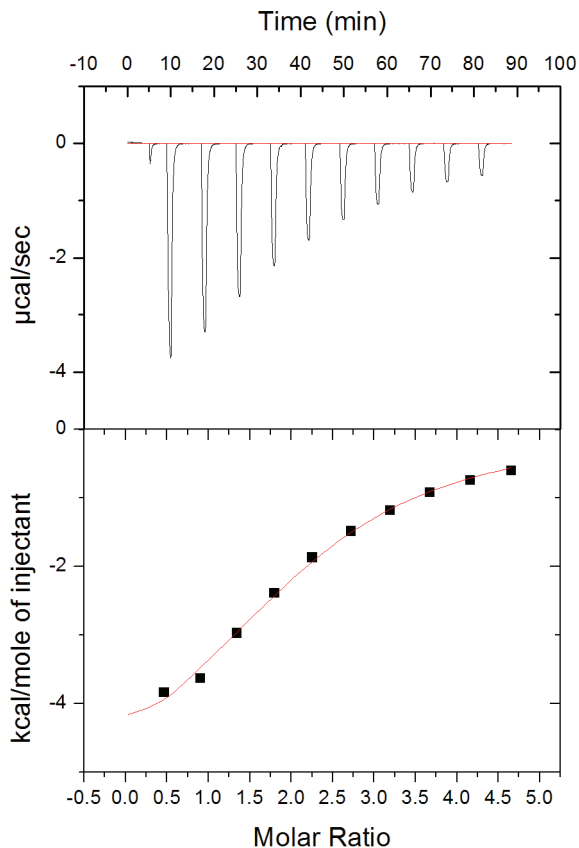
Figure 4.1: Isothermal titration calorimetry plot of 1,3-bis(1-adamantyl)imidazolium

chloride/β-cyclodextrin guest/host complex

With experimental evidence for the desired 2:1 inclusion complex inorganic reactions were performed to investigate if the product phase could be perturbed from that obtained with 1,3-bis(1-adamantyl)imidazolium alone. The initial focus was at the moderately aluminum-rich reaction condition using NaY as aluminum source. It was anticipated that the polar, hydrophilic β-CD external surface would provide favorable interactions in the moderately polar aluminosilicate gel. Products from alkali metal/crown ether complexes are typically hydrophilic, with product silica to alumina (SAR) ratios of 5-8 in FAU/EMT to approximately 28 in MSO[17]. The results are presented in Table 4.2 and

show no perturbation with added β-CD or Me-O-β-CD at NaOH/SiO$_2$=0.25. At NaOH/SiO$_2$=0.05, SSZ-16 was obtained when Me-O-β-CD while addition of β-CD gave an amorphous product. In addition, the cyclodextrins appeared to degrade significantly under reaction conditions. All reactions with cyclodextrins gave very dark colored gels that smelled like burnt sugar. Reactions using β-CD appeared fluid when opened but solidified upon stirring. Therefore, no pH measurements could be made on these reactions. Figure 4.2 plots pH as a function of time for reactions involving no cyclodextrin and Me-O-β-CD. The pH measurements for Me-O-β-CD reactions show opposite behavior at the two sodium hydroxide concentrations studied. At the higher concentration the pH was consistently higher than the corresponding gel without CD, and even though the gel was visibly discolored pH did not decrease. In contrast, the low sodium hydroxide reaction showed a sustained pH decline over the measurement period. A sample worked-up for analysis after 10 days was amorphous with no sign of NaY reflections. Further heating lead to the formation of SSZ-16 with no residual NaY (Figure 4.3 shows XRD patterns for all three reactions at NaOH/SiO$_2$=0.05). This suggests Me-O-β-CD addition may offer improved product purity under certain reaction conditions.

Table 4.2: Products obtained from inorganic reactions using 1,3-bis(1-adamantyl) imidazolium hydroxide / β-cyclodextrin inclusion complexes. Gel compositions were 1.0 SiO_2:0.029 Al_2O_3:0.20 SDA^+OH^-:x CD:y NaOH:30.0 H_2O (x=0.0 or 0.40).

Cyclodextrin	y = 0.25	y = 0.05
None	Mordenite	SSZ-16
β-CD	Mordenite	Amorphous
Me-O-β-CD	Mordenite	SSZ-16
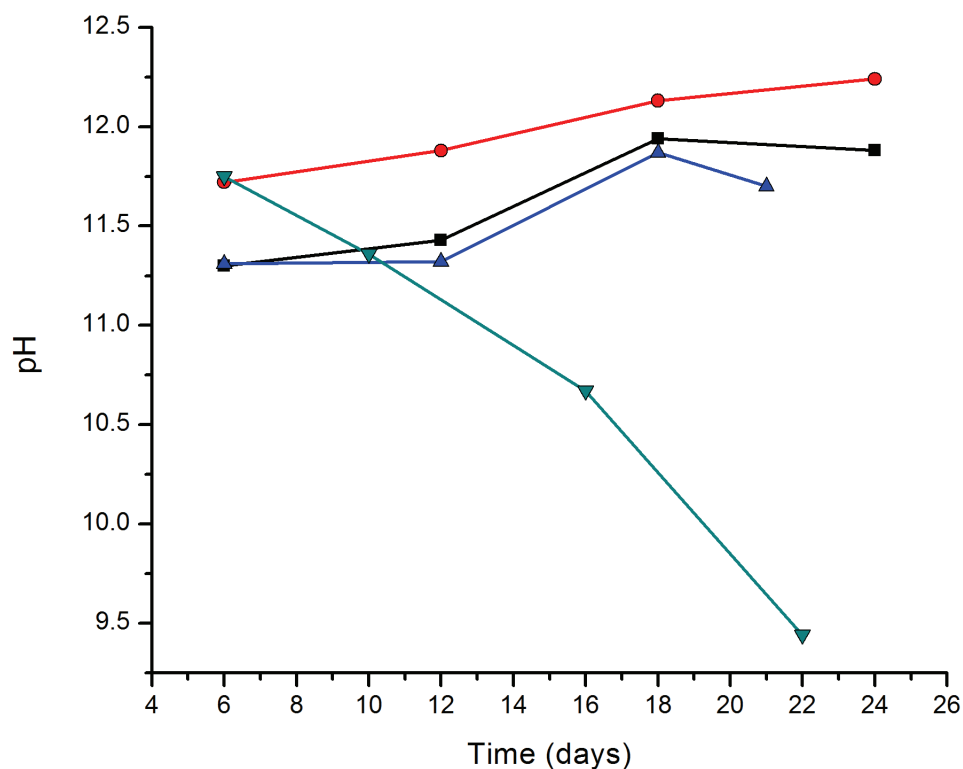
Figure 4.2: Plot of pH versus reaction time for SAR=35 reactions with no cyclodextrin and Me-O-β-CD. $NaOH/SiO_2$=0.25+CD/SiO_2=0.0 (■),$NaOH/SiO_2$=0.25+CD/SiO_2=0.4 (●),$NaOH/SiO_2$=0.05+CD/SiO_2=0.0 (▲) and $NaOH/SiO_2$=0.05+CD/SiO_2=0.4 (▼)
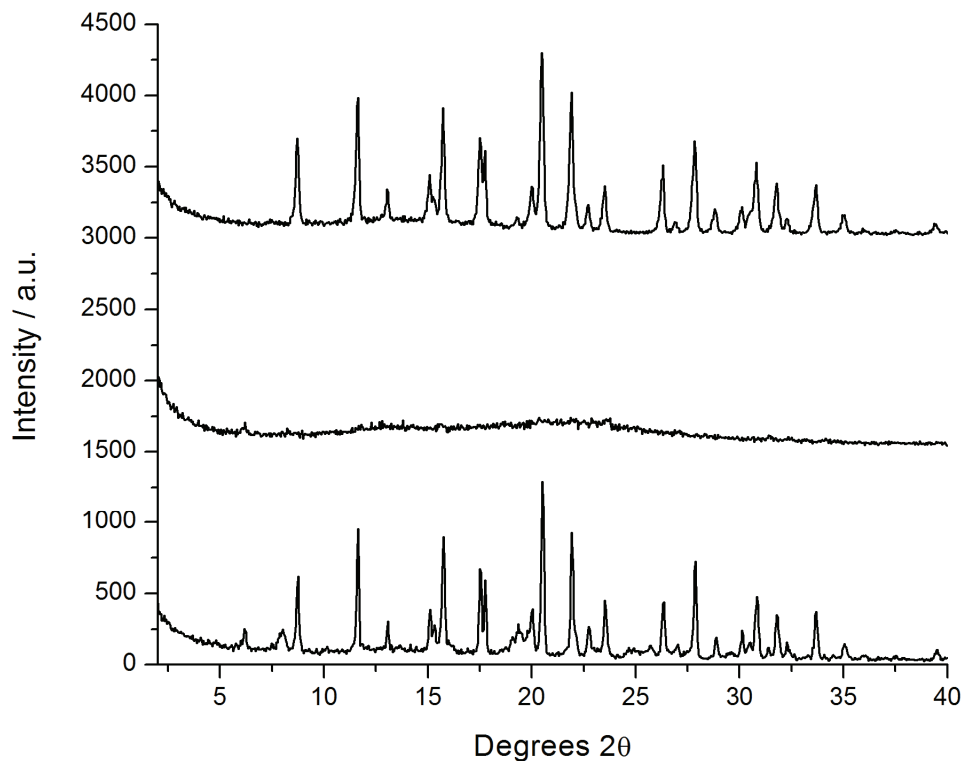
Figure 4.3: XRD patterns for 1,3-bis(1-adamantyl)imidazolium hydroxide/β-cyclodextrin

inclusion complex. Top= Me-O-β-CD (SSZ-16), middle = β-CD (amorphous) and

bottom = no cyclodextrin (SSZ-16 + minor NaY)

The results from the initial inorganic reactions using bis(adamantyl)/cyclodextrin inclusion complexes did not show any desirable product perturbation.   In addition, cyclodextrin degradation was significant as indicated by rapid discoloration and sustained pH decline in the low sodium hydroxide NaY reaction. The results in Chapter Two using this large bis(adamantyl) SDA suggest relatively narrow composition windows for SSZ-16, SSZ-35 and CIT-5 phases. Also, all reactions required >10 days at 150°C (or higher). The slow kinetics posed a very significant obstacle given the cyclodextrin degradation. In this regard the large bis(adamantyl) SDA must organize a large amount of silicate species

before nucleation occurs. For the STF case two cavities contain 66 tetrahedral atoms (3x10MR plus 2x18MR) so clearly a complex self-assembly process is required to coordinate adjacent silicate/organic complexes to nucleate the crystalline product. It should be noted that the final product has a lower tetrahedral atom to SDA ratio due to sharing between adjacent channels. Even accounting for this the self assembly process with such a large SDA appears very complex; adding additional size through inclusion complex formation would only increase complexity.

At this point it was not considered likely that a 2:1 inclusion complex would succeed in making a crystalline phase for the reasons outlined above. Therefore, a change to 1:1 inclusion complexes using β-CD and N,N,N-trimethyl-1-adamantanammonium hydroxide was made. It was anticipated that a smaller supramolecular SDA might be able to nucleate a crystalline product before significant cyclodextrin degradation occurred.

Inorganic reactions with TMADOH have been extensively studied and reported in the literature. Product phases in hydroxide reactions are largely determined by the inorganic components. With a number of products possible for a given inorganic composition multiple phases can be encountered and/or temporal evolution shows an initial product being displaced, presumably via an Ostwald ripening process[21]. Products obtained with this SDA include[1] SSZ-13 (CHA), SSZ-23 (STT), SSZ-24 (AFI), SSZ-25 (MWW), ITQ-1 (MWW)[22], SSZ-31(*STO) and VPI-8 (VET)[23]. These products span a wide range of lattice substitution with SSZ-13 materials often aluminum (or boron) rich (SAR~20) through to pure silica SSZ-24 and ITQ-1 (SAR=∞). Also, rapid product formation has been reported, e.g. SSZ-13 via conversion of various faujasites in as little as 40 hours at 135°C[24]. In pure silica fluoride reactions CHA, STT and *STO are observed depending on

the water to silica ratio[25, 26]. Similar to the hydroxide reactions, the initial products at low and high water to silica ratios are displaced upon continued heating. The initial product at $H_2O/SiO_2 < 6$ is CHA while at $H_2O/SiO_2 > 15$ *STO is observed. STT displaces both phases on prolonged heating, and is the only phase observed for $6 < H_2O/SiO_2 < 15$[27].

The inorganic reactions can be grouped into three general categories: aluminosilicate or borosilicate; zincosilicate and miscellaneous. Representative examples are presented in Tables 4.3, 4.4 and 4.5 below. The first group contains gel compositions favorable for three-dimensional product formation with SiO_2/Al_2O_3 (or B_2O_3) < 50. Both hydroxide and fluoride mediated reactions were attempted to probe cyclodextrin stability at high pH (hydroxide reactions) and approximately neutral pH (fluoride reactions). The zincosilicate reactions were largely built around reported VET syntheses with lithium hydroxide in an attempt to obtain fast product formation[23]. The final group lists additional reaction attempts where no trivalent lattice element was introduced, aluminophosphate (AlPO) reaction attempts and reactions where no adamantyl component was introduced. Several reactions investigated an alternative supramolecular SDA using α-CD/polyethylene glycol (PEG) threading complex. In addition, γ-CD was also tested in place of β- or Me-O-β-CD.

Table 4.3: Aluminosilicate and borosilicate reactions employing N,N,N-trimethyl-1-adamantanammonium hydroxide (SDA$^+$OH$^-$) / β-cyclodextrin inclusion complex as structure directing agent

Entry	Gel Composition	Cyclodextrin	Product
1	1.0 SiO$_2$:0.1 B$_2$O$_3$:0.25 SDA$^+$OH$^-$:0.0 CD:23.0 H$_2$O	None	CHA
2	1.0 SiO$_2$:0.1 B$_2$O$_3$:0.25 SDA$^+$OH$^-$:0.25 CD:23.0 H$_2$O	Me-O-β-CD	Amo+CHA
3	1.0 SiO$_2$:0.02 Al$_2$O$_3$:0.25 SDA$^+$OH$^-$:0.00 CD:0.25 NH$_4$F:10.0 H$_2$O	None	Amorphous
4	1.0 SiO$_2$:0.02 Al$_2$O$_3$:0.25 SDA$^+$OH$^-$:0.25 CD:0.25 NH$_4$F:10.0 H$_2$O	Me-O-β-CD	Amorphous
5	1.0 SiO$_2$:0.02 Al$_2$O$_3$:0.25 SDA$^+$OH$^-$:0.25 CD:0.25 NH$_4$F:10.0 H$_2$O	Me-O-β-CD	Amorphous
6	1.0 SiO$_2$ 0.02 Al$_2$O$_3$ 0.25 SDA$^+$OH$^-$:0.25 CD:0.25 HF:5.0 H$_2$O	β-CD	Amorphous
7	1.0 SiO$_2$:0.02 Al$_2$O$_3$:0.25 SDA$^+$OH$^-$:0.25 CD:0.25 HF:5.0 H$_2$O	Me-O-β-CD	Amorphous
8	1.0 SiO$_2$ 0.10 Al$_2$O$_3$:0.05 SDA$^+$OH$^-$:0.05 CD 0.20 LiOH:30.0 H$_2$O	Me-O-β-CD	Amorphous
9	1.0 SiO$_2$:0.067 Al$_2$O$_3$:0.11 SDA$^+$OH$^-$:0.11 CD:1.09 NaOH:21.0 H$_2$O	Me-O-β-CD	FAU[a]

[a]Reaction performed at 90°C

Entries 1 and 2 in Table 4.3 used very similar inorganic compositions to the boron rich hydroxide reactions investigated in Chapter Two for SSZ-70. Cyclodextrin absence gave the expected B-CHA product[28]. In contrast, Me-O-β-CD inclusion resulted in a mostly amorphous product with very weak CHA reflections. Figure 4.4 shows the XRD patterns for entries 1 and 2. Significant discoloration was observed with cyclodextrin incorporation where the corresponding reaction with adamantyl SDA only exhibited almost no discoloration.

The next reaction subset employed fluoride either as hydrofluoric acid or ammonium fluoride. The expectation in this series was for significantly reduced cyclodextrin degradation under the approximately neutral pH reaction conditions. Initial inspection of all reactions with cyclodextrin and fluoride addition showed black gels with a

distinct smell of burnt sugar. With rapid and significant degradation apparent the reactions were stopped after several days at 150°C.
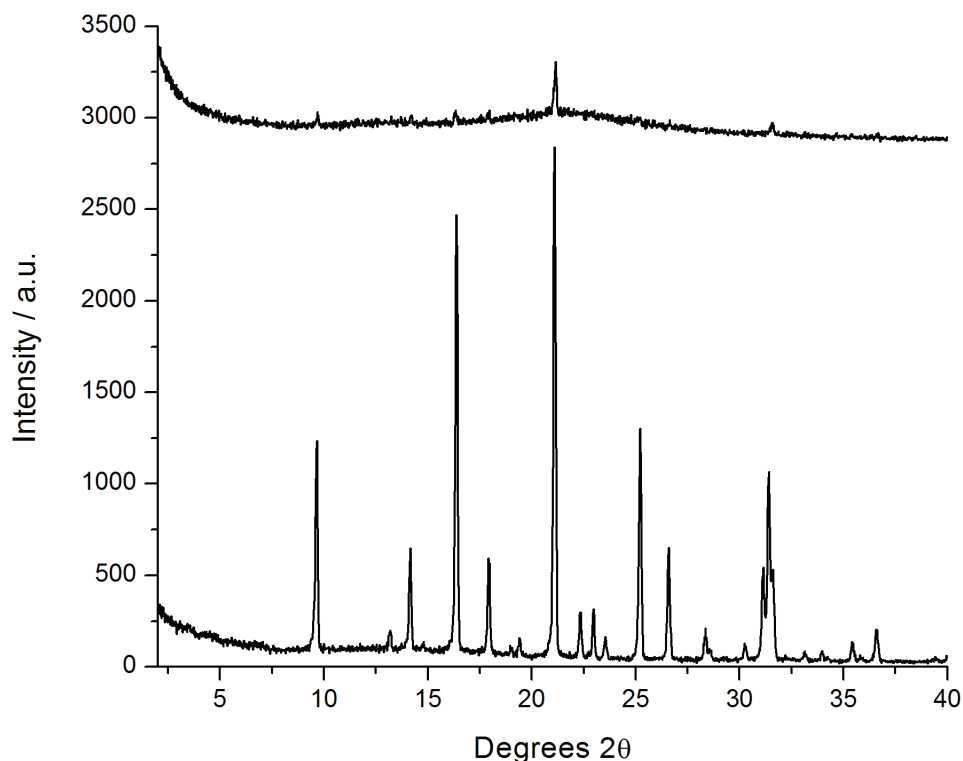
Figure 4.4: XRD patterns for borosilicate reactions employing N,N,N-trimethyl-1-adamantanammonium hydroxide/Me-O-β-CD inclusion complex as SDA. Top=Adamantyl SDA/Me-O-β-CD complex (amorphous + CHA) and bottom=Adamantyl SDA only (CHA)

The final entry in Table 4.3 represents an attempt to reduce cyclodextrin degradation by performing the reaction at lower temperature (90°C). The inorganic conditions were modeled after those used to synthesize Gmelinite (GME) using quaternary polymers [29]. Here the total hydroxide to silica ratio was 1.2 and silica to alumina ratio was

15. The aim was to mitigate degradation while providing enough hydroxide for silicate organization to occur. Reference 16 states FAU and P (GIS) were observed in the absence of quaternary polymer: the reaction studied above gave FAU with significant discoloration even at the lower temperature.

The reactions summarized in Table 4.3 show no desirable product perturbation. In all cases cyclodextrin degradation was significant, with fluoride addition appearing to accelerate degradation. For entries 2 and 9 crystalline phases were observed in the presence of Me-O-β-CD. In both cases the cyclodextrin was not responsible for structure direction.

Table 4.4: Zincosilicate reactions employing N,N,N-trimethyl-1-adamantanammonium hydroxide (SDA$^+$OH$^-$) / β-cyclodextrin inclusion complex as structure directing agent

Entry	Gel Composition	Cyclodextrin	Product
1	1.0SiO$_2$:0.01ZnO:0.05SDA$^+$OH$^-$:0.00 CD:0.2LiOH:30.0 H$_2$O	None	Amorphous
2	1.0SiO$_2$:0.01ZnO:0.05SDA$^+$OH$^-$:0.05 CD:0.2LiOH:30.0 H$_2$O	β-CD	Amorphous
3	1.0SiO$_2$:0.01 ZnO:0.05SDA$^+$OH$^-$:0.05 CD:0.2LiOH:30.0 H$_2$O	Me-O-β-CD	Amorphous
4	1.0SiO$_2$:0.04GeO$_2$:0.01ZnO:0.05SDA$^+$OH$^-$: 0.05CD:0.2LiOH:30.0 H$_2$O	Me-O-β-CD	Amorphous
5	1.0SiO$_2$:0.1ZnO:0.4SDA$^+$OH$^-$:0.4CD:0.2LiOH:60.0 H$_2$O	Me-O-β-CD	VET
6	1.0 SiO$_2$:0.04GeO$_2$:0.05ZnO:0.3SDA$^+$OH$^-$: 0.3CD:0.2LiOH:45.0 H$_2$O	Me-O-β-CD	VET+layered

Table 4.4 summarizes representative zincosilicate reactions using TMAD$^+$OH$^-$/β-CD inclusion complexes. Entries 1–4 were run at low SDA$^+$OH$^-$ to silica ratios in an

attempt to add just enough SDA to fully occupy the final product. Lithium hydroxide was used to supply the remaining hydroxide to give total hydroxide/silica=0.25. This total hydroxide content was sufficient in many borosilicate and aluminosilicate reactions presented in Chapters Two and Three. Entry 4 included germanium in an attempt to enhance product nucleation. Germanium incorporation often increases the population of 4MR in the product due to the longer Ge-O bond length and tetrahedral angle flexibility[30]. Unfortunately, no crystalline phase was obtained for all entries, presumably due to insufficient hydroxide to facilitate silicate organization in the presence of zinc.

Entries 5 and 6 were performed at higher SDA^+OH^- concentrations and VET was observed in both cases in the presence of Me-O-β-CD. Entry 5 stands out as no evidence of layered material could be detected by XRD. Previous syntheses with $TMAD^+OH^-$ under similar conditions gave VET plus a layered impurity[31]. The layered impurity appears as a relatively broad reflection at ~6°2θ as shown in Figure 4.5. The absence of layered material for entry 14 further supports the observation in Table 4.2 that Me-O-β-CD addition may improve product phase purity.
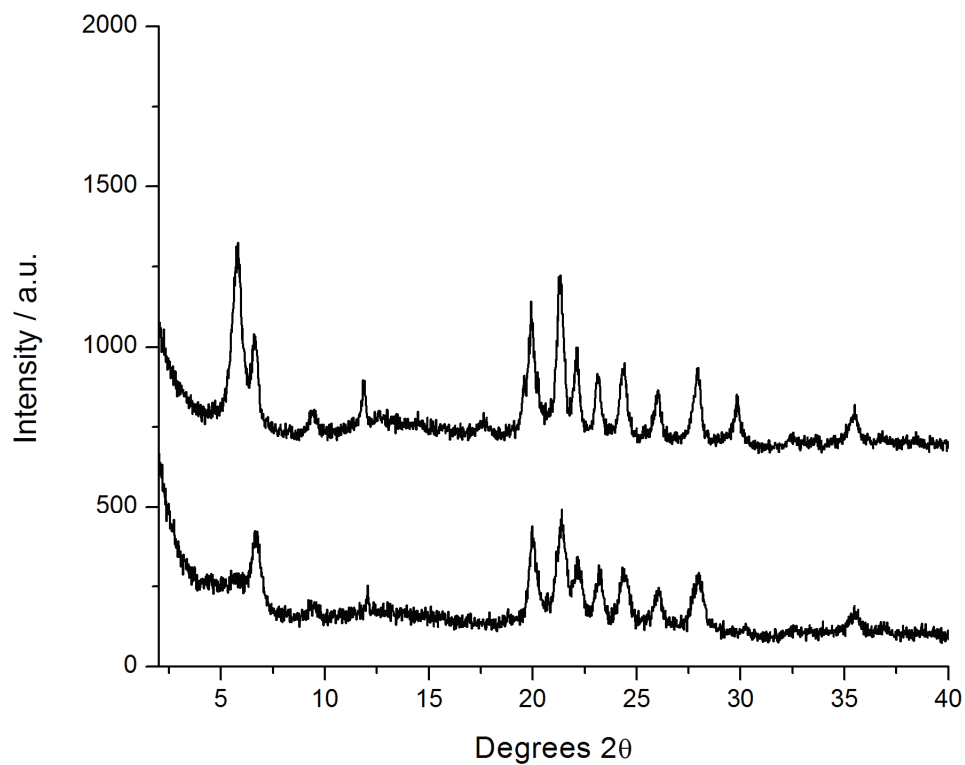
Figure 4.5: XRD patterns for zincosilicate reactions employing N,N,N-trimethyl-1-adamantanammonium hydroxide/Me-O-β-CD inclusion complex as SDA. Top=Adamantyl SDA/Me-O-β-CD complex + GeO$_2$(VET+layered) and bottom= Adamantyl SDA/Me-O-β-CD complex (VET)

Table 4.5: Gel compositions and product phases for miscellaneous reactions employing cyclodextrins

Entry	Gel Composition	Cyclodextrin	Product
1	$1.0\ SiO_2:0.04GeO_2:0.30\ SDA^+OH^-:0.00\ CD:0.2LiOH:45.0\ H_2O$	None	Layered+AFI
2	$1.0\ SiO_2:0.04GeO_2:0.30\ SDA^+OH^-:0.30\ CD:0.2LiOH:45.0\ H_2O$	Me-O-β-CD	Layered
3	$1.0\ SiO_2:0.10\ CD:0.48NaOH:0.48HF:14.0\ H_2O$	α-CD	Amorphous
4	$1.0\ SiO_2:0.24\ CD:0.24NH_4F:14.0\ H_2O$	α-CD	Amorphous
5	$1.0\ SiO_2:0.24\ CD:0.24NH_4F:14.0\ H_2O$	Me-O-β-CD	Amorphous
6	$1.0\ SiO_2:0.24\ CD:0.24NH_4F:14.0\ H_2O$	γ-CD	Amorphous
7	$1.0\ SiO_2:0.3\ ZnO:0.1CD:0.48NaOH:0.24HCl:20.0\ H_2O$	Me-O-β-CD	Amorphous
8	$1.0\ SiO_2:0.3\ ZnO:0.1CD:0.48NaOH:25.0\ H_2O$	Me-O-β-CD	Amorphous[a]
9	$1.0SiO_2:0.3\ ZnO:0.1CD:0.48NaOH:25.0\ H_2O$	Me-O-β-CD	Amorphous[b]
10	$1.0SiO_2:0.3\ ZnO:0.1CD:0.48NaOH:25.0\ H_2O$	Me-O-β-CD	Amorphous[c]
11	$1.0SiO_2:0.1ZnO:0.06CD:0.00PEG:0.1LiOH:25.0\ H_2O$	α-CD	Amorphous
12	$1.0SiO_2:0.1ZnO:0.06CD:0.01PEG_{400}:0.1LiOH:25.0\ H_2O$	α-CD	Amorphous
13	$1.0SiO_2:0.1ZnO:0.06CD:0.01PEG_{3350}:0.1LiOH:25.0\ H_2O$	α-CD	Amorphous
14	$1.0SiO_2:0.1ZnO:0.06CD:0.00PEG:0.1LiOH:25.0\ H_2O$	α-CD	Amorphous[d]
15	$1.0SiO_2:0.1ZnO:0.06CD:0.01PEG_{400}:0.1LiOH:25.0\ H_2O$	α-CD	Amorphous[d]
16	$1.0SiO_2:0.1ZnO:0.4\ TEA^+OH^-:0.0CD:0.2LiOH:30.0\ H_2O$	None	VET
17	$1.0SiO_2:0.1ZnO:0.4\ TEA^+OH^-:0.05CD:0.2LiOH:30.0\ H_2O$	Me-O-β-CD	VET
18	$1.0SiO_2:0.1Al_2O_3:0.1CD:0.48NaOH:0.48HF:14.0\ H_2O$	Me-O-β-CD	Amorphous
19	$0.66SiO_2:0.34GeO_2:0.1Al_2O_3:0.1CD:0.48NaOH:25.0\ H_2O$	Me-O-β-CD	AST
20	$0.95SiO_2:0.05GeO_2:0.05Al_2O_3:0.05CD:0.1NaOH:25.0\ H_2O$	Me-O-β-CD	Amorphous
21	$0.98SiO_2:0.02GeO_2:0.03Al_2O_3:0.05CD:0.1NaOH:25.0\ H_2O$	Me-O-β-CD	Amorphous
22	$1.0SiO_2:0.1B_2O_3:0.05CD:0.1NaOH:25.0\ H_2O$	Me-O-β-CD	Amorphous
23	$1.0Al_2O_3:1.0P_2O_5:0.25SDA^+OH^-:0.00CD:100H_2O$	None	Dense
24	$1.0Al_2O_3:1.0P_2O_5:0.25SDA^+OH^-:0.25CD:100H_2O$	Me-O-β-CD	Dense
25	$1.0Al_2O_3:1.0P_2O_5:0.25SDA^+OH^-:0.25CD:100H_2O$	β-CD	Dense

[a]Reaction performed at 90°C with 4 hour periods at 135°C

[b]Reaction performed at 90°C with 8 hour periods at 135°C

[c]Reaction performed at 90°C with 4 hour periods at 150°C

[d]Reaction performed at 90°C

Table 4.5 provides additional inorganic reaction examples where various cyclodextrins were added to the reaction gel. Entries 1–6 contained no trivalent lattice element (aluminum or boron) in contrast to the previous syntheses outlined in Tables 4.1–4.4. With no trivalent lattice element one dimensional products (or clathrates) were expected. Entry 1 shows SSZ-24 (AFI) plus a layered impurity was obtained in a germanosilicate reaction using only TMAD$^+$OH$^-$. The same gel composition with Me-O-β-CD gave the layered phase only. In this instance cyclodextrin incorporation lead to an undesirable phase dominating in contrast to those cases discussed above where cyclodextrin incorporation suppressed undesirable impurity phases. The high lithium hydroxide content most likely contributed to layered phase formation. No attempts were made to repeat the reactions at lower lithium hydroxide concentration.

The remaining pure silica reactions investigated α- and γ-CD in addition to Me-O-β-CD. As α-CD could not form an inclusion complex with adamantane none was added. One reaction used NaF as fluoride source whereas the remaining reactions used NH$_4$F. All four examples gave amorphous products and reaction gels were dark brown to black in color when first opened. Given the severe degradation observed in all cases no insight could be gained into the relative stability of each cyclodextrin.

Entries 7–17 summarize additional zincosilicate reaction attempts with no adamantane component added. Entries 7–10 used inorganic compositions closer to those reported for VPI-7 (VSV)[32]. An additional aspect of these reactions was an attempt to manage cyclodextrin degradation by performing the reactions at two temperatures. For example, entry 8 used 90°C for six days then four hours at 135°C before returning to 90°C. The intention was to find a temperature where minimal degradation occurred (as evidenced

by color change) and holding at this temperature to hopefully facilitate some silicate bond rearrangement. Trial experiments revealed 90°C was the upper temperature limit for the given hydroxide to silica ratio (NaOH/SiO$_2$=0.48; recall significant discoloration was observed for entry 9 in Table 4.3 at 90°C with OH$^-$/SiO$_2$=1.2). The period at higher temperature was included to provide additional thermal energy that might induce nucleation while not long enough for significant degradation to occur. If nucleation occurred at elevated temperature crystal growth could continue at lower temperature. Entries 7, 9 and 10 showed significant discoloration (deep brown to black), whereas entry 8 was tan colored. Therefore, it did appear that degradation could be managed to some extent but ultimately no crystalline phase was obtained for all entries.

Entries 11–15 explored α-CD/PEG threading complexes as alternative supramolecular SDAs. Low alkali hydroxide concentrations were used with the intention of minimizing cyclodextrin degradation. The initial reactions at 150°C gave amorphous products and significant discoloration was observed. This prompted experiments performed entirely at 90°C (entries 14 and 15) whereby discoloration was greatly reduced but again no crystalline product evolved.

The above examples where Me-O-β-CD addition still gave SSZ-16 and VET suggested the cyclodextrin and decomposition products had a neutral to slightly positive effect on phase purity. For the SSZ-16 case a potential hypothesis was the cyclodextrin components prevented stabilization of the NaY reagent thereby giving full transformation. In contrast, the VET example suggested suppression of a competing layered phase. Entries 16 and 17 were included to further investigate the role Me-O-β-CD addition had on phase selectivity and purity. Specifically, could Me-O-β-CD addition effect a reaction where no

adamantyl component was added? Entry 16 represents a control experiment where tetraethylammonium hydroxide was used in a zinc-containing gel to produce VET[33]. Addition of Me-O-β-CD in entry 17 did not change the product phase. This indicated the cyclodextrin decomposed and acted as a neutral species in the reaction gel.

The next reaction group summarizes reactions where no adamantyl component was added in moderately polar gels. Entry 18 was adapted from the reaction condition used by Burkett when investigating FAU/EMT structure direction using alkali metal/crown-ether complexes[15]. α-CD was attempted with degradation noted; therefore Entry 18 was performed under approximately neutral conditions with HF addition. Significant degradation was observed for this reaction consistent with all other cyclodextrin reactions with fluoride addition. Entries 19–21 explored germanosilicate reactions with not adamantyl component added. AST was obtained at Si/Ge=2 with amorphous products at higher Ge/Si ratios. As discussed previously, AST is rich in D4R and appears frequently at low Si/Ge ratios. For the gel composition studied, aluminum incorporation could be balanced by sodium cations and this might be sufficient to stabilize the cages. Alternatively, decomposed sugar moieties could be small enough to become occluded within the cage (intact CD would be too large to fit). No structure directing role can be directly attributed to the cyclodextrin, although decomposition fragments might play a minor role with the inorganic composition largely dictating the product. The final reaction in this group explored a borosilicate reaction. Here the SiO_2/B_2O_3 was 10 and the $NaOH/SiO_2$ ratio was kept low at 0.1 to minimize degradation. At these conditions there would be insufficient positive charge to balance negative framework charge if all boron was incorporated. However, studies have shown boron tends to be drawn into the growing

crystal as required[34]. This offered a potential window where borate buffering could offer reduced pH and hence improved CD stability. Unfortunately, no product was obtained and discoloration was observed indicating degradation.

The final entries give details of AlPO reactions. These reactions were attempted as many AlPO products form with little or no induction period. Cyclodextrin degradation was expected under the acidic reaction conditions but if degradation was slightly slower than crystallization novel phases could evolve. The results show an unidentified dense phase was obtained for all three reactions and Figure 4.6 gives the XRD pattern. Both gels with CD added became deep black and particularly pungent smelling. It should be noted that AFI has been reported in AlPO reactions using the adamantyl SDA[24]. Fine tuning the gel composition should enable replication; however, severe CD degradation did not warrant further reactions.
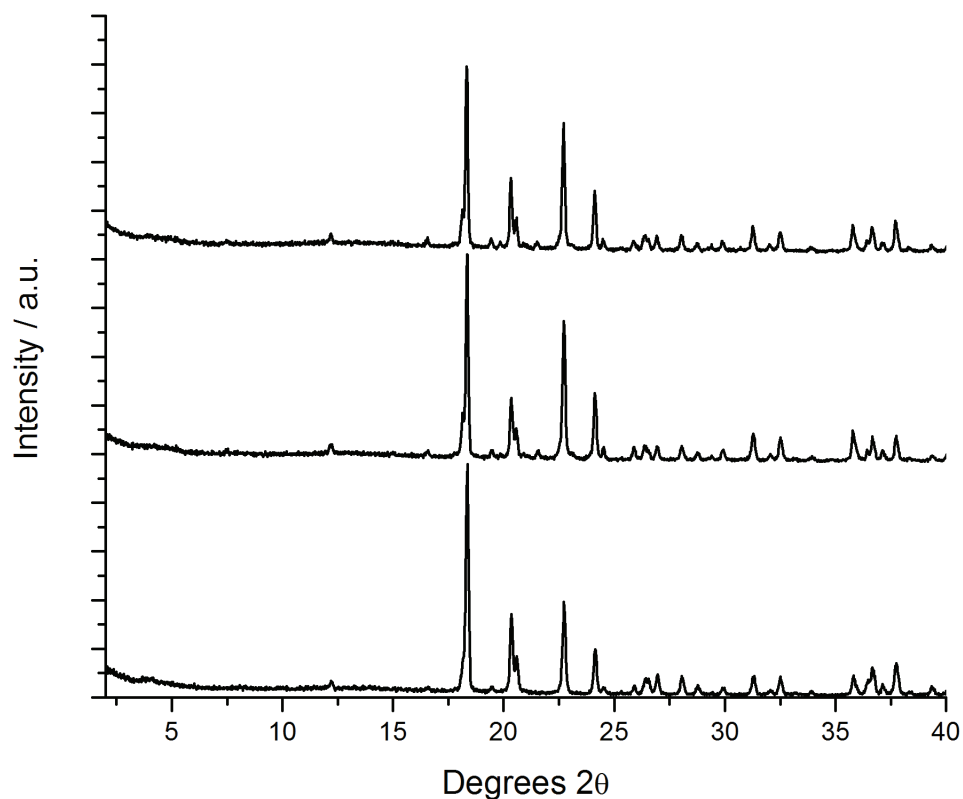
Figure 4.6: XRD patterns of unknown dense aluminophosphate phase. Top to bottom=Adamantyl SDA/β-CD complex, adamantyl SDA/Me-O-β-CD and adamantyl SDA only

4.4: Conclusions

Supramolecular SDAs based on adamantyl/β-CD inclusion complexes were not able to perturb the observed product. Inorganic reactions containing β-CD or Me-O-β-CD yielded AFX, MOR, CHA, FAU, VET and AST under appropriate inorganic conditions with all remaining products amorphous or layered. No structure direction could be attributed to CD addition for any crystalline phase observed. All reactions with CD

addition performed above 90°C showed significant discoloration indicating degradation occurred. Reactions at approximately neutral pH using fluoride gave faster discoloration. Overall, cyclodextrins were not stable under molecular sieve synthesis conditions thereby preventing any structure direction.

Even with degradation some inorganic reactions containing Me-O-β-CD gave products with fewer impurities (AFX and VET). This was not observed for all products and β-CD did not show similar improvements. Therefore, Me-O-β-CD addition in reactions containing adamantyl SDAs could be a useful technique to improve product purity.

4.5: References

1. S. I. Zones, Y. Nakagawa, G. S. Lee, C. Y. Chen and L. T. Yuen, Microporous and Mesoporous Materials **21** (4–6), 199–211 (1998).

2. Y. Nakagawa, US Patent No. 5,271,922 (1993).

3. M. Yoshikawa, P. Wagner, M. Lovallo, K. Tsuji, T. Takewaki, C. Y. Chen, L. W. Beck, C. Jones, M. Tsapatsis, S. I. Zones and M. E. Davis, Journal of Physical Chemistry B **102** (37), 7139–7147 (1998).

4. I. Ogino and M. E. Davis, Microporous and Mesoporous Materials **67** (1), 67–78 (2004).

5. K. Tsuji, P. Wagner and M. E. Davis, Microporous and Mesoporous Materials **28** (3), 461–469 (1999).

6. A. Burton, S. Elomari, C. Y. Chen, R. C. Medrud, I. Y. Chan, L. M. Bull, C. Kibby, T. V. Harris, S. I. Zones and E. S. Vittoratos, Chemistry—a European Journal **9** (23), 5737–5748 (2003).

7. C. C. Freyhardt, M. Tsapatsis, R. F. Lobo, K. J. Balkus and M. E. Davis, Nature **381** (6580), 295–298 (1996).

8. M. E. Davis and M. E. Brewster, Nature Reviews Drug Discovery **3** (12), 1023–1035 (2004).

9. M. E. Davis, C. Saldarriaga, C. Montes, J. Garces and C. Crowder, Zeolites **8** (5), 362–366 (1988).

10. A. Corma, M. J. Diaz-Cabanas, J. L. Jorda, C. Martinez and M. Moliner, Nature **443** (7113), 842–845 (2006).

11. C. T. Kresge, M. E. Leonowicz, W. J. Roth, J. C. Vartuli and J. S. Beck, Nature **359** (6397), 710–712 (1992).

12. S. L. Burkett and M. E. Davis, Chemistry of Materials **7** (8), 1453–1463 (1995).

13. A. Corma, F. Rey, J. Rius, M. J. Sabater and S. Valencia, Nature **431** (7006), 287–290 (2004).

14. F. Delprato, L. Delmotte, J. L. Guth and L. Huve, Zeolites **10** (6), 546–552 (1990).

15. S. L. Burkett and M. E. Davis, Microporous Materials **1** (4), 265–282 (1993).

16. E. W. Valyocsik, US Patent No. 5,670,131 (1997).

17. D. F. Shantz, A. Burton and R. F. Lobo, Microporous and Mesoporous Materials **31** (1–2), 61–73 (1999).

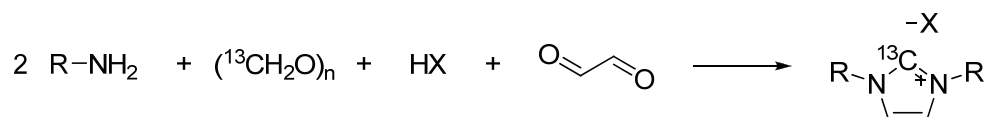18. J. Tellinghuisen, The Journal of Physical Chemistry B **109** (42), 20027–20035 (2005).

19. M. J. Blandamer, P. M. Cullis and J. Engberts, Journal of the Chemical Society-Faraday Transactions **94** (16), 2261–2267 (1998).

20. P. Wagner, Y. Nakagawa, G. S. Lee, M. E. Davis, S. Elomari, R. C. Medrud and S. I. Zones, Journal of the American Chemical Society **122** (2), 263–273 (2000).

21. S. I. Zones, S. J. Hwang and M. E. Davis, Chemistry—a European Journal **7** (9), 1990–2001 (2001).

22. M. A. Camblor, C. Corell, A. Corma, M.-J. Diaz-Cabanas, S. Nicolopoulos, J. M. Gonzalez-Calbet and M. Vallet-Regi, Chemistry of Materials **8** (10), 2415–2417 (1996).

23. M. Yoshikawa, S. I. Zones and M. E. Davis, Microporous Materials **11** (3–4), 127–136 (1997).

24. S. I. Zones, Journal of the Chemical Society-Faraday Transactions **87** (22), 3709–3716 (1991).

25. S. I. Zones, S. J. Hwang, S. Elomari, I. Ogino, M. E. Davis and A. W. Burton, Comptes Rendus Chimie **8** (3–4), 267–282 (2005).

26. M. A. Camblor, M. J. Diaz-Cabanas, J. Perez-Pariente, S. J. Teat, W. Clegg, I. J. Shannon, P. Lightfoot, P. A. Wright and R. E. Morris, Angewandte Chemie International Edition **37** (15), 2122–2126 (1998).

27. In *Verified Syntheses of Zeolitic Materials*, edited by H. Robson and K. P. Lillerud (Elsevier Science B.V., 2001).

28. L. T. Yuen and S. I. Zones, Patent No. 20060115422 (2006).

29. R. H. Daniels, G. T. Kerr and L. D. Rollmann, J. Am. Chem. Soc. **100** (10), 3097–3100 (1978).

30. R. D. Shannon, Acta Crystallographica Section A **32** (SEP1), 751–767 (1976).

31. M. A. Camblor, M. Yoshikawa, S. I. Zones and M. E. Davis, in *Synthesis of Microporous Materials: Zeolites, Clays, Nanocomposites* (Marcel Dekker, New York, 1996), pp. 243.

32. M. J. Annen, M. E. Davis, J. B. Higgins and J. L. Schlenker, Journal of the Chemical Society-Chemical Communications (17), 1175–1176 (1991).

33. C. C. Freyhardt, R. F. Lobo, S. Khodabandeh, J. E. Lewis, M. Tsapatsis, M. Yoshikawa, M. A. Camblor, M. Pan, M. M. Helmkamp, S. I. Zones and M. E. Davis, Journal of the American Chemical Society **118** (31), 7299–7310 (1996).

34. S. I. Zones and S.-J. Hwang, Microporous and Mesoporous Materials **58** (3), 263–277 (2003).

Chapter Five: Conclusions and Future Considerations

The guest/host study presented in Chapter Two successfully expanded the SSZ-70 composition window to pure-silica and aluminum containing materials. Other phases observed in the study were TON, MFI, MTT, MTW, Beta, EUO, CFI, SSZ-16 (AFX) and STF. The aluminum-containing SSZ-70 materials were shown to be active catalysts for hydrocarbon cracking. One aspect that remained unsolved was the structure of SSZ-70. In particular, the physical characterization showed strong similarity to MWW materials but catalytic behavior was different. Additional catalytic investigations, such as methanol to higher hydrocarbons, could provide complementary information about possible structural features[1]. Recent advances in combining electron microscopy with high resolution XRD data might offer a path to structure solution. These techniques have been recently used to solve several complex structures from crystals too small for single-crystal analysis[2]. Successful application of these techniques requires sufficient long range order within SSZ-70. It is possible that disorder occurs throughout SSZ-70 making structure solution more difficult. If disorder is present, advanced two-dimensional NMR techniques might offer insight into local structure through $^{29}Si\{^{29}Si\}$ 2D experiments[3, 4]. Solid-state NMR measurements showed well resolved ^{29}Si resonances indicating strong local order suggesting this approach holds promise. In addition, understanding where the SDA molecules are located might offer insight into the observed differences in catalytic behavior. One area of interest is the relative proximity of the charge center to the silicate framework. Again, 2D NMR techniques could offer valuable information although the

relatively weak ^{13}C resonance associated with the imidazolium C(2) carbon could hamper investigations. This potential limitation could be overcome if an imidazolium SDA with ^{13}C enrichment at the C(2) position was employed. Reports of 2-^{13}C-4,5-diphenylimidazole using ^{13}C-formic acid suggest this could be a viable strategy[5]. The proposed synthesis would employ ^{13}C-labeled paraformaldehyde as shown in Scheme 5.1.

$$2 \; R{-}NH_2 \;\; + \;\; (^{13}CH_2O)_n \;\; + \;\; HX \;\; + \;\; O{\diagdown}{\diagup}O \;\; \longrightarrow \;\; R{-}N{\overset{-X}{\underset{\diagdown{=}\diagup}{\overset{^{13}C}{\cdots}}}N}{-}R$$

Scheme 5.1: Proposed synthesis of ^{13}C-labeled imidazolium SDA

The proposed ^{13}C-labeling could help understand organic/silicate interactions with 1,3-bis(1-adamantyl)imidazolium hydroxide. This SDA was able to produce three crystalline phases whereas the two other SDA with quaternary carbons adjacent to nitrogen were not nearly as successful. Information about the distance between the charge center and silicate species would help discriminate the structure direction mechanism.

The apparent similarity between SSZ-70 and MWW should be investigated further through layer manipulation experiments. MWW materials can be swollen, delaminated, pillared and exfoliated with enhanced catalytic properties towards larger molecules[6–8]. Investigations into MWW delamination have focused on aluminosilicate products. As demonstrated in Chapter Two, SSZ-70 can be synthesized as a borosilicate and aluminosilicate. Different delamination behavior might be observed between borosilicate and aluminosilicate materials.

The second guest/host study presented in Chapter Three investigated chiral imidazolium SDAs in the synthesis of polymorph A enriched Beta. Both 1,3-bis((S)-3,3-dimethylbutan-2-yl)imidazolium hydroxide and 1,3-bis((S)-1-cyclohexylethyl)imidazolium hydroxide produced Beta, and many of the XRD patterns were distinctly different than those for regular Beta. EUO was the only other crystalline phase observed in the study. The observed differences in XRD patterns did not correspond to simulated patterns for polymorph A enrichment. Molecular modeling suggested both SDAs occupied the straight 12MR pores. This arrangement did not project chirality across the [001] fault planes providing an explanation for absence of polymorph A enrichment. Modeling showed careful consideration must be given to efficiently filling the entire void space with large SDAs. This obstacle could be overcome using a dual SDA strategy where a large chiral SDA (>10Å length) could be combined with a smaller SDA. The large SDA would be able to span [001] fault planes thereby projecting "handedness" between adjacent layers. The smaller SDA is envisioned to occupy void volume in a similar manner to pore filling agents (PFAs)[9, 10]. A dual SDA approach was recently used to synthesize pure-silica LTA (ITQ-29) using tetramethylammonium hydroxide as the second SDA[11]. Competing nucleation selectivity between the large chiral SDA and smaller SDA is an obvious barrier to overcome. Recent advances in high-throughput (HT) methods could be applied to screen large combinations of SDAs and inorganic compositions[12, 13].

The third study presented in Chapter Four investigated supramolecular SDAs created through adamantyl/β-cyclodextrin inclusion complexes. Experimental evidence for a 2:1 inclusion complex between β-CD and 1,3-bis(1-adamantyl)imidazolium chloride was

obtained from ITC. Initial inorganic reactions with the desired 2:1 inclusion complex showed no desirable perturbation to the product and significant cyclodextrin degradation was observed. Additional attempts using a 1:1 β-CD/N,N,N-trimethyl-1-adamantanammonium complex gave similar degradation. Ultimately, carbohydrate-containing SDAs were not stable under molecular sieve synthesis conditions.

5.1: References

1. S. I. Zones, C. Y. Chen, A. Corma, M. T. Cheng, C. L. Kibby, I. Y. Chan and A. W. Burton, Journal of Catalysis **250** (1), 41–54 (2007).

2. L. B. McCusker and C. Baerlocher, Chemical Communications (12), 1439–1451 (2009).

3. D. H. Brouwer, R. J. Darton, R. E. Morris and M. H. Levitt, Journal of the American Chemical Society **127** (29), 10365–10370 (2005).

4. S. Cadars, D. H. Brouwer and B. F. Chmelka, Physical Chemistry Chemical Physics **11** (11), 1825–1837 (2009).

5. P. Kang and C. S. Foote, Journal of the American Chemical Society **124** (32), 9629–9638 (2002).

6. A. Corma, V. Fornes, S. B. Pergher, T. L. M. Maesen and J. G. Buglass, Nature **396** (6709), 353–356 (1998).

7. W. J. Roth, C. T. Kresge, J. C. Vartuli, M. E. Leonowicz, A. S. Fung and S. B. McCullen, Catalysis by Microporous Materials **94**, 301–308 (1995).

8. S. Maheshwari, E. Jordan, S. Kumar, F. S. Bates, R. L. Penn, D. F. Shantz and M. Tsapatsis, Journal of the American Chemical Society **130** (4), 1507–1516 (2008).

9. H. Lee, S. I. Zones and M. E. Davis, Journal of Physical Chemistry B **109** (6), 2187–2191 (2005).

10. S. I. Zones and S. J. Hwang, Chemistry of Materials **14** (1), 313–320 (2002).

11. A. Corma, F. Rey, J. Rius, M. J. Sabater and S. Valencia, Nature **431** (7006), 287–290 (2004).

12. M. Moliner, J. M. Serra, A. Corma, E. Argente, S. Valero and V. Botti, Microporous and Mesoporous Materials **78** (1), 73–81 (2005).

13. A. Corma, M. J. Diaz-Cabanas, J. L. Jorda, C. Martinez and M. Moliner, Nature **443** (7113), 842–845 (2006).